
**Unraveling the role of the RNA-binding protein
MUSASHI1
in chemoresistance and malignancy of
Glioblastoma**

Dissertation

zur Erlangung des akademischen Grades

doctor rerum naturalium

(Dr. rer. nat)

der

Naturwissenschaftlichen Fakultät I -Biowissenschaften-

der Martin-Luther-Universität Halle-Wittenberg

vorgelegt

von Rebecca Pötschke

geboren am 3.11.1988 in Räckelwitz

1. Gutachter: Prof. Dr. Stefan Hüttelmaier
2. Gutachter: Prof. Dr. Elmar Wahle
3. Gutachter: Prof. Dr. Luiz Penalva

Datum der öffentlichen Verteidigung: Mittwoch, 14.10.2020

„Mit jeder Antwort [wächst] die Neugierde weiterzufragen [..].
Man sieht nur was man weiß. Das heißt, dass mehr Wissen den Menschen auch mehr sehen
lässt und ein Mehr-Sehen wieder zu mehr Wissen und zu mehr Interesse führt.“

M. Beck

Table of Contents

1	Introduction.....	1
1.1	Insights into eukaryotic gene regulation.....	1
1.1.1	The Role of RNA-binding Proteins in Gene Regulation.....	1
1.1.2	The Role of miRNAs in Gene Regulation.....	3
1.2	RNA-binding proteins and miRNAs in Cancer.....	5
1.3	The RNA-binding protein Musashi1.....	7
1.3.1	MSI1 in embryogenesis.....	10
1.3.2	MSI1 in tumorigenesis.....	11
1.4	Glioblastoma and Glioblastoma Cancer Stem Cells.....	13
1.4.1	MSI1 as marker in GBM cancer stem cells.....	16
1.4.2	CD44 as marker in GBM cancer stem cells.....	17
1.4.3	Therapy of GBM.....	18
1.5	Aim of the Study.....	20
2	Material and Methods.....	21
2.1	Material.....	21
2.1.1	Chemicals, Enzymes, Ladders and Cell culture supplies.....	21
2.1.2	Bacteria.....	21
2.1.3	Cell lines.....	21
2.1.4	Antibodies.....	22
2.1.5	Vectors.....	22
2.1.6	Oligonucleotides.....	23
2.1.7	Systems and Kits.....	25
2.1.8	Standardbuffers and Reagents.....	26
2.1.9	Equipment.....	27
2.2	Methods.....	27
2.2.1	Cell biological techniques.....	27
2.2.1.1	Cell culture of adherent cells.....	27
2.2.1.2	Isolation and cultivation of primary cells from tumor tissue.....	27
2.2.1.3	Lipofection of DNA and RNA.....	28
2.2.1.4	Generation of CRISPR/Cas mediated knockout cell lines.....	28
2.2.1.5	Inhibition of RNA synthesis.....	29
2.2.2	Analysis of cell phenotypes.....	29
2.2.2.1	2D-Growth curve.....	29
2.2.2.2	Cell viability assay.....	29
2.2.2.3	Colony formation assay.....	30
2.2.2.4	3D-Spheroid growth assay.....	30
2.2.2.5	Anoikis resistance assay.....	30
2.2.2.6	Compound testing.....	31
2.2.2.7	Immunohistochemistry.....	31
2.2.2.8	Immunofluorescence staining.....	32
2.2.2.9	Single cell migration analysis.....	32
2.2.3	Molecular biological techniques.....	33
2.2.3.1	Extraction of protein.....	33
2.2.3.2	SDS-Polyacrylamide gel electrophoresis (SDS-PAGE).....	33
2.2.3.3	Western Blot-Analysis.....	33
2.2.3.4	Preparation of human tumor tissues.....	33
2.2.3.5	Isolation of total RNA from cell lines (TRIzol/Chloroform extraction).....	34
2.2.3.6	Reverse Transcription.....	34
2.2.3.7	Quantitative Real-Time Polymerase-Chain-Reaction (qRT-PCR).....	35
2.2.3.8	Extraction of genomic DNA.....	35
2.2.3.9	DNA amplification.....	36
2.2.3.10	Oligo-Annealing.....	36
2.2.3.11	Molecular Cloning.....	36

2.2.3.12	Plasmid digestion.....	37
2.2.3.13	Agarose-gel electrophoresis	37
2.2.3.14	DNA extraction from Agarose gels.....	37
2.2.3.15	Ligation.....	37
2.2.3.16	Transformation of <i>E. coli</i> TOP10.....	38
2.2.3.17	DNA Preparation from TOP10 E.Coli (MiniPrep / MidiPrep)	38
2.2.3.18	Sequencing of isolated Plasmid-DNA	38
2.2.3.19	Luciferase-reporter assay.....	38
2.2.3.20	RNA-co-immunoprecipitation (RIP).....	39
2.2.4	Microscopy.....	39
2.2.4.1	Brightfield microscopy	39
2.2.4.2	LSM microscopy	40
2.2.5	Mouse orthotopic xenografts	40
2.2.6	Next generation sequencing (NGS) analysis.....	40
2.2.7	Database research	41
2.2.8	Statistics.....	41
3	Results.....	43
3.1	Expression of MSI1.....	43
3.1.1	MSI1 is highly expressed during early brain development.....	43
3.1.2	MSI1 is highly expressed in high-grade glioma.....	44
3.1.3	MSI1 expression in GBM cell lines	46
3.2	MSI1 affects cancer cell phenotypes	47
3.3	MSI1 conveys oncogenic potential in GBM-derived cells	52
3.4	MSI1 regulates CD44 expression in a 3'UTR-dependent manner.....	55
3.5	Treatment with MSI1 inhibitor luteolin	60
3.6	MSI1 impacts on chemoresistance <i>in vitro</i>	62
3.7	Additional Results:.....	66
	Alternative Splicing results in a second functional MSI1 isoform	66
4	Discussion	71
4.1	MSI1 is an oncofetal RBP.....	71
4.2	MSI1 affects cancer cell phenotypes	72
4.3	Identification of CD44 as a new post-transcriptionally regulated target of MSI1	75
4.4	A treatment with the MSI1 inhibitor Luteolin resembles MSI1 KD and KO phenotypes.....	77
4.5	MSI1 affects chemoresistance <i>in vitro</i>	78
4.6	Alternative splicing results in a second functional MSI1 protein isoform	79
5	Summary	81
6	References	83
7	Appendix.....	99
7.1	Abbreviations.....	99
7.2	List of Figures.....	102
7.3	Eidesstattliche Erklärung.....	104
7.4	Danksagung.....	105
7.5	Curriculum Vitae	106
7.6	Publikationsliste	107

1 Introduction

1.1 Insights into eukaryotic gene regulation

Gene expression comprises well-coordinated events, individually for each cell type, which is a basic necessity to form a multicellular organism with different gene expression patterns for a specific tissue. It is assumed, that mammalian cells contain approximately ~22,000 to ~500,000 messenger RNAs (mRNAs) with varying length (~500 to ~10,000 nt) and distinct cell type specific copy numbers (1 to ~7,000 in copies/cell) (Singh et al. 2015; Islam et al. 2011; Marinov et al. 2014). To orchestrate those sequences carefully, several levels of gene regulation occur within the cell. Regulation of gene expression is categorized into three steps, namely epigenetic, transcriptional and post-transcriptional control. Furthermore, protein expression can be controlled by post-translational modifications (PTMs) and subsequent degradation. Transcriptional control is mainly accomplished via transcription factors which are binding to the DNA, while their functions are influenced by chromatin remodeling and epigenetic regulation (Lelli et al. 2012). Post-transcriptional control comprises regulatory processes occurring on an mRNA. An mRNA consists of different parts – a 5' and 3' untranslated region (UTR) and the coding sequence (CDS). The CDS contains the protein-encoding information, whereas the UTRs modulate mRNA fate by *cis*-regulatory elements, which serve functions in terms of mRNA transport, translation and turnover. To date, most well-characterized post-transcriptional regulatory factors are RNA-binding proteins (RBPs) and microRNAs (miRNAs) (Garneau et al. 2007).

1.1.1 The Role of RNA-binding Proteins in Gene Regulation

RBPs are able to control the fate of an mRNA, from its genesis in the nucleus to its degradation in the cytoplasm. With the beginning of transcription of a protein-coding gene from DNA into mRNA, messenger ribonucleoprotein (mRNP) assembly from different types of RBPs begins to direct the path of an RNA within the cell. The composition of the mRNP complex defines the processing, splicing, localization, stability, translational efficiency, and degradation of the target transcript (Figure 1). Thus, RBPs are potent regulators of post-transcriptional processing steps that influence the overall gene expression pattern of a cell. Accurate control of these processes is necessary to ensure the development and differentiation of any tissue to form an organism (Glisovic et al. 2008).

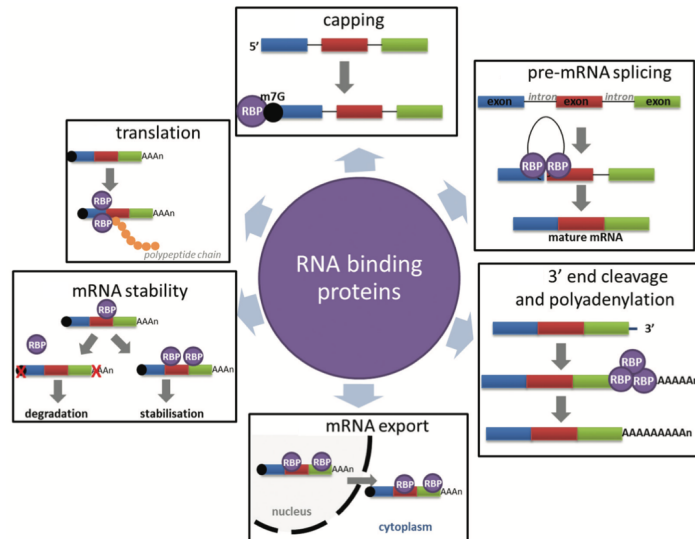


Figure 1. Mechanisms of posttranscriptional gene regulation by RBPs. *Capping* involves the generation of a 7-methylguanosine to the 5' end of a pre-mRNA RBPs bind to the cap and promote mRNA stability. *Pre-mRNA splicing* induces the excision of intronic regions from nascent pre-mRNA. This process is facilitated by the spliceosome. *3'-end cleavage and polyadenylation* involves the cleavage at a defined site and the 3'-end of fully transcribed pre-mRNAs, followed by the addition of a poly-adenosine (poly(A)) tail. *mRNA export* refers to the shuttling of mature mRNAs through the nuclear pore complex to the cytoplasm and subcellular sorting, e.g. during embryonal development. *mRNA stability* can be modulated by association of transcript with specific RBPs, for instance by sequestration in protective cytoplasmic compartments. *Translation* is facilitated by ribosomes, large complexes consisting of RBPs, modulating the mRNA fate. Schematic derived from (Sutherland et al. 2015).

The association of an RBP to RNA is mediated in a specific or non-specific manner. The non-specific binding is influenced by different RBP/RNA concentration levels within the cell, the rate constant for RNA substrate binding/dissociation, and RBP additive or synergistic interactions of co-factors (Jankowsky et al. 2015). Specific mRNA binding is enabled via sequence-specific motifs and or RNA secondary structures. RBPs have a modular structure with protein domains responsible for the different functions. Over 50 different binding domains have been proposed. The most prominent ones are the RNA-recognition motif (RRM) and the human heterogeneous nuclear ribonucleoprotein (hnRNP) K-homology (KH) domain. An RRM consists of approximately 90 amino acids and folds into two alpha-helices packed against a four-stranded beta-sheet. Contrary to that, a KH domain consists of approximately 70 amino acids and folds into three alpha-helices packed against a three-stranded beta-sheet (Pereira et al. 2017; Hentze et al. 2018).

Recently, a set of 1,542 human RBPs (7.5% of the proteome) was defined (Gerstberger et al. 2014) and has been supported by projects within the ENCODE consortium, which investigated 250 of those RBPs for their specific binding by improved high-throughput

techniques, including enhanced crosslinking and immunoprecipitation (eCLIP) (Van Nostrand et al. 2016). Initially, these RBPs were identified with different methods, which decipher the RBP-mRNA interaction (Tenenbaum et al. 2000; Ascano et al. 2013; McHugh et al. 2014; Gerstberger et al. 2014). To get a broad overview of RBP-mRNA associations within the cell and to identify RBPs in separate subcellular compartments, the RNA interactome capture (RIC) can be applied (Castello et al. 2012; Baltz et al. 2012). But novel CLIP techniques, including PAR-CLIP (photoactivatable-ribonucleoside-enhanced CLIP), iCLIP (individual-nucleotide resolution UV-CLIP) or the beforementioned eCLIP, which determine the direct binding site of an RBP on the mRNA with single-nucleotide resolution (Van Nostrand et al. 2016). Therefore, new downstream targets of RBPs were revealed with additional information of 3'UTR, CDS, or 5'UTR regulation.

1.1.2 The Role of miRNAs in Gene Regulation

Very well characterized molecules for post-transcriptional gene regulation are miRNAs, which are able to influence cell growth, proliferation, and differentiation, most likely by inducing gene silencing. They are evolutionary conserved non-coding RNAs with a length of ~22nt with approximately 2200 miRNAs identified in humans (Ameres et al. 2013; Ardekani et al. 2010). The gene silencing occurs via miRNAs through a combination of translational repression, deadenylation, decapping and finally mRNA degradation (miRNA-mediated gene silencing reviewed by (Jonas et al. 2015; Huntzinger et al. 2011; Fabian et al. 2012)). In the canonical biogenesis of miRNAs, their respective genes are transcribed from the RNA-polymerase II into a primary transcript (pri-miRNA), which contains the mature miRNA sequence within its stem-loop. Further processing into a pre-miRNA is performed by the ribonuclease III Droscha within the nucleus. Subsequently, the pre-miRNA is transported into the cytoplasm by Exportin V. There, the ribonuclease III Dicer finally processes the pre-miRNA into a ~22nt long double-stranded RNA. In humans, the association of the RNA-duplex molecule with one of four potential Argonaut (AGO) proteins (preferentially AGO 2) results in the pre-RNA-induced silencing complex (RISC). The mature miRNA-incorporating RISC (miRISC) is assembled by the separation of the double-stranded miRNA, while the guide strand stays associated to the complex, and the passenger strand is degraded (Bartel 2004; Kwak et al. 2010). Within the miRISC, the sequence of the miRNA serves to specifically mediate the process of post-transcriptional gene regulation via partially complementary base pairing between the miRISC and the 3'UTR of the target mRNA (Figure 2). The AGO-protein

recruits the GW182 proteins (in mammals there are three paralogues, termed trinucleotide repeat-containing 6 (TNRC6) proteins), which interact with the cytoplasmic poly(A)-binding protein (PABPC) and the deadenylation complexes PAN2-PAN3 and CCR4-NOT. The interactions result in dissociation of PABPC from the poly(A)-tail of the target mRNA, which is subsequently deadenylated. Following this, the decapping protein 2 (DCP2) removes the 5' cap structure from the mRNA, which is finally degraded via the 5' to 3' exonuclease XRN1. Additionally, the GW182 proteins induce the dissociation of the poly(A)-tail and PABPC to disrupt the 'closed loop' between the 3' end termination site and 5'-cap to inhibit the formation of the translation initiation complex eIF4F. Furthermore, it is assumed, that miRNAs directly suppress the assembly and activity of the eIF4F complex (Fabian et al. 2009; Jonas et al. 2015).

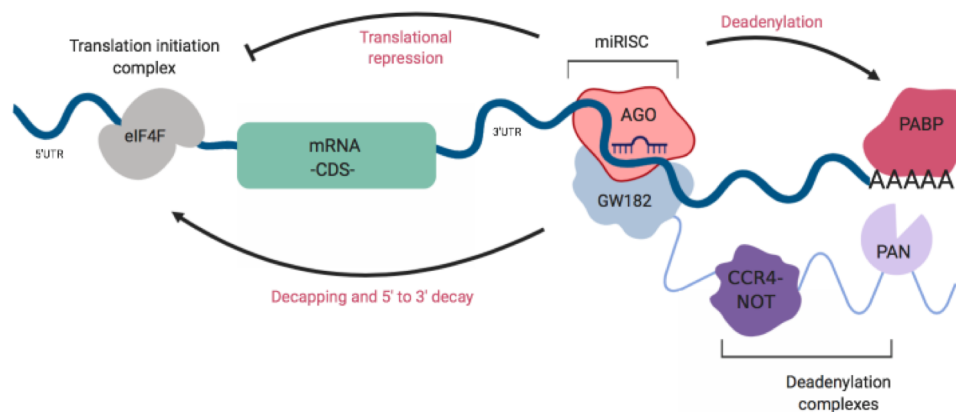


Figure 2: Schematic illustration of miRNA-mediated silencing. MicroRNAs (miRNAs) associate with Argonaute (AGO) proteins in miRNA-induced silencing complexes (miRISCs) and recognize their mRNA targets by base-pairing to partially complementary miRNA recognition elements (MRE). These are predominantly located in the 3' untranslated regions of mRNAs. The AGOs interact with the GW182 proteins, which further interacts with the cytoplasmic poly(A)-binding protein (PABPC) and with the cytoplasmic deadenylase complexes PAN2–PAN3 (Pan) and CCR4–NOT. These interactions catalyze the deadenylation of the mRNA target, and subsequently initiate decapping, followed by 5' to 3' decay. In addition, the miRISC can repress translation by inhibiting the activity and/or assembly of the eukaryotic initiation factor 4F (eIF4F) complex, whereas this mechanism is still not fully understood. Schematic modified from (Jonas et al. 2015).

For complementary binding of the miRNA within the 3'UTR of the mRNA, the complete match of the 'seed region' from nucleotides 2-7 is essential. Supportive binding efficiency is provided by nucleotides 13-16, while between nucleotide 8-12 a bulge is formed (Bartel 2009). Different criteria contribute to the efficiency of the miRNA-mRNA interaction, e.g. the distance from the stop codon (at least 15nt) as well as from the poly(A)-tail and secondary structures have an impact on the effectiveness of miRISC association (Grimson et al. 2007). A 3'UTR can contain multiple binding sites for one or more miRNAs. Thus, transcripts with a

longer 3'UTR tend to contain more regulatory sites for expression control than a gene with a short 3'UTR (Cheng et al. 2009).

1.2 RNA-binding proteins and miRNAs in Cancer

Cancers are characterized by a series of hallmarks acquired during tumorigenesis. These include sustained proliferation, evasion from growth suppression, resistance to cell death, induction of angiogenesis, activation of invasion and metastasis, metabolic rewiring and immune modulation (Hanahan et al. 2011; Fouad et al. 2017). Both post-transcriptional regulators, RBPs and miRNAs as described above, were identified to show aberrant expression in several cancer types (Sassen et al. 2008; Kechavarzi et al. 2014). Due to their impact on diverse cellular processes, they are involved in the hallmarks of cancer (Iorio et al. 2012; Pereira et al. 2017). The aberrant miRNA expression in cancer is ascribed to epigenetic alterations, genetic depletions, amplifications, and mutations, but also an incorrect miRNA biogenesis (Jansson et al. 2012; Iorio et al. 2012). MiRNAs promote tumorigenesis through acting as oncogenes (also called onco-miRs) or tumor suppressive miRNAs, as their expression can be down- or upregulated in cancers (Zhang et al. 2007). MiR-21 or members of the miR-17-93 cluster are representatives of oncogenic miRNAs in general. For the latter, the overexpression is for example described in medulloblastoma (Uziel et al. 2009), neuroblastoma (Mestdagh et al. 2010) and lung cancer (Hayashita et al. 2005), leading to a poor survival outcome for patients. MiR-21 is one of the most abundant expressed miRNAs, and is associated with proliferation, apoptosis and invasion. Its upregulated expression is reported in glioblastoma (GBM) (Malzkorn et al. 2010), breast cancer (Yan et al. 2008) and chronic lymphocytic leukemia (Fulci et al. 2007). The most studied tumor suppressive miRNA family is miR-*let-7*, consisting of 10 family members. Its reduced expression is associated with cancer types like leukemia, lung and ovarian carcinoma (Nair et al. 2012).

In contrast to aberrant miRNA expression, genetic alterations seem to play a minor role for dysregulated RBP expression in cancer (Wang et al. 2018). A recent study identified that only ~15% of all RBPs have mutations affecting their protein sequence. Exceptions are copy number variations in genomic regions containing RBP loci. Gene amplifications are more frequent than gene losses and lead to an upregulated expression of the particular RBP (Sebestyen et al. 2016). In this respect, somatic copy number alterations (SCNA) of RBPs were observed for IGF2BP1 in neuroblastoma (Bell et al. 2015) and the splicing factor PTBP1 in

GBM (Ferrarese et al. 2014). In addition to genetic alterations, the upregulation of specific transcription factors promotes expression of RBPs. For instance, the epithelial-mesenchymal-transition (EMT) related transcription factor ZEB1 represses the mRNA of the RBP ESPR1, which in turn leads to a higher expression of a mesenchymal splicing variant of CD44, thereby inducing a more stemness/invasive phenotype in lung, breast and pancreatic cancer cells (Larsen et al. 2016; Preca et al. 2015). Further, dysregulated expression of RBPs in cancer can be related to post-transcriptional control by non-coding RNAs. The expression of the RBP MSI1 is identified to be translationally repressed by tumor-suppressive miRNAs, resulting in slower tumor growth in GBM and medulloblastoma (Vo et al. 2012). Additionally, the function of RBPs is altered in cancer via PTMs, including (de-) acetylation, phosphorylation, methylation, and ubiquitination. Specifically, RNA-binding domain-forming regions of RBPs are frequently modified (Castello et al. 2016). The PTMs of RBPs can affect RNA-binding properties (Babic et al. 2004), influence their enzymatic activity (Zhang et al. 2013) as well as their intracellular localization (Lee 2012). Although RBPs can bind along an mRNA, most regulatory elements described to date are located within the 5' or 3' UTRs. A mechanism to undergo 3'UTR-dependent regulation is, that for instance cancer cells express mRNAs with a truncated 3'UTR (by alternative cleavage or alternative polyadenylation). The consequences of such processes are fewer miRNA- and RBP binding elements. This process is often associated with activation of oncogenes in cancer cells and enhanced tumorigenesis (Sandberg et al. 2008; Mayr et al. 2009).

Some RBPs show an oncofetal expression pattern, like MSI1 (Sakakibara et al. 1996), IGF2BP1/3 (Bell et al. 2013), LIN28B and HMGA2 (Boyerinas et al. 2008). Oncofetal proteins are highly expressed during development of an organism and are downregulated or entirely absent in adult tissues, but often show re-expression in malignancies. This could be attributed to their function in pathways necessary for proliferation to which the tumor growth depends on. Due to their distinctive appearance, oncofetal proteins are interesting candidates for drug development, and thus, they are under special attention in research. In an optimal case, drugs would not affect normal tissue since they lack expression of the targeted oncofetal proteins.

As already mentioned, RBPs impact the behavior of a cancer cell via influencing alternative splicing, polyadenylation, stability, translation and subcellular localization of their target mRNAs. Thereby, they alter the cancer cell phenotype (e.g., sustained proliferation) and promote an aggressive tumor development (reviewed in (Pereira et al. 2017)). Thus, investigating the interaction of RBPs and their cancer-related target mRNAs and the resulting

network will help to decipher the biology of a tumor and, most importantly, may help patients suffering from these malignancies.

1.3 The RNA-binding protein Musashi1

Musashi1 (MSI1) belongs to the Musashi family of RBPs, which comprises MSI1 and MSI2. MSI proteins are evolutionarily conserved proteins across several species. In the course of evolution, MSI expression includes *Drosophila melanogaster* Msi (Nakamura et al. 1994), *Xenopus laevis* nervous system-specific RNP proteins (Richter et al. 1990), *Mus musculus* Msi1 (Sakakibara et al. 1996) and Msi2 (Sakakibara et al. 2001) as well as human MSI1 (Good et al. 1998) and MSI2 (Barbouti et al. 2003). In *Drosophila m.*, Msi was identified as a protein involved in sensory organ development and asymmetric cell division (Nakamura et al. 1994). MSI1 and MSI2 differ in their expression pattern and their functional role within the mammalian cell. While MSI1 is claimed to be an oncofetal protein with a major expression in stem cells (Siddall et al. 2006), MSI2 is expressed ubiquitously along during development and mainly found in the hematopoietic system after birth (Sakakibara et al. 2001; Kharas et al. 2010).

The *MSI1* gene contains 15 exons. The respective mRNA possesses a 3'UTR of 1776 nt in length and the resulting coding sequence codes for a protein of 362 amino acids (AA). A schematic representation of MSI1 transcript and protein is depicted in Figure 3. Within the N-terminal region, two RRM motifs mediate the RNA binding ability. Both RRMs are connected with a short linker sequence. Two highly conserved sequence motifs RNP1 (Ribonucleoprotein octamer) and RNP2 (Ribonucleoprotein hexamer) are located within the RRMs. Typically, those sequences are (R/K)-G-(F/Y)-(G/A)-(F/Y)-V-X-(F/Y) for RNP1 and (L/I)-(F/Y)-(V/I)-X-(N/G)-L for RNP2 (Burd et al. 1994). It was observed that both RRMs from MSI1 recognize motifs variously defined as [(G/A)U(n)AGU(n=1-3)], r(GUAG) and r(UAG), but preferentially bind to core motif UAG within the 3'UTR of the target mRNAs (Imai et al. 2001; Katz et al. 2014; Zearfoss et al. 2014; Ohyama et al. 2008; Ohyama et al. 2012). Studies on MSI1 RNA-binding revealed that mostly RRM1 is responsible for recognition of the core motif sequence within the target mRNA. RRM2 seems to increase binding affinity about 10-fold in combination with RRM1 but might do not directly contribute to binding specificity (Zearfoss et al. 2014).

While the N-terminus of MSI1 and MSI2 show high sequence homology, the less structured C-terminal region seems to be less conserved. Within the C-terminal half of mammalian MSI1 protein, two protein interaction domains were identified. In proximity to RRM2, a binding site for PABP was reported (Kawahara et al. 2008). Interestingly, it is reported, that PABP interaction domain overlaps with a Germ Line Development 2 (GLD2) binding site in *Xenopus laevis*. This interaction is reported to induce activation of translation via GLD2-mediated polyadenylation and thereby stabilization of the target mRNA (Cragle et al. 2014). Another protein interaction domain is reported for LIN28A. It is assumed that MSI1 associates with a poly-alanine motif within LIN28A to block neural differentiation via impairment of miRNA biogenesis, identifying the potential role of MSI proteins in miRNA-dependent post-transcriptional regulation (Kawahara et al. 2011). Interestingly, both RRMs contain a nuclear localization signal (NLS). Kawahara et al. postulated that due to their localization within the RRMs, both NLS are blocked during target mRNA binding while an RRM-deficient mutant of MSI1 localizes preferentially to the nucleus. The NLS may regulate MSI1 localization to the nucleus by importin- α protein (Kawahara et al. 2011).

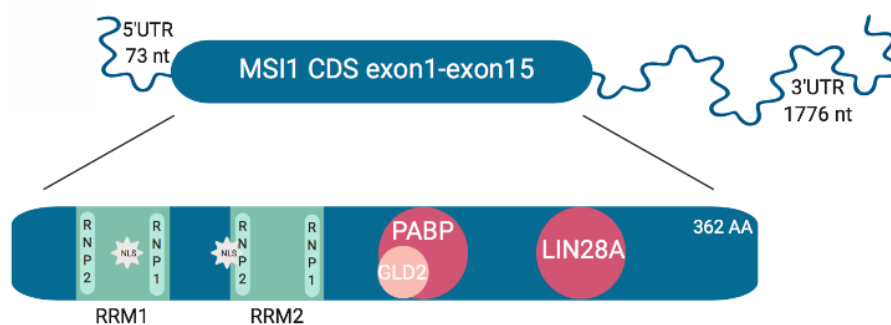


Figure 3: Schematic of MSI1 protein domain composition. Two RRMs are located at the N-terminus. In proximity of the second RRM, protein binding domains were identified. In humans, a PABP binding site and a LIN28 site is reported. In *Xenopus laevis*, a GLD2 site, instead of the PABP site was reported. Schematic modified from (Fox et al. 2015).

The first identified downstream target of MSI1 is NUMB, the major antagonist of the Notch signaling pathway (Imai et al. 2001). This pathway is known to promote proliferative signaling during neurogenesis. It was identified, that MSI1 modulates translation by direct binding with its two RRMs to a specific motif within the 3'UTR of NUMB in neuronal stem cells (NSC), which in turn leads to a downregulated NUMB protein expression. Due to translational repression of NUMB, proliferative signaling through Notch is promoted in neural progenitor cells. Thus, these cells could keep their undifferentiated state as well as their self-renewal potential. Seven years after publication of this observation, the mechanism of MSI1-

dependent translational repression was unraveled (Figure 4). It is reported, that MSI1 contains a direct PABP protein interaction domain. PABP is essential for initiation of translation via binding of eIF4G (eukaryotic initiation factor 4 G), thereby recruiting the 80S ribosomal subunit. It is proposed, that MSI1 competes with eIF4G for the PABP binding. Thus, MSI1 blocks the ribosome assembly and subsequently the formation of the translation initiation complex. Therefore, cap-dependent initiation of translation is repressed (Kawahara et al. 2008). Other identified mRNA targets for translational repression by MSI1 are CDKN1A (Batelli, 2006), doublecortin (Horisawa, 2009), Jagged1 (Katz, 2014), Tensin3 (Chen, 2017) and NF-YA (Lagadec, 2014). In addition, it was found that MSI1 interferes with the time-dependent memory loss in *C. elegans* via translational control of the Arp2/3 actin branching regulator complex (Hadziselimovic et al. 2014).

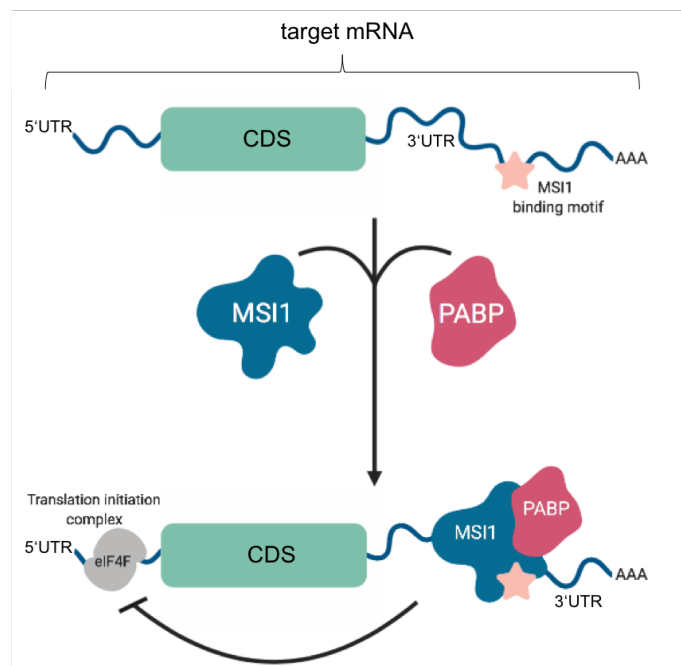


Figure 4: Mechanism of MSI1-dependent translational repression of its target mRNA. MSI1 binds to consensus sequence (MSI1 binding motif) in 3'UTR. There, it can also interact with PABP via a separate domain (see Figure 3). This interaction competes with eIF4G for PABP, which results in the blockage of ribosome assembly and subsequent translation. Schematic modified from (Fox et al. 2015).

MSI1 seems to interfere with fatty acid synthesis since it was found to promote the expression of the enzyme SCD, which catalyzes the conversion of saturated fatty acid into monounsaturated fatty acids. Thus, SCD is essential for normal cellular proliferation, metabolism, and signaling (Clingman et al. 2014). In contrast, MSI1 was identified to promote translation of Robo3 in mice (Kuwako et al. 2010), which regulates axonal navigation during neurogenesis, and the proto-oncogene *c-mos* in *Xenopus* oocytes, which is necessary for meiotic cell cycle progression (Charlesworth et al. 2006). Thus, MSI1 exerts a dual function on

translation within a cell. How both potentially opposing mechanisms are regulated needs to be clarified in future work. Furthermore, Cambuli et al. assumed an mRNA stabilizing function by MSI1 for the targets CCND1, CDK6, and Sox4 in the whole intestinal epithelium in mice (Cambuli et al. 2015).

To further elucidate new downstream targets of MSI1, high-throughput screenings were applied. Those techniques revealed that MSI1 directly or indirectly controls the expression of a large number of genes. The first genomic analyses of MSI1 downstream targets was performed via RNA-immunoprecipitation (RIP)-Chip method in HEK293T cells and revealed 64 MSI1-associated mRNAs involved in cell proliferation, differentiation, cell cycle control, apoptosis, and protein modification (de Sousa Abreu, 2009). Later on, the same group used the iCLIP technique with a GBM-derived cell line U251MG and thereby identified MSI1 as a regulator of cell adhesion pathways (Uren et al. 2015). Another RIP-Chip analysis performed in a Medulloblastoma-derived cell line showed that MSI1 controls a complex network of cancer-related genes and claimed it as a therapeutic target (Vo et al. 2012). Katz et al. performed Ribo-seq analyses to define new translationally regulated targets (Katz et al. 2014).

1.3.1 MSI1 in embryogenesis

After Msi was identified to be involved in the development of the sensory organs in *Drosophila m.*, it was also described that especially MSI1 is a key player in neural development in mammals later on (Sakakibara et al. 1996). The respective study showed that MSI1 is predominantly enriched in neural tissue (olfactory bulb, cerebellum, cerebral cortex, hippocampus, brain stem), in the small intestine, ovary as well as in stem cells of the central nervous system (CNS). Additionally, MSI1 expression pattern regarding brain development was further analyzed. Its mRNA expression in the whole brain of embryonic and postnatal mice was investigated. Highest levels were detected at embryonic day 12 when neurogenesis is actively occurring in mice brain. mRNA expression declines in the course of the developmental process, and only faint MSI1 levels were detectable in adult animals. Although MSI1 expression is dramatically decreased in postnatal stages, in some regions of the adult brain MSI1 levels are still detectable, in association with mitotic activities and expression of NSCs (e.g., cerebellum or subventricular zone) (Sakakibara et al. 1996).

MSI1 interferes with several pathways necessary for a proper self-renewal like the Notch signaling, Wnt-signaling pathway (Rezza et al. 2010) as well as Sonic Hedgehog pathway

(SHH) (Hong et al. 2013). These are known to regulate cell cycle progression and proliferation (Batista et al. 2014). Moreover, MSI1 and also MSI2 seem to be required for brain stem-cell renewal, since a double knockout of both members led to decreased neurosphere formation (Sakakibara et al. 2002). Additionally, both proteins could potentially compensate for their loss due to their RRM sequence similarity and their similar mRNA binding motif. Despite these findings, the same study reported generation of *Msi1*^{-/-} knockout mice, which were uncoordinated, developed hydrocephalus, showed ataxia, and died within 1-2 months after birth. Furthermore, their brains were smaller, contained an increased amount of early lineage progenitor cells, and showed less differentiated cells than control mice. Embryonic neurospheres cultured from the *Msi1*^{-/-} double knockout mice showed reduced capacity to differentiate into neurons and oligodendrocytes.

1.3.2 MSI1 in tumorigenesis

The tightly controlled process of differentiation during development enables stem cells to reproduce themselves, like it is predetermined due to their genetic program. If this course degenerates, an aggressive proliferating process is initiated, which could lead to the development of a tumor. MSI1 is identified to be re-expressed in several cancer types where it is claimed to be an oncogenic driver (Kudinov et al. 2017). It is mostly unknown how MSI1 re-expression is mediated. However, some regulatory mechanisms of MSI1 expression regulation were unraveled so far. At the epigenetic level, promotor methylation seems to affect MSI1 expression. Kagara et al. reported a correlation between MSI1 and hypomethylated regulatory CpG sites (Kagara et al. 2012). At the transcriptional level, it is reported that expression of mouse *Msi1* is regulated by Regulatory factor X (RFX) in NSCs (Kawase et al. 2014). Also, a TCF/LEF-binding site upstream of *Msi1* transcription start site seems to have a regulatory function (Rezza et al. 2010). Post-transcriptionally, MSI1 mRNA is assumed to be stabilized via the RNA-binding protein HuR shown for neural stem/progenitor cells and GBM cells (Vo et al. 2012). As mentioned above, MSI1 mRNA stability is claimed to be regulated by tumor suppressive miRNAs (Vo et al. 2011). Arumugam et al. reported an autoregulatory function of MSI1 for its own translation through binding to its 3'UTR during oocyte maturation in *Xenopus laevis* (Arumugam et al. 2012). Additionally, two extracellular factors were identified to modulate MSI1 expression, thyroid hormone T3 (Cuadrado et al. 2002) and TenascinC (Oskarsson et al. 2011). MSI1 function can be inhibited via oleic acid, which is a

fatty acid (Clingman et al. 2014). It binds to the N-terminal RRM of MSI1 and induces a conformational change that prevents further RNA association. Thus, MSI1 is no longer able to control its downstream targets mainly involved in control of cell proliferation.

In breast cancer, MSI1 expression was analyzed in 140 primary breast tumors by immunohistochemistry (IHC), where only 45 tumors were negative for MSI1 staining. Interestingly, MSI1 was found in 100% of lymph node metastases. Kaplan-Meier analysis revealed MSI1 as a prognostic marker for breast cancer, since patients with MSI1⁺ tumors showed a significantly lower 5-year survival rate compared to patients with MSI1⁻ tumors (Wang, Penalva, et al. 2010). In colon cancer, MSI1 expression was significantly increased in 10 out of 15 tumor samples compared to paired surrounding uninvolved tissue. In this study, the expression was detected on RNA level (Sureban et al. 2008). Further investigations of MSI1 in colon cancer revealed it as a prognostic biomarker (Li et al. 2011). Additionally, high MSI1 levels were detected in lung cancer (Wang et al. 2013), medulloblastoma (Nakano et al. 2007) and ovarian adenocarcinoma (Chen et al. 2015). Expression of MSI1 in gliomas was reported first in 2001 (Kanemura et al. 2001; Toda et al. 2001), where it was described as a potential molecular marker for prognosis and diagnosis. Kanemura et al. assumed that gliomas might derive from progenitor cells. Thus, they detected MSI1 in regard to examining if gliomas express phenotypic markers which are selective to NSCs and/or progenitor cells since MSI1 was identified to be expressed in mice neural stem-like cells, neuronal progenitor cells and astroglial progenitor cells (Sakakibara et al. 1996; Kaneko et al. 2000). They found an intense MSI1 IHC staining in 17 out of 25 GBMs. Interestingly, two different morphological MSI1-positive cell types were observed. One showed a large soma and a co-expression with Glial Fibrillary Acidic Protein (GFAP, a marker for astrocytes) in their cell bodies and processes, but only a moderate level of MSI1. They assumed that those cells will differentiate to astrocytes. The other MSI1-positive cell type showed no GFAP expression and a small cell body. These cells were located in areas with high cellularity at the border between tumor and normal tissue. The authors concluded that those cells correspond to immature glial progenitor cells with high proliferative activity (Kanemura et al. 2001). Toda et al. investigated MSI1 expression via IHC and reverse transcription polymerase chain reaction (RT-PCR) in gliomas and other types of cancer. MSI1 mRNA expression was significantly higher in gliomas compared to normal brain and other cancers (e.g., melanoma or prostate cancer). All six GBM tissues showed a strong MSI1 staining. Moreover, MSI1 expression increases with tumor

grade malignancy and correlates with proliferative activity. This finding underlines a less differentiated tumor environment of GBM (Toda et al. 2001).

1.4 Glioblastoma and Glioblastoma Cancer Stem Cells

GBM is the most prevalent and lethal primary brain tumor. It is a WHO grade IV glioma, which represents the most malignant form. Gliomas are categorized as WHO grades I-IV based on histological characteristics (nuclear atypia, mitosis, vascular endothelial proliferation, and necrosis) and genetic alterations, which both carry prognostic and survival correlates. The majority of GBMs are found in the frontal lobes of the supratentorial compartments, but they can also occur in all cortical areas, cerebellum, brain stem and spinal cord. The median survival rate for patients after diagnosis is about 14 months, and the 5-year survival rate is about 2% (Lathia et al. 2011; Adamson et al. 2009).

In order to understand molecular biology, GBM displays one of the malignancies being best characterized genomically by high-throughput technologies. Loss of function mutations within the signaling pathways of the tumor suppressor p53 and Rb were detected in 87% and 78% of all GBM cases collected in the TCGA dataset, respectively (Cancer Genome Atlas Research 2008). Frequent genomic amplifications are reported for *EGFR* (~ 40%) and *PDGFRA* (~13%). The activation of receptor tyrosine kinases (RTKs) and their downstream signaling pathways are described as the primary oncogenic drivers in GBM. Additionally, dysregulated alterations in the pathways of PI3K-AKT-mTOR and RAS-MAPK were observed (Huse et al. 2009). Verhaak et al. defined pro-neural, neural, classical, and mesenchymal subtypes of GBM based on transcription profiles (Verhaak et al. 2010). Noushmehr et al. found alterations in promoter DNA methylation and identified a distinct glioma-CpG island methylation phenotype, which belongs to the proneural subgroup and is associated with mutations of *IDH1* (Noushmehr et al. 2010). The four subgroups were refined into six groups in the study of Sturm et al., where mutations in *H3F3A* and *IDH1* were unraveled to define a distinct epigenetic and biological subgroup of GBM. Long-term survivors are often patients harboring a mutation in *IDH1* (Sturm et al. 2012). Also, the promoter methylation of the methyl guanine methyltransferase (*MGMT*) gene increases patient's survival since they are responding better to the chemotherapy treatment (Hegi et al. 2005). However, genetic characterization of GBM mostly failed to impact on patient's survival outcome (Lathia et al. 2015).

The current treatment consists of maximal tumor resection, concurrent radiation therapy with temozolomide (TMZ) chemotherapy, and adjuvant chemotherapy with TMZ (Stupp et al. 2009). Nevertheless, tumor recurrence occurs in >90% of cases. Also, GBM are known for their high degree of invasiveness. During tumor progression, tumor cells infiltrate adjacent brain parenchyma; thus, a complete resection is not possible. Invading cells stay quiescent within the normal brain tissue and start to proliferate, which initiates reiterated tumor growth (Furnari et al. 2007) (Figure 5). Thus, those cells are resistant to standard cytotoxic therapies compared to partially differentiated tumor cells. Several molecular processes are claimed to activate therapeutic resistance, including increased DNA damage response, Notch, NF- κ B, EZH2, and PARP pathways (Lathia et al. 2015). Additionally, development of a hypoxic environment within the tumor increases resistance (Filatova et al. 2013).

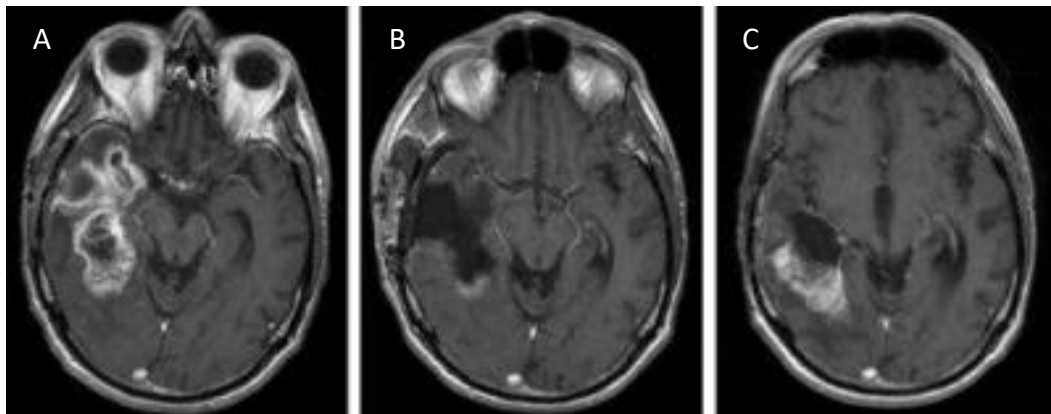


Figure 5: MRT scans of a patient's brain suffering from GBM. A) Brain before surgery with a GBM, localized in left hemisphere (white expansion). B) Brain after surgery. C) Brain shows tumor recurrence (Schlegel 2009).

GBM displays a high cellular heterogeneity, which is maybe responsible for tumor invasion, proliferation, tumor maintenance, and therapy resistance (Lathia et al. 2015). Most of the cells within a tumor mass appear to be non-tumorigenic. It is assumed that only a less differentiated cell population is responsible for tumor initiation and recurrence, called GBM cancer stem cells (GBM-CSC) (Das et al. 2008). First identified tumors with a portion of stem cells possessing extensive proliferation and self-renewal capacity were reported from acute myeloid leukemia (AML) (Bonnet et al. 1997). Hereafter, CSCs have been found in further hematopoietic and solid tumors, including melanoma (Fang et al. 2005), breast, colon and lung cancer (Al-Hajj et al. 2003; Ricci-Vitiani et al. 2007; Eramo et al. 2008). Within the brain tumors medulloblastoma and low-grade glioma (LGG), CSCs were identified via the surface marker CD133 (Singh et al. 2003). Cells expressing this antigen were able to resemble the

original tumor phenotypically. For those experiments establishing a primary sphere formation assay was necessary. CSCs were extracted from a primary tumor and cultured in a defined serum-free neural stem cell medium containing epidermal growth factor (EGF) and basic fibroblast growth factor (bFGF). Tumor spheres could be differentiated with fetal bovine serum (FBS) conditioned medium and were investigated with immunocytochemical staining of differentiation markers (GFAP and β -tubulin 3). At the same time Singh et. al. reported CSCs in medulloblastoma and LGG, another group showed the existence of CSCs in the pediatric brain tumors (Hemmati et al. 2003; Singh et al. 2003). They concluded their findings by similar neurosphere culture experiments but without selecting for CD133. Solely the ability of brain tumor stem cells to form neurospheres *in vitro* was their selection criteria. Both groups suggested that those tumor-derived progenitor cells can give rise to tumorigenic process. Thus, it is crucial to identify and understand the physiology of cells, which are potentially responsible for tumor formation and recurrence. Therapies that do not target GBM-CSCs will presumably be inefficient in tumor treatment. Additionally, it has to be addressed how high the impact on normal NSCs in the normal brain is since they are essential for recovery of damaged areas (Batista et al. 2014).

Stem cells are immature cells with the capacity for self-renewal and to generate mature cells due to induction of differentiation (Reya et al. 2001). Multipotent NSCs have the ability to differentiate into neurons and glia (astrocytes and oligodendrocytes). The process of neurogenesis occurs in two major regions of the adult mammalian brain: in the subventricular zone of the lateral ventricles (from which progenitor cells migrate to the olfactory bulb) and in the subgranular layer of the hippocampal dentate gyrus (Das et al. 2008). New neurons are integrated into the mature neuronal circuitry and take on various functions, thereby contributing to the structural and functional plasticity of the CNS with a crucial role in the neurobiological basis of learning and memory. The subventricular zone is the most substantial neurogenic niche, which supports the maintenance, survival, and proliferation of NSCs. Thus, it is thought that this region gives rise to the most GBM (Batista et al. 2014). However, GBM-CSCs and their progeny are not restricted to neurogenic niches, since they own the ability to migrate away from their place of origin. The majority of neoplastic cells are found within the tumor bed and within 2 cm of borders (Adamson et al. 2009). However, migrating cells can be found several centimeters away from the tumor bulk and even in the contralateral hemisphere, but GBM cells do not metastasize outside the CNS. Like GBM demonstrates a high level of intra-and inter-tumor heterogeneity, GBM-CSCs show a heterogeneous pattern.

GBM-CSCs lines can be classified into oligodendrocyte progenitor cells (OPC), astrocyte progenitor cells (APC), and neural progenitor cells (NPC) based on their expression profile (Pointer et al. 2014).

Pathways for regulation of neuronal differentiation of adult NSCs include Notch, BMP, Wnt, and SHH (Batista et al. 2014). GBM-CSCs are claimed to share properties similar to NSCs such as capacity of self-renewal, proliferation, migration, and differentiation in at least one specific lineage. Also, they express common markers and share signaling pathways responsible for proliferation (Reya et al. 2001). Transcription factors that play a significant role in brain tumors include Bmi1, Olig2, c-Myc, Sox2, Oct4, and Nanog. These factors are associated with high grade glioma (HGG), promoting tumorigenic activity, and GBM-CSC proliferation (Batista et al. 2014).

Tumors require a large amount of nutrients and oxygen to support their rapid growth, which occurs mostly during angiogenesis. The vascular niches in brain tumors are abnormal and contribute directly to the generation of GBM-CSCs and tumor growth (Filatova et al. 2013). These niches protect GBM-CSCs from environmental aggression and provide resistance to therapies. GBM-CSCs are capable of modulating their own microenvironment to produce signals for the recruitment of other immature cells. One of the main components of the extracellular matrix, which is Hyaluronan (HA), was shown to provide a beneficial microenvironment for the self-renewal and maintenance of stem cells. CD44 is the major receptor of HA, and their interaction was shown to propagate stemness of CSCs (Chanmee et al. 2015). Other identified cell surface markers of GBM-CSCs, which mediate the interaction between cells and the microenvironment, are CD15, CD133, integrin α 6, L1CAM, and A2B5 (Lathia et al. 2015). A structural protein, which is identified to be essential for GBM-CSCs, is Nestin (Dahlstrand et al. 1992). Additionally, the RBP MSI1 is known to be a GBM-CSCs marker by maintaining self-renewal potential (Hemmati et al. 2003).

1.4.1 MSI1 as marker in GBM cancer stem cells

As already mentioned, brain tumor stem cells are one of the first CSCs identified in solid tumors. These studies also reported MSI1 expression in CSCs and claimed MSI1 as marker for GBM-CSCs. MSI1 was formerly shown to be expressed in CNS stem cells and neural progenitor cells. Thus, it was thought that normal NSCs and GBM-CSCs share similar expression patterns (Good et al. 1998; Kaneko et al. 2000). Hemmati et al. investigated CSCs in the pediatric brain tumors medulloblastoma, anaplastic astrocytoma as well as in GBM

(Hemmati et al. 2003). They stained clonal neurosphere cells derived from anaplastic astrocytoma with MSI1 and Nestin to show the undifferentiated state of these cells. Via semiquantitative RT-PCR, three medulloblastoma tumors, one anaplastic astrocytoma, and one GBM were analyzed regarding their stem cell marker expression pattern. While GBM whole tumors show a weak MSI1 expression, tumor-derived undifferentiated neurospheres revealed a moderate signal and differentiated neurospheres lacked MSI1 expression. MSI1 expression was further reported in other cancer stem cells, including breast cancer (Wang, Penalva, et al. 2010).

CSCs are able to migrate into the surrounding tissue away from the tumor bulk, where they are claimed to induce tumor recurrence after an uncertain amount of time (Cheng et al. 2011). It was shown, that MSI1 binds several targets (e.g. integrins like ITGA1, ITGAV or ITGB8) of cell adhesion pathways (Uren et al. 2015). Thus, MSI1 impacts on cell migration and invasion supporting CSCs to leave the tumor towards adjacent normal tissue.

CSCs are claimed to expose a high resistance to standard chemo- and radiotherapy (Bao et al. 2006; Chen et al. 2012). Two studies associated MSI1 to increase tumor therapy resistance in GBM. First, MSI1 is assumed to control interleukin-6 synthesis in an AKT-dependent manner and thereby, it inhibits drug-induced apoptosis (Chen et al. 2016). Further, MSI1 was described as a regulator of response to radiotherapy. The depletion of MSI1 led to decreased expression of the catalytic subunit of the DNA-protein-kinase catalytic subunits (DNA-PKcs). This resulted in an increase in DNA damage due to reduced capacity for non-homologous end joining (NHEJ), a distinct DNA-repair mechanism (de Araujo et al. 2016).

In order to these findings, MSI1 is investigated as a potential drug target to treat GBM patients, as it could be a promising starting point for novel (combinatorial) treatment options. Its oncofetal expression pattern could allow a targeted therapy with an MSI1 inhibitor, since it would not interfere with normal cells. One identified MSI1 inhibitor is Luteolin, which is claimed to inhibit MSI1 binding to its target mRNAs (Yi et al. 2018). Luteolin (3', 4', 5,7-tetrahydroxyflavone) is a common dietary flavonoid, which is applied in cardiac diseases and inflammatory disorders. Its effect is investigated in colon cancer, gastric cancer, breast cancer, prostate cancer, and GBM.

1.4.2 CD44 as marker in GBM cancer stem cells

CD44 evolved as a marker for CSC and is highly expressed in several human tumors including colorectal, prostate, breast cancer and AML (Bendall et al. 2000). In GBM, it was shown that

CD44 expression correlates with increasing tumor grade (Yoshida et al. 2012) and high CD44 levels indicate poor prognosis for patient survival (Wei et al. 2010). The transmembrane glycoprotein consists of an N-terminal HA-binding link-homology module, a stem region, a transmembrane domain and a short C-terminal cytoplasmic domain (Zoller 2011). CD44 consists of 20 exons, whereas exons 6-10 are often found to be excluded by alternative splicing. Thus, CD44 has multiple transcript variants which are expressed in a tissue- and stage-specific manner during embryogenesis and carcinogenesis. Notably, CD44 standard isoform (CD44s) is encoded by ten exons, lacking exons 6 to 15, and is translated into a polypeptide with a molecular mass of approx. 85kDa. Post-translational modifications of CD44 include N- and O-glycosylation which enormously influence molecular mass and also its function. CD44 is the major receptor for HA, which is a main component of the extracellular matrix. The interaction was shown to propagate stemness of CSC (Bourguignon et al. 2012). CD44 has a high impact in cell invasion, since adhesion of CD44 to its ligands induces upregulation of other adhesion molecules like integrins (Lundell et al. 1997). Furthermore, upon HA binding to CD44, a cytoskeletal reorganization through signal transduction pathways occurs, which are necessary for cell migration (Oliferenko et al. 2000). The HA-CD44 interaction was identified to enhance chemoresistance in CSCs. HA binding to CD44 increases multidrug efflux regulated via ankyrin. Additionally, the binding of HA to CD44 promotes the interaction of Nanog with Stat-3 leading to Stat-3-dependent Multidrug-resistance protein1 (MDR1) expression (Bourguignon et al. 2008).

1.4.3 Therapy of GBM

GBM is a highly radio- and chemotherapy resistant tumor, leaving it as a non-curable disease. Still, the standard therapy of GBM includes surgical resection, which is not curative approach, followed by radiation with a total dose of 60 Gy and concomitant administration of chemotherapy with the alkylating agent TMZ. Unfortunately, sensitivity to TMZ is restricted to a subset of GBM patients lacking expression of the DNA-repair enzyme MGMT. TMZ induces methyl adducts that are removed by MGMT and thereby resulting in enhanced drug resistance (Esteller et al. 2000; Vogelbaum 2012; Perkins et al. 2016).

Although the understanding of the origin and biological features of GBM through the application of genome- and epigenome-wide molecular profiling techniques has greatly improved, there have been no significant achievements made in terms of patient survival for decades. Thus, it is crucial to find new therapeutic approaches to increase chemotherapy

response as well as to investigate key mechanisms involved in drug resistance in order to find novel, effective GBM targeting strategies (Lathia et al. 2015).

Commonly, patients suffer from tumor recurrence, due to the infiltration of the surrounding brain tissue, potentially by GBM-CSCs. These are reported to be highly radio- and chemoresistant, resulting in the overcoming of the aggressive treatment. The GBM-CSCs can then resemble the primary tumor (Singh et al. 2003). Several recent studies have identified a number of molecular mechanisms that mediate the therapeutic resistance of CSCs to cytotoxic therapies, including the DNA damage checkpoint, as well as Notch- or PARP-signaling, to only name a few (Venere et al. 2011; Wang, Wakeman, et al. 2010; Bao et al. 2006). This suggests that CSCs could be able to exploit multiple mechanisms to achieve resistance, which may require combinations of agents for successful therapy.

In this respect, various histone-deacetylase inhibitors (HDACi) are applied in clinical studies. HDACi are claimed to induce apoptosis, cell cycle arrest and DNA damage repair (Mottamal et al. 2015). One current treatment option for pediatric GBM employs a combination of radiochemotherapy and TMZ with valproic acid (VPA) (clinical trial HIT-HGG-2013; NCT03243461). VPA is an FDA-approved HDACi and is primarily applied for seizure disorders and is widely used in child diseases. It is involved in modulating chromatin structures by histone acetylation, thereby increasing DNA accessibility and cytotoxicity of drugs targeting DNA (Barker et al. 2013). *In vitro* studies showed increased sensitivity for TMZ and radiotherapy upon VPA treatment (Van Nifterik et al. 2012; Hosein et al. 2015).

Besides agents with multiple targets (for instance HDACi) or rather unspecific action (like TMZ by damaging DNA at many genetic loci), current research focuses on immuno- and targeted therapy. Immunotherapy approaches focused on the administration of VEGF or EGFR antibodies with minor to none benefit for patients. Furthermore, direct targeting of frequently altered pathways in GBM are being considered. But inhibiting RTK by imatinib or sunitinib in combination with additional compounds or with radiotherapy revealed only limited activity in primary and recurrent GBM, as shown by several clinical trial studies. A promising approach could be the direct targeting of the EphA3 receptor, an RTK which is overexpressed in 40-60 % of GBMs. Previously tested use of a chemical, GLPG1790, revealed promising results in *in vitro* and *in vivo*-experiments if applied alone, but did not improve benefit over the current therapies when applied in combination with other agents or radiotherapy. Nonetheless, ifabotuzumab, a EphA3-targeting monoclonal antibody is now subject of an early-phase clinical trial (reviewed by (Taylor et al. 2019)).

1.5 Aim of the Study

RBPs are known to regulate gene expression on the post-transcriptional as well as on the post-translational level. The RBP MSI1 is postulated to mainly control mRNA translation of its target transcripts in mammals. Thereby, MSI1 regulates cell proliferation and is able to modulate cellular plasticity and cell differentiation. MSI1 expression is highly abundant during brain development, but is barely detectable in adults, except for NSCs. However, MSI1 is *de novo* synthesized in various types of cancers, including GBM, where it is presumed to promote tumor progression.

In order to these findings, the here presented study aimed to identify the function of MSI1 in GBM cell self-renewal, differentiation, migration and therapy resistance. To achieve the aim, first MSI1 associated phenotypes in a GBM derived cell line were investigated. Since MSI1 is claimed to be a stem cell marker, it was examined if MSI1 drives an aggressive stemness-like tumor cell phenotype. During GBM progression, tumor recurrence occurs as a typical feature due to invading tumor cells. Thus, it was of interest if MSI1 has an impact on cell migration. Furthermore, the impact of MSI1 in a mice survival experiment was investigated. Although MSI1 is considered to mainly control mRNA translation, the here presented study evaluated the impact of MSI1 on the regulation of mRNA turnover of a newly identified target. Potential MSI1 target mRNAs were determined by RNA-sequencing upon MSI1 depletion in GBM-derived cells. To proof the relevance of resulting downstream targets in brain tumors, MSI1 impact was tested also in GBM-CSCs. Therefore, an experimental procedure was established to extract and cultivate GBM-CSCs from primary tumor tissues.

Since MSI1 shows an oncofetal expression pattern, the demand for a MSI1 specific inhibitor arose to target it directly within a tumor. It was investigated how the effects of a therapeutic strategy manifests on cell phenotype as well as on the molecular level. Additionally, MSI1's impact on chemoresistance was tested with a combinatorial compound treatment.

2 Material and Methods

2.1 Material

2.1.1 Chemicals, Enzymes, Ladders and Cell culture supplies

All chemicals used in this study were purchased from Thermo Fisher Scientific, Sigma-Aldrich and Carl Roth, if not indicated otherwise. Enzymes with respective reaction buffers were purchased from Promega and New England Biolabs. DNA and Protein ladders were purchased from Thermo Fisher Scientific and New England Biolabs. Transfection reagents were acquired from Thermo Fisher Scientific. Cell culture plates were purchased from Techno Plastic Products, TPP. Cell culture solutions were acquired from Thermo Fisher Scientific and Sigma-Aldrich.

2.1.2 Bacteria

Stamm	Genotype
<i>E. coli</i> TOP10	F- <i>mcrA</i> Δ (<i>mrr-hsdRMS-mcrBC</i>) Φ 80 <i>lacZ</i> Δ M15 <i>ΔlacX74 recA1 araD139 Δ(ara leu) 7697 galU galK</i> <i>rpsL</i> (StrR) <i>endA1 nupG</i>

For bacteria cultivation, LB (Luria Bertani) medium, consisting of 1 % (w/v) Tryptone, 0,5 % (w/v) yeast extract and 1 % (w/v) NaCl. For LB-Agar, 1,5% (w/v) Agar was added.

For selection of recombinant clones, LB medium was supplemented with antibiotics, according to the respective vector-mediated resistance (30 μ g Kanamycin/mL or 150 μ g Ampicillin/mL).

2.1.3 Cell lines

Table 1: Established cell lines and isolated CSC lines used in this study.

Name	Origin	Reference
HEK293T	Human embryonic kidney	DuBridg e et al., 1987
MCF-7	Breast Cancer (female, 69 yrs)	Brooks et al., 1973
KNS42	Pediatric Glioblastoma (male, 16yrs)	Takeshita et al., 1987
SF188	Pediatric Glioblastoma (male, 8yrs)	Rutka et al., 1987
U251MG (provided by Penlava)	Glioblastoma (male)	Westermar k et. al, 1973

U87MG	Glioblastoma (female, 44yrs)	Macyintyre et al, 1972
U343MG (provided by Penlava)	Glioblastoma (male, 54 yrs)	Nister et al., 1987
T98G	Glioblastoma (male, 61 yrs)	Stein et. al, 1979
LN18	Glioblastoma (male, 65yrs)	Diserens et al., 1981
HAL1 (CSC)	Glioblastoma	this study
HAL8 (CSC)	Glioblastoma	this study
HAL10 (CSC)	Glioblastoma	this study

2.1.4 Antibodies

Table 2: Primary and secondary antibodies used in this study.

Primary Antibodies	Species	Company
anti-MSI1	rabbit	Abcam
anti-MSI1	rabbit	GeneTEch
anti-MSI1	mouse	Millipore
anti-GFAP	mouse	Cell Signalling
anti-CD44, HCAM	rabbit	Sigma-Aldrich
anti-CD44-APC	mouse	Miltenyi
anti-SOX2	rabbit	Cell Signalling
anti-GFP	mouse	Santa Cruz
anti-PABP	rabbit	Cell Signalling
anti-IGF2BP1 (6A9)	mouse	AG Hüttelmaier
anti-GAPDH	rabbit	Cell Signalling
anti-Vinculin, hVin1	mouse	Sigma-Aldrich
anti- PARP	rabbit	Cell Signalling
anti-TUBA4A	mouse	Sigma-Aldrich
anti-Ago2	mouse	Merck Millipore
Secondary Antibodies	Antigen	Company
mouse-IRDye680/800	mouse IgG	LiCor
rabbit-IRDye680/800	rabbit IgG	LiCor
anti-mouse Cy5	mouse IgG	Dianova
anti-rabbit FITC	rabbit IgG	Dianova
anti-rabbit Cy3	rabbitIgG	Dianova

2.1.5 Vectors

Table 3: Cloning vectors used in this study.

Name	Company
pCR [®] -blunt	Invitrogen

pEGFP-C1	CLONTECH
pEGFP-C2	CLONTECH
pLVX-TO(zeo)-GFP	Invitrogen
pmirGlo Dual Luciferase	Promega
pSG-RFP-BbsI-GFP	AG Hüttelmaier
pcDNA_Cas9_T2A_GFP	Addgene

2.1.6 Oligonucleotides

Oligonucleotides and siRNAs were purchased from MWG.

Table 4: Oligonucleotides for molecular cloning.

Name	Sense (5'→3')	Restriction Site
MSI1_CDS_fw	gcgGGATCCatggagactgacgcgccccagc	EcoRI
MSI1_CDS_rev	gccTCTAGAGTCGACtcagtggtaccattggggaagg	SalI/XbaI
MSI1_IF_fw	CCCGAGGTCTCGAGTCATGCCCTACG	
MSI1_IF_rev	CCCGAGGTCTCGAGTCATGCCCTACG	
MSI1_RRMmut_fw	tgaccaagagatccaggggtCtcggcCtcgtcactCtcattggaccaggcgggggtgg	
MSI1_RRMmut_rev	ccacccccgcctggccatgaGagtgacgaGgccgaGaccctggatctcttggtca	
CD44_3p_fw	gcgGAATTCACCTACACCATTATCTTGG AAAGAAACAAC	EcoRI
CD44_3p_mid_fw	ggAGTACTGGCTTTATCCTCTAACC	ScaI
CD44_3p_mid_rev	ggAGTACTCTCTTGTGTTGGTCATAAA	ScaI
CD44_3p_rev	gcgCTCGAGctgttcccttagctcttttaattgtagccttttaattttcc	XhoI

Table 5: Oligonucleotides for Antisense Reporter.

Name	Sequence (5'→3')
hsa-miR-199a-3p_as	aattcACAGTAGTCTGCACATTGGTTAgggcccc
hsa-miR-199-3p_s	tcgagggggcccTAACCAATGTGCAGACTACTGTg
hsa-miR-27b-3p_as	tcgagggggcccTTCACAGTGGCTAAGTTCTGCG
hsa-miR-27b-3p_s	aattcGCAGAACTTAGCCACTGTGAaggcccc
hsa-miR-143-3p_as	aattcTGAGATGAAGCACTGTAGCTCgggcccc
hsa-miR-143-3p_s	tcgagggggcccGAGCTACAGTGCTTCATCTCAG
CD44_miR-27b-3p_1_s	aattcTAATGGCCACCTGTTCTCTCCTGTGAA AGGCTTTGCAAAGTCACATTAGGGCCCC
CD44_miR-27b-3p_1_as	tcgagggggcccTAATGTGACTTTGCAAAGCCT TTCACAGGAGAGAACAGGTGGCCATTAG
CD44_miR-27b-3p_2_s	aattcTGAAAACTTCTTTCTCTTCTGTGA ACATCATTGGCCAGATCCATTTGGGCCCC
CD44_miR-27b-3p_2_as	tcgagggggcccAAATGGATCTGGCCAATGATG

	TTCACAGAAGAGAAAGGAAGTTTTTCAG
CD44_miR-143-3p_s	aattcAAGGAGACTCTTCTAAGTCTTCATCT CAGAGACCTGAGTTCCACTCGGGCCCC
CD44_miR-143-3p_as	tcgaggggccGAGTGGGAACTCAGGGTCTCT GAGATGAAGACTTAGAAGAGTCTCCTTG

Table 6: Oligonucleotides for semiquantitative RT-PCR.

Name	Sequence (5'→3')
3pCD44_s1	CACCTACACCATTATCTTGAAAGAAACAAC
3pCD44_r1	CAAAAAGAGTAGAAAATTTTATGCTAAAAAAGATTTCGC
3pCD44_r2	TATACTGATCAAAGGACTGATCCAGGGT
3pCD44_r3	GAAGATCGAAGAAGTACAGATATTTATTATGAATCAGT
3pCD44_r4	CTGTTTCCTTTAGTCTTTTAATGTTAGCCTTTTAATATTTTCC
CD44 3p fw	GGAGTGCTGGTTGTTATGAGTCTGG
CD44 3p rev 1 (KO)	CCCTTTTGTGCCTCTGACAAAGTAAC
CD44 3p rev 2 (KO)	GTGCTTTCAACTCAGCAATATACATATCATGC
MSI1_ex10_fw	GTTACCCAGGTTTCCAAGC
MSI1_ex12_rev	CTGTCCCTCGAACCACA
MSI1_exon11fw	AATTCGTGTAGAGCGG
MSI1_exon12rev2	CTGTCCCTCGAACCACA

Table 7: Oligonucleotides for qRT-PCR.

Name	Sense (5'→3')	Antisense (5'→3')
GAPDH	CATCAAGAAGGTGGTGAAGCAG	TGTCATACCAGGAAATGAGCTT
EEF2	CCTTGTGGAGATCCAGTGTCC	TTGACCACAAACATGGGGGT
RPLP0	CCTCGTGGAAAGTGACATCGT	ATCTGCTTGGAGCCCACATT
MSI1	GCTCAGCCAAAGGAGGTGAT	GGGCGAGGCCTGTATAACTC
GFAP	AAAGAGATCCGCACGCAGTA	CCAGCGCCTCCTGATAACTG
SOX2	ATGCACCGCTACGACGTGA	CTTTTGCACCCCTCCATTT
NES	GCGGGATACTGAAAAGTTCC	CCTGGGGTCCTGAAAGCTGA
CD44	CATCAGTCACAGACCTGCCCAATGC	ATGTAACCTCCTGAAGTGCTGCTCC
NUMB	CGTTCGCACCGGAAAATGTA	TTCCAGTTTTTCCAAAGAAGCCT

Table 8: Oligonucleotides for siRNA mediated gene knock-down.

Name	Sequence (5' → 3')	Binding site within the MSI1 transcript (nt)
Control (siC, miR-cel-239b-5p)	UUGUACUACACAAAAGUACUG	-
MSI1#1	GGAGAAAGUGUGUGAAAUU	578-596
MSI1#2	GGAUAAAGUGCUGGCGCAA	311-329

MSI1#3	UGGAGGACGUGAAGCAAUA	454-472
MSI1#4	AGGAAGGGCUGCGCAAUA	187-205
MSI1#5	GGUCUCGAGUCAUGCCUA	685-703
MSI1#6	GGGUUUGUCACGUUUGAGA	546-564
MSI1#7	CAGCCUUCACCAAUGGGUA	1153-1171
MSI1#8	GGUUCGGGUUUGUCACGUU	541-559
MSI1#9	GCUCAGCCAAAGGAGGUGA	639-657
MSI1#10	CGAGGGUUCGGGUUUGUCA	537-555

Table 9: Oligonucleotides for CRISPR/Cas9 mediated gene knock-out.

Name	Sequence (5' -> 3')
sgMSI1-1_s	caccgCGAATACTTCGGCCAGTTCG
sgMSI1-1_as	aaacCGAACTGGCCGAAGTATTTCGc
sgMSI1-3_s	caccgGAGACTGACGCGCCCCAGCC
sgMSI1-3_as	aaacGGCTGGGGCGCGTCAGTCTCc
sg_CD44_3p_1_s	caccgTTGGAACATAACCATTACA
sg_CD44_3p_1_as	aaacTGTAATGGTTATGTTTCCAAc
sg_CD44_3p_2_s	caccgTTGATGGATCAATAATAATG
sg_CD44_3p_2_as	aaacCATTATTATTGATCCATCAAc

2.1.7 Systems and Kits

Table 10: Systems and kits used in this study.

Name	Company
WIZARD® SV Gel and PCR Clean-Up System	Promega
WIZARD® Plus SV Miniprep	Promega
Qiagen Plasmid Midi Kit (100)	Qiagen
Zero Blunt™ PCR Cloning Kit	Life Technologies
Phusion® High-Fidelity PCR Kit	New England Biolabs
DC Protein Assay	Biorad
Dual-Glo™ Luciferase Assay System	Promega
CellTiter-Glo® Assay Sytem	Promega
Caspase-Glo® 3/7 Assay System	Promega

2.1.8 Standardbuffers and Reagents

Table 11: Receipts used for buffers and reagents.

Name	Receipt
Phosphate buffered saline (PBS, 0,01M)	137 mM NaCl 2,7 mM KCl 10 mM Na ₂ HPO ₄ 2 mM KH ₂ PO ₄
PBS-Tween (PBS-T)	0,01 M PBS 1% Tween-20
Total-Lysisbuffer	50 mM Tris pH 7,4 50 mM NaCl 1 % SDS (v/v) 2 mM MgCl ₂ 0,2 % (v/v) Benzonase (Millipore)
RIP Gradientbuffer	10 mM Hepes pH 7,4 150 mM KCl 5 mM MgCl ₂ 0,5 % (v/v) NP40
Gradient Lysis-Buffer	10 mM HEPES 150 mM KCl 5 mM MgCl ₂ 0,5 % NP40
NuPage Blotting Buffer	50 mM Tris pH 8,5 40 mM Glycin 10 % MeOH 0,04 % SDS
Ponceaus-S	0,1 % (w/v) Ponceau 5 % Acetic Acid Nuclease-free Water
TRIzol	0,8 M Guanidiumthiocyanat 0,4 M Ammoniumthiocyanat 0,1 Natriumacetat pH 5 5 % Glycerin 48 % Roti-Aqua-Phenol Nuclease-free Water
AlamarBlue	75mg Resazurin 12,5mg Methylene Blue 164,5mg Potassium hexacyanoferrate (III) 211mg Potassium hexacyanoferrate (II) trihydrate 500ml sterile PBS

2.1.9 Equipment

Table 12: Equipment used in this study.

Name	Company
Spectroscopy	Tecan Infinite 2000
SDS-PAGE	Life Technologies NuPAGE MOPS Electrophoresis System
Western-Blot	Trans-Blot Turbo Transfer System (BioRad)
Infrared-Scanner	Odyssey Infrarot Scanner (LiCOR)
Luminescence	GloMAX [®] 96 Luminometer (Promega)
Real-Time PCR	LightCycler [®] 480 II (Roche)
Flow Cytometry	MACSQuant Analyzer (Miltenyi Biotec)
Thermocycler	Mastercycler gradient (Eppendorf)
Centrigue	Heraeus Biofuge Stratos Heraeus Biofuge fresco Eppendorf miniSpin
Microscopy	Leica SP5X Nikon TE-2000E Nikon Eclipse TS100 IncuCyte (Essen BioScience)

2.2 Methods

2.2.1 Cell biological techniques

2.2.1.1 Cell culture of adherent cells

Adherent cell lines were cultivated in DMEM (Dulbecco's modified Eagle's medium), supplemented with 10 % Fetal bovine serum (FBS) and 1 % GlutaMAX (L-Alanyl-L-glutamin) at 37°C and 5 % CO₂. For passaging, cell medium was removed and cells were washed with PBS. Cells were detached with 0,05 % Trypsin in PBS and 0,4 mM EDTA. Detaching was stopped via addition of DMEM (10 % FBS, 1 % GultaMAX). Cells were resuspended and seeded into new plates.

2.2.1.2 Isolation and cultivation of primary cells from tumor tissue

Human glioblastoma brain tumor samples were obtained from the neurosurgery, university clinics Halle (Saale). Transfer and use of samples were performed with permission of the local ethics committee. Primary cells were isolated from fresh surgical specimens of human

primary GBM according, as previously described (Azari et al. 2011). In brief, resected GBM was placed in a tube with PBS supplemented with antibiotics (Penicillin/Streptomycin) and stored on ice. The samples were processed under sterile condition. Medium was removed and the sample was washed with PBS to remove blood and debris. The samples were placed in a cell culture dish and dissected with a scalpel. Afterwards, the minced tissues were trypsinized in pre-warmed trypsin-EDTA for 10-15 min at 37°C. The trypsinisation was stopped with a soybean trypsin inhibitor. The suspension was then centrifuged (800 rpm, 5 min) and the supernatant was discarded. The remaining tissue pieces were resuspended in neural stem cell (NSC) medium (DMEM/F-12 and Neurobasal medium (1:1) supplemented with B27 supplement, bFGF and EGF (20 ng/ml each)). The cell suspension was filtered through a 40 µm cell strainer and again centrifuged (800 rpm, 5 min). Subsequently, the cells were cultured in NSC medium. Neurospheres were subcultured upon the reached an approximate diameter of 150-200 µm. Upon trypsinisation, the cells were replated at a concentration of 5×10^4 cells/ml in NSC medium. Secondary neurospheres formed within 7-10 days (incubated at 37°C, 5 % CO₂).

2.2.1.3 Lipofection of DNA and RNA

Transient transfections were performed with Lipofectamine 3000 or RNAiMAX (ThermoFisher), according to the manufacturer's protocol. In brief, 5×10^5 cells in 1.8 ml were seeded into 6-well plates. For siRNA mediated knockdown, 15 nM siRNA in 100 µl serum-free medium (Optimem, ThermoFisher) and 5 µl RNAiMAX in 100 µl Optimem were mixed, incubated for 5 min at RT and added to the cell suspension. Knockdown efficiencies and effects on downstream target were analyzed 72 h post-transfection on RNA and protein level. For transfection with Lipofectamine 3000, 2,5 µg vector DNA and 3,75 µl P3000 reagent in 100µl Optimem and 3,75 µg Lipofectamine 3000 in 100 µl Optimem were mixed, incubated for 5 min at RT and added to the cell suspension. For selection, cells were incubated with antibiotics according to the respective vector-mediated resistance.

2.2.1.4 Generation of CRISPR/Cas mediated knockout cell lines

For generation of knockout cell lines, the clustered regularly interspaced short palindromic repeat (CRISPR)/Cas9 method was used. Knockouts were generated via inserted mutations within the genome, if a *protospacer adjacent motif* (PAM, 5'-NGG-3') is located directly 3' of the target sequence. This PAM motif gets recognized by a Cas9 nuclease, which is able to

insert a break into the DNA-strand. To guide the Cas9 to a specific target sequence, a *single guide* (sg) RNA builds a complex with the nuclease. The sgRNA consists of a CRISPR-RNA (crRNA, 20 nucleotides), which is complementary to the 3' strand of the target sequence and a Cas9 nuclease-recruiting sequence (tracrRNA). For generation of MSI1 knockouts, sgRNA-plasmids were generated with specific target sequences and transfected in addition with a Cas9-coding vector as described in 2.1.1.3. Successful co-transfection was tested by using fluorescence microscopy. The Cas9-plasmid coded for a detectable green fluorescent protein (GFP) and pSG-MSI1-plasmid coded for a red fluorescent protein (RFP). Transfected cell populations were sorted (BD FACS Aria II, core facility 'Cell Analysis and Cell Sorting', MLU Halle) for double positive fluorescence into 96-well plates after 24 h post-transfection. To increase the survival rate of single cells, conditioned medium was used (according to cell type, 20% FBS total, sterile filtered). Cells were cultured at 37°C and 5 % CO₂. Successful knockouts were verified via Western blot analysis.

2.2.1.5 Inhibition of RNA synthesis

For RNA decay analysis, RNA transcription of siRNA-transfected cells was blocked by treatment with actinomycin D [5 µM] for indicated time points, 72 h post-transfection. RNA abundance was measured by qRT-PCR.

2.2.2 Analysis of cell phenotypes

2.2.2.1 2D-Growth curve

To analyze cell growth, 1x10⁴ cells were seeded into 24-well plates in triplicates for each measuring point. Cell numbers were determined via flow cytometry (MACSQuant[®], Miltenyi Biotec) every two days. Dead cells were identified by adding propidium iodide. Initial cell numbers were counted via flow cytometry as input control.

2.2.2.2 Cell viability assay

Cell viability was determined by using the *CellTiter-Glo[®] Luminescence Cell Viability Assay* (Promega) according to the manufacturer's protocol. Cell viability is measured via intracellular ATP-concentration, which signals the presence of metabolically active cells. The CellTiter-Glo[®] reagent was applied in a 1:1 ratio to cell culture medium and incubated for 10

min. The resulting luminescence signal is a product by the luciferase reaction and was detected with a GloMAX[®] luminometer (Promega).

2.2.2.3 Colony formation assay

To investigate anchorage-independent cell growth, a colony formation assay was performed. Therefore, 3,5 % and 5,0 % agarose suspension was generated out of SeaPlaque[™] Agarose (Lonza) and PBS. The 5,0 % agarose suspension was heated and diluted to 0,5 % with DMEM (10 % FBS, 1 % GlutaMAX[™]) and used for coating (1 ml) of a 12-well plate and left at 4°C over night. Per well, 1×10^3 cells in 900 μ l DMEM and 100 μ l of liquid 3,3 % agarose suspension were mixed, seeded and left for 5 min at 4°C. Afterwards, cell culture medium (0,5 ml/well) was added. After 14 days of cell culturing at 37°C, cell viability was measured via adding methylthiazolyldiphenyl-tetrazolium bromid (MTT). Therefore, 100 μ l of 5 mg/ml MTT-solution (in PBS) was added per 12-well and incubated for 20 min at 37°C. Documentation was performed with a Scanjet G4010 photo scanner (HP). Number and size (colony size $\geq 5 \times 10^5 \mu\text{m}^2$) of MTT-stained colonies were analyzed with the *SoftAgarPipeline* software.

2.2.2.4 3D-Spheroid growth assay

For spheroid formation and growth, 3×10^3 cells in 100 μ l were seeded into a 96-well of a round bottom ultra-low attachment surface plate (Corning). After plating, cells were centrifuged for 3 min at 2000 rpm. Initial cell viability was measured as input control. 100 μ l of cell suspension and 50 μ l of CellTiter-GLO[®] were added into a white microtiterplate and incubated for 10 min. Luminescence was measured with a GloMax[®] 96 Luminometer (Promega). Cells were grown at 37°C and 5 % CO₂. Pictures of spheres were taken with an IncuCyte device or a Nikon Ts2 microscope. The spheroid size was determined with IncuCyte Software or Fiji Particle Analyzer. Cell viability was measured after four to six days, as described in 2.2.2.2.

2.2.2.5 Anoikis resistance assay

For an anoikis resistance assay, 3×10^3 cells in 100 μ l per well were seeded into a 96-well flat bottom ultralow attachment surface plate (Corning). Cell medium was changed from DMEM (10% FBS, 1% GlutaMax[™]) to DMEM (w/o FBS, 1%GlutaMax[™]). After plating, cells were centrifuged for 3 min at 300 rpm. Initial cell viability was measured as input control, as described in 2.2.2.4. Cells were grown at 37°C and 5% CO₂. Pictures of spheroids were taken

with an IncuCyte device (Essen BioScience) or a Nikon Ts2 microscope. Cell viability was measured after seven days, as described in 2.2.2.2.

2.2.2.6 Compound testing

KNS42 or SF188 cells were plated onto a 96-well plate in 200 μ l complete culture media (KNS42 5×10^3 cells/well, SF188 1×10^3 cells/well). Cells were treated with varying concentrations of VPA (Sigma-Aldrich) (diluted in H₂O) and or TMZ (Sigma-Aldrich) (diluted in DMSO), or vehicle control. Cells were treated for 96 h at 5 % CO₂ and 37°C. To assess cell viability in response to TMZ and VPA treatment, AlamarBlue™ was used, which was added (1:10) to each well and incubated for 3 h at 5 % CO₂ and 37°C. The color change and fluorescence increase indicates cell viability. Fluorescence (excitation 560 nm, emission 590 nm) was measured with an Infinite® 200 Pro plate reader (Tecan).

For treatment with MSI1 inhibitor Luteolin (Sigma-Aldrich) of KNS42 and HAL8 cells, 5×10^5 cells in 100 μ l were seeded as duplicate into a 96-well plate. DMSO served as vehicle. Tested concentrations ranged from 100 μ M down to 0.39 μ M. Cell viability was measured 72 h after drug addition with alamarBlue™ assay. AlamarBlue™ solution was added 1:10 to cell medium and incubated for approximately 4 h at 37°C. Change in fluorescence was determined with Tecan Infinite 2000 (excitation 560 nm, emission 590 nm; bottom reading; gain: optimal). The half-effective concentration (EC₅₀) was determined with Prism Software.

2.2.2.7 Immunohistochemistry

IHC stainings were generated by Gerrit Gielen, Bonn.

The neuropathological analysis of pediatric glioma samples (diffuse astrocytoma (WHO grade II, IDH-mutant), anaplastic astrocytoma (WHO grade III, IDH-mutant) and glioblastoma (WHO grade IV, IDH-wildtype), were diagnosed according the 2016 WHO classification of tumors of the central nervous system. Control tissue origins from cerebellum of a five year old girl (cause of death not neoplastic) was retrieved from the archive of the Institute of Neuropathology, University of Bonn Medical Centre. IHC was performed on a Ventana Benchmark XT Immunostainer (Roche Ventana, Darmstadt, Germany) with a monoclonal antibody directed against Musashi-1 (clone 7B11.1; Merck/Millipore, MABE268, dil. 1/400). Antibody labeling was assessed microscopically by an experienced neuropathologist. Specific cytoplasmic and or nuclear staining was considered as positive staining. Human cerebellar tissue served as a positive control. The analysis was approved by the IRB review of the

University clinic Goettingen (Germany), as part of the HIT-HGG-2013 (for HGG) and SIOP LGG 2004 (for LGG) clinical trial. Patients, respectively parents gave their informed consent for storage and use of tumor material for future research, like the present one.

2.2.2.8 Immunofluorescence staining

Cells were grown in 24-well plates on coverslips for at least 24 h. All following steps were carried out at room temperature. Cells were fixed using 4 % PFA solution for 20 min at RT and permeabilized with 0,5 % (v/v) Triton X-100 in PBS for 5 min. For tubulin staining, cells were fixated with 80 % methanol at -20°C for 15 min. Cells were washed three times with PBS. Unspecific binding was blocked with 1 % BSA in PBS for 1 h. Primary antibodies were diluted in 1 % BSA/PBS and incubated for 1 h (antibodies listed in 1.1.4). After washing with PBS, cells were incubated with FITC-, Cy3- or Cy5-fluorescently labeled secondary antibodies and/or phalloidin-TRITC (for F-Actin staining, Sigma-Aldrich, 1:500) in 1 % BSA/PBS solution for 1 h. Unbound secondary antibodies were removed with PBS. Nuclei were stained with DAPI (for nuclei staining, 1:10 000 in PBS, Sigma-Aldrich) for 5 min. Stained cells were washed several times with PBS, two times with distilled water and two times with 96 % ethanol for dehydration. Afterwards, cells were conserved on cover slips with ProLong® Gold Antifade (Thermo Fisher Scientific). Images were acquired by confocal microscopy.

2.2.2.9 Single cell migration analysis

For single cell migration analyses, cells were seeded on a collagen coated 24-well plate (3×10^3 cells /500 μ l). Single cell migration was monitored over 10 h by time lapse analyses (1 frame/5 min) based on a Leica TCS SP5 confocal microscope equipped with a Ludin cube incubation chamber using a 20x objective. The speed of cell migration was determined as mean displacement [μ m/min] of tracked cells using the ‘manual tracking’ plugin (<http://rsbweb.nih.gov/ij/plugins/track/track.html>) for ImageJ. Statistical significance was determined by Student’s T-test.

2.2.3 Molecular biological techniques

2.2.3.1 Extraction of protein

For extraction of protein from cells, cell medium was aspirated and washed with PBS. By using a spatula, cells were scraped from the plate and harvested in 1ml PBS. After centrifugation at 4000 rpm for 5 min and aspiration of PBS, the pellet was dissolved in total lysis buffer. Protein concentration was determined with the DC Protein Assay (BioRad) and BSA in serial dilution as standard. Measurements were done with Tecan Infinite 200 at 750 nm.

2.2.3.2 SDS-Polyacrylamide gel electrophoresis (SDS-PAGE)

Separation of proteins according to their size was performed by SDS-PAGE. Equal protein amount of different samples were buffered with 4xNuPage LDS Sample Buffer (containing 1:10 DTT [1 M]). Samples were denatured at 95°C for 5 min and loaded on a NuPage® Novex 4-12% Bis-Tris Protein Gel (Life Technologies). Electrophoresis was performed at 180 V in NuPAGE® MOPS SDS Running Buffer (Life Technologies).

2.2.3.3 Western Blot-Analysis

For detection of proteins with specific antibodies, SDS-PAGE separated proteins were transferred with Tank-Blot method to a Hybond-ECL Nitrocellulosemembrane (GE Healthcare). Whatman-paper and membrane were pre-incubated in 1xNuPAGE-blotting buffer, supplemented with 10 % MeOH. Proteins were blotted on the membrane at 33 V for 75 min. Accurate blotting was ensured via Ponceau staining, which can be removed with PBS-T. Unspecific antibody binding was prevented by blocking the membrane with 5 % milk in PBS-T for 30 min. Primary antibody was incubated for 1 h at RT or overnight at 4°C. The secondary antibody was incubated for 45 min at RT. Afterwards, the membrane was washed with PBS-T. Protein abundance was detected with an Odyssey Infrared Imaging System (LI-COR) at 680 nm or 800 nm. Quantification of protein signals was done with the Image studio Software (LI-COR).

2.2.3.4 Preparation of human tumor tissues

Adult glioblastoma tumor samples were provided by the Neuropathology Department, University Magdeburg.

Frozen tumor samples were shredded in liquid nitrogen with a mortar and allotted into 1,5ml Eppendorf tubes. For isolation of tissue RNA, ceramic beads were added to the frozen tissue pulver and supplemented with 1ml TRIzol. The vessel content was homogenized for 20 s with a Precellys® 24 homogenizer and stored for 5 min on ice. RNA was isolated by using TRIzol/Chloroform extraction, as described in 2.2.3.5.

2.2.3.5 Isolation of total RNA from cell lines (TRIzol/Chloroform extraction)

For isolation of total RNA with TRIzol, cell medium was discarded, cells were rinsed two times with PBS and incubated with 1ml TRIzol per 6-well plate for several minutes. The suspension was transferred into a safe lock Eppendorf tube and stored at -80°C or was further processed. Therefore, 200 µl Chloroform were added and the samples were vortexed subsequently. Phase separation was achieved by centrifugation for 5 min at 13000 rpm and 4°C. The aqueous (upper) phase was transferred into a new Eppendorf tube. RNA precipitation was ensued by addition of 500 µl isopropanol and incubation at 4°C for 20 min. Afterwards, the precipitated RNA was pelletized via centrifugation at 13000 rpm and 4°C for 10 min. The pellet was washed for two times with 1 ml 80% ethanol and dried off at 65°C for 1 min. RNA was dissolved in 30 µl ultra-pure water and stored at -80°C. Concentrations were determined with a Tecan Infinite 2000.

2.2.3.6 Reverse Transcription

For cDNA-Synthesis, 2 µg RNA (unless otherwise stated) was added with ultra-pure water to a total volume of 13,5 µl. 1 µl random-hexamer (R6) was added and incubated for 5 min at 65°C. This incubation step dissolves secondary structures and allows a proper binding of primers to RNA. After a cool down to 4°C, 5,5 µl Master mix (containing 1 µl 10 mM dNTPs, 4 µl Reverse Transcriptase 5xBuffer (Promega) and 0,5 µl M-MLV Reverse Transcriptase (Promega)) was added to each sample. Following program was used to achieve reverse transcription:

Table 13: Program for reverse transcription.

Step	Temperature	Time
Denaturation	65°C	5 min
Cool Down	4°C	2 min
Addition of 5,5 µl Master Mix		

R6-Annealing	20°C	5 min
	25°C	5 min
	30°C	5 min
Reverse Transcription	42°C	60 min
Inactivation	72°C	15 min
End	4°C	-

The cDNA was stored at -20°C or further processed.

2.2.3.7 Quantitative Real-Time Polymerase-Chain-Reaction (qRT-PCR)

qRT-PCR was done for quantitative analysis of mRNA-abundance. cDNA was diluted 1:7-1:10 with ultra-pure water. Measurement was done in a 384-well microtiter plate. Per well, 2,5 µl of diluted cDNA was mixed with 2,5 µl ORA qPCR-Green ROX L Mix 2x (HighQu) and 0,02 µl of each specific primer (100 µM). Measurements were done duplicates. For qRT-PCR measurement a Roche Light Cycler 480 II was used with the following:

Table 14: Program for RT-qPCR.

Step	Temperature	Time	
DNA polymerase activation	95°C	5 min	
Denaturation	95°C	10 s 10 s 20 s	40 cycles
Primer-Annealing	60°C		
Elongation	72°C		
Melting curve	65°C-95°C	-	

Resulting C_q-values (cycle of quantification) from first point of inflection of second derivation (second derivative maximum) were used for calculation of changes in mRNA levels compared to control with $\Delta\Delta C_q$ -method (Livak and Schmittgen, 2001).

2.2.3.8 Extraction of genomic DNA

For extraction of genomic DNA of KNS42 cells, cell pellets were solved in total lysis buffer (500 µl). 5 µl of Proteinase K (NEB) was added and incubated for 60 min at 55°C. For DNA precipitation, 500 µl Isopropanol was added and the sample was inverted several times. Precipitated DNA was transferred with a needle into a new Eppendorf tube. Afterwards, 1ml 80 % Ethanol was added. After three washing steps with Ethanol (centrifugation for 5 min, 13000 rpm), the pellet was dried via aspiration and diluted in distilled H₂O.

2.2.3.9 DNA amplification

For amplification of the sequence of interest for cloning purposes, Phusion High-Fidelity DNA Polymerase (Thermo Fisher Scientific) was used. The reaction mix composed as follows:

Table 15: Reaction mix for DNA amplification.

Component	Amount
cDNA	10-100 ng
10 mM dNTPs	0.5 μ l
10 μ M sense/antisense Oligonucleotide	1 μ l each
5xGC Buffer	5 μ l
Phusion High Fidelity DNA Polymerase	0.5 μ l
Ultra-pure water	add to 25 μ l

Following protocol was used for amplification:

Table 16: Program for DNA amplification

Step	Temperature	Time	
Initial Denaturation	98°C	5min	
Denaturation	98°C	10 s	35 cycles
Primer-Annealing	60-65°C	30 s	
Elongation	72°C	30 s-90 s	
Final Elongation	72°C	-	

2.2.3.10 Oligo-Annealing

For oligo annealing, 5 μ l 100 μ M sense oligonucleotides, 5 μ l 100 μ M antisense oligonucleotides and 10 μ l ultra-pure water was mixed. The oligonucleotides were incubated for 5 min each at starting temperature 95°C, followed by 65°C and afterwards cooled down to RT.

2.2.3.11 Molecular Cloning

For cloning purposes, a sequence of interest was amplified with Phusion® High-Fidelity DNA polymerase (Thermo Fisher scientific) with specific oligonucleotides, which added specific restriction sites. The purified PCR product (described in 2.2.3.14) was inserted into a pCR™-Blunt vector. All variants of MSI1 coding sequence were amplified by RT-PCR from total

KNS42 RNA. The MSI1 amplicons were subcloned via EcoRI/SalI into pcDNA3.1zeo-Flag and pLVX-TO(zeo)-GFP, respectively. To generate an RNA-binding deficient MSI1 mutant, three phenylalanines within the RRM1 were mutated to lysine, as described by (Imai et al. 2001). MSI1 Δ 11 was generated via fusion PCR (1. Fragment MSI1 CDS fw primer, MSI1 IF rev primer; 2. Fragment MSI1 IF fw primer, MSI1 CDS rev primer). For luciferase reporter assay, the 3'UTR of CD44 was amplified from total KNS42 cDNA. The amplified CD44 3'UTR was subcloned into the pmirGlo Dual Luciferase Expression Vector with EcoRI/XhoI restriction sites. For luciferase miRNA-antisense reporter assay, constructs were generated by oligo-annealing and cloned with EcoRI/XhoI restriction enzymes into the pmirGlo Dual Luciferase Expression Vector.

2.2.3.12 Plasmid digestion

For restriction cloning, 1 μ g vector DNA was digested with 1 unit of restriction enzyme. Digestion Batch had a total volume of 10 μ l. If not indicated otherwise, 10x CutSmart[®] buffer (NEB) was used. Incubation time was set according to enzymes preferences, mostly at 37°C for 30 min to 2 h.

2.2.3.13 Agarose-gel electrophoresis

Preparative digestions, test-digestions and PCR products were separated by gel electrophoresis. 6x Gel loading dye (NEB) was added to the samples and loaded onto a 1-2 % agarose gel. Quick-load 2-log DNA-ladder (NEB) was used as size marker. DNA was separated at 140 V and visualized with Ethidium bromide by UV light.

2.2.3.14 DNA extraction from Agarose gels

DNA extraction from agarose gels was performed with the Wizard[®] SV Gel and PCR Clean-Up system (Promega), according to manufacturer's protocol.

2.2.3.15 Ligation

For ligation, extracted DNA, digested vector, 1 μ l 10x T4 Ligase buffer and 1 μ l T4 Ligase (NEB) were incubated at RT for 1 h. The molecular proportion of insert to vector was 5:1. Total volume of a ligation reaction was 10 μ l.

2.2.3.16 Transformation of *E. coli* TOP10

For Transformation of ligated DNA, the respective ligation reaction was added to *E. coli* TOP10 bacteria (1:10) and incubated on ice for 20 min. After a heat shock at 42°C for 50 sec, the bacterias were incubated on ice for 3 min, followed by the addition of 500 µl LB medium. Subsequently, the bacteria were incubated at 37°C for 60 min. Afterwards, they were plated on LB-agar, containing antibiotics according to the vector-mediated resistances and were grown over night at 37°C.

2.2.3.17 DNA Preparation from TOP10 E.Coli (MiniPrep / MidiPrep)

For MiniPrep (QIAprep Spin Miniprep Kit, Qiagen) or Midi Prep (QIAprep Spin Miniprep Kit, Qiagen), cells were grown in LB-medium over night at 37°C. Isolation of DNA was done according to manufacturer's protocol.

2.2.3.18 Sequencing of isolated Plasmid-DNA

The sequences of isolated plasmid DNA was verified by Sanger-sequencing by Eurofins Genomics GmbH. For this purpose, 250 ng-1500 ng DNA/15 µl ultra-pure water and 2 µl sequencing primer were mixed.

2.2.3.19 Luciferase-reporter assay

Luciferase reporter assays were performed to investigate 3'UTR-dependent regulation and to analyse miRNA activity. Respective constructs were transfected into cells with Lipofectamine 3000, according to the manufacturer's protocol. 48 h post-transfection, luciferase activity was measured by using the Dual-Glo® Luciferase assay system. Therefore, the cell medium was aspirated and cells were washed with PBS. Afterwards, 50 µl PBS and 50 µl Dual-Glo® Luciferase substrate were added to each well and incubated for 10min. The mix was transferred into a white 96-well-luminometer plate, luminescence of the firefly luciferase was detected with a GloMAX® 96 Microplate Luminometer (Promega). Afterwards, 50 µl Dual-Glo Stop&Glo substrate was added to each well, incubated for 10 min and luminescence of the renilla luciferase was measured. Firefly luminescence was normalized to renilla luminescence. Relative luminescences were calculated as ratio from condition to control.

2.2.3.20 RNA-co-immunoprecipitation (RIP)

RIP was used to determine the association of MSI1 with target mRNAs. GFP-, GFP-MSI1- and GFP-MSI1-RNPmutant overexpressing KNS42 cells were used for the analysis. For each RIP, 5×10^6 cells were used, which were grown on a 10 cm plate at 37°C overnight and harvested by trypsinisation. Upon centrifugation at 1500 rpm for 3 mins, each cell pellet was lysed in 500 µl gradient buffer for 5 min on ice and centrifuged at 13000 rpm. The lysate was split for 10 % Input (50 µl) and 90 % RIP (450 µl). Per RIP, 2.5 µg GFP-antibody (Roche) was coupled to 20 µl Protein G Dynabeads® (Thermo Fisher). Therefore, beads and the antibody were incubated in gradient buffer on a rotating wheel for 20 min. After coupling, unbound antibody was removed by immobilizing beads with a magnet (DynaMag™-2; Thermo Fisher) and 3 subsequent washing steps in 300 µl gradient buffer. For elution of GFP, GFP-MSI1 and GFP-MSI1-RNPmutant, beads were incubated at 65°C for 5 min and incubated with 110 µl gradient buffer with 1% SDS. The eluate was transferred into new tubes after immobilizing beads with a magnet. For measurement of RNA enrichment, 70 µl of eluate was added to 930 µl TRIzol and either stored at -80°C or used for subsequent use. For proof of antibody binding by Western blotting, 30 µl of eluate was added to 4x sample puffer (NuPAGE® LDS Sample Buffer, 1:10 DTT; Invitrogen).

The RNA was purified by TRIzol-chloroform extraction as described in 2.2.3.5. Finally, the pellet was solved in 14 µl for IP and 30 µl for Input-RNA. A volume of 13,5 µl of the RNA was used for the reverse transcription with M-MLV reverse transcriptase and random hexamer primers, as described in 2.2.3.6. RNA abundance was assessed by qRT-PCR using primers listed in table 7.

2.2.4 Microscopy

2.2.4.1 Brightfield microscopy

Brightfield microscopy was used to analyze cell viability and confluence of growing cells. Additionally, cell morphology upon knockdown of MSI1 was examined. Representative images were acquired using a Nikon Coolpix 990 camera attached to a Nikon Eclipse TS100 microscope.

2.2.4.2 LSM microscopy

Confocal laser scanning microscopy was used for acquisition of images from immunostained cells. Image acquisition was performed with a Leica SP5 microscope with a 63x Plan Apo objective, a white light laser and LAS AF software.

2.2.5 Mouse orthotopic xenografts

The injection of KNS42 sgMSI1 cells and KNS42 control cells into the brains of nude swiss mice (CrI:Nu(Ico)-Foxn1 nu) was performed by Prof. Dr. Mawrin at the Neuropathology Department, University Magdeburg within license of authorization for animal experiments (Uni MD 2-12-14). KNS42 cells were injected orthotopically, i.e. into the mouse brain. In brief, nude mice were anesthetized with ketamine/xylazine. Afterwards, the head was fixated and the skin was cut open. 2 mm in front of the bregma and 1,5 mm lateral of it, a 1,5 mm deep borehole was generated. Per mice, two boreholes with 2.5×10^5 cells diluted in PBS were injected. Skin flaps were stuck together with tissue glue. Per condition, 4 mice were operated. The experiment lasted 3 months.

2.2.6 Next generation sequencing (NGS) analysis

mRNA-sequencing upon MSI1 KD in KNS42 cells was performed by Novogene (HongKong). Total RNA was isolated via TRIzol/Chloroform extraction (Chomczynski et al. 1987), as in 2.2.3.5. The RNA quality was assessed by using a Bioanalyzer (Agilent). NEB Next[®] Ultra[™] RNA Library Prep Kit was used for RNA library preparation. RNA sequencing was performed on an Illumina HiSeq X platform. miRNA-sequencing of wildtype KNS42 cells was performed by the Deep Sequencing Facility, TU Dresden. Again, total RNA was isolated via TRIzol/Chloroform extraction. For the generation of small RNA-seq libraries, 50 ng of total RNA served as input using the NEXTflex Small RNA Library Prep Kit v3 (Bio Scientific). Sequencing was performed on an Illumina HighSeq 2000 platform.

Analysis of NGS data was performed by Dr. Glass (AG Hüttelmaier, University Halle). Low quality read ends, as well as remaining parts of sequencing adapters were clipped off using Cutadapt (v 1.14). For mRNA and miRNA-seq analyses, reads were aligned to the human genome (UCSC GRCh38) using HiSat2 (v 2.1.0; (Kim et al. 2015)) or Bowtie2 (V 2.3.2; (Langmead et al. 2012)), respectively. FeatureCounts (v 1.5.3; (Liao et al. 2014)) was used for summarizing gene-mapped reads. Ensembl (GRCh38.89; (Yates et al. 2016)) or miRBase (v

21; (Kozomara et al. 2014)) was used for annotations. Differential gene expression (DE) was determined by the R package edgeR (v 3.18.1; (Robinson et al. 2010)) using TMM normalization.

2.2.7 Database research

For mRNA expression analysis and gene correlation studies of glioblastoma tumor samples, publicly available datasets of *R2: Genomic Analysis and Visualization Platform* (<https://hgserver1.amc.nl/cgi-bin/r2/main.cgi>) were used. Analyzed datasets were mentioned within figures legends and the text.

For the prediction of putative miRNA binding sites within CD44 3'UTR, TargetScan (http://www.targetscan.org/vert_72/) was used. For detection of alternative spliced forms of MSI1, ASPedia (ASpedia 2017) and VastDB (Tapial et al. 2017) databases were used.

2.2.8 Statistics

Unless otherwise stated, all experiments were performed at least three times. Error bars indicate standard deviation. To analyze the data, GraphPad Prism software (v 7.0) was used. Statistical significance was determined by Mann-Whitney-test or Student's t-test, as indicated. To define statistical significance, p-values were indicated with asterisks in the respective diagrams as follows: (*) $P \leq 0.05$, (**) $P \leq 0.01$ and (***) $P \leq 0.001$.

3 Results

3.1 Expression of MSI1

3.1.1 MSI1 is highly expressed during early brain development

MSI1 is evolutionary conserved across several species (Kaneko et al. 2000). Initially, it was identified in *Drosophila melanogaster*, where MSI1 plays a critical role in the asymmetrical division of stem cells for the proper external sensory organ development (Nakamura et al. 1994). Later on, MSI1 was described as translational repressor of its targets to support a sustained cell proliferation, which is necessary during an organism's development (Imai et al. 2001). During the progression of murine development, overall Msi1 expression declines and remains expressed only in tissues enriched with stem cells, e.g. dentate gyrus of the hippocampus or within the olfactory bulb (Sakakibara et al. 1996). This expression pattern is also observed for human MSI1 during fetal brain development by RNA sequencing data of hippocampus-derived tissues (Figure 6) (BrainSpan database, (Miller et al. 2014)). The highest MSI1 mRNA level was found at 9 post-conception weeks (pcw) and steadily declined to the age of 4 months (mos). At the age of 2 years (yrs), only a minor MSI1 mRNA expression was detectable, which persisted for the rest of the organism's life. The tight control of MSI1 expression suggests a distinct function during early brain development. Another protein with a similar expression pattern is IGF2BP1, which is also reported to serve in embryogenesis (Bell et al. 2013). In comparison, the mRNA level of the MSI1 homologue MSI2 was lower and it shows continuous expression in analyzed timepoints, suggesting a different role in the nervous system.

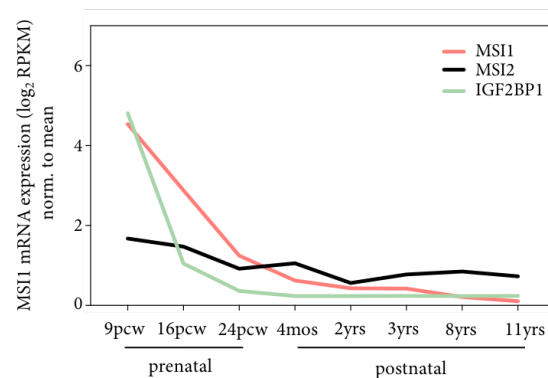


Figure 6. Expression of MSI1, MSI2 and IGF2BP1 across human fetal hippocampus development. MSI1, MSI2 and IGF2BP1 expression across eight stages of the human hippocampus development, ranging from nine pcw up to eleven yrs, as profiled by RNA-sequencing (data from the BrainSpan database). For each gene, RPKM (reads per kilobase per million mapped reads) values were normalized to the fold changes by dividing the expression value by the mean expression value across developmental stages.

3.1.2 MSI1 is highly expressed in high-grade glioma

Interestingly, MSI1 is reported to be re-expressed in several cancers (Kudinov et al. 2017) indicating it as an oncofetal RBP. Re-evaluation of the expression profile of MSI1 in RNA sequencing data from The Cancer Genome Atlas (TCGA) (Cancer Genome Atlas Research et al. 2013) across various types of tumors showed highest amounts of MSI1 expression in GBM (Figure 7A). MSI1 expression was also comparably high in ovarian and prostate cancer, whereas the lowest expression of MSI1 was detected in acute myeloid leukemia (AML). Noteworthy, in AML a high MSI2 expression was reported (Kharas et al. 2010).

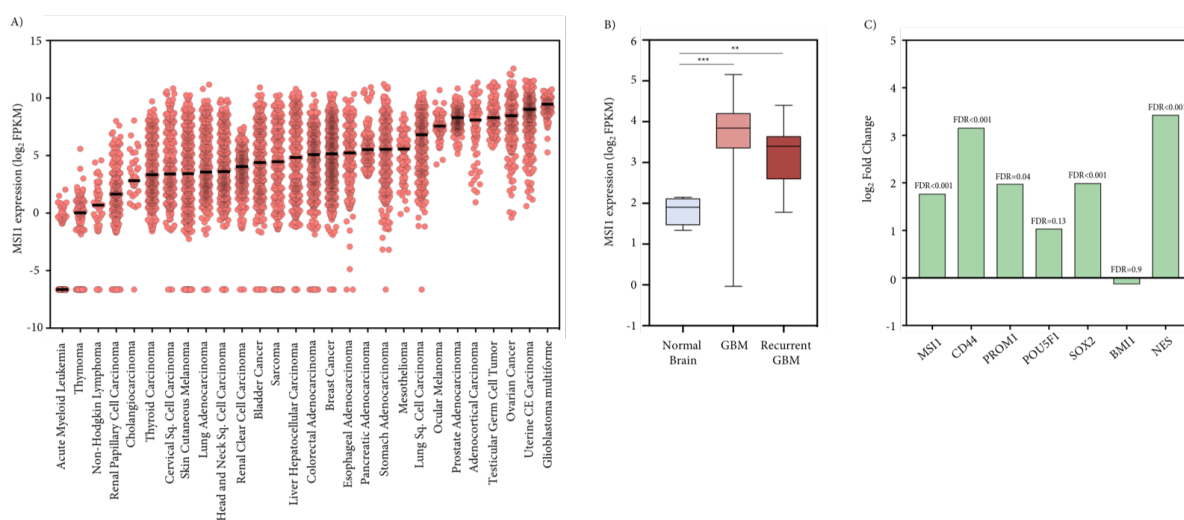


Figure 7. MSI1 expression in TCGA cancer cohorts. A) MSI1 mRNA expression in different cancer types, provided by TCGA. B) MSI1 mRNA expression in primary GBM and paired recurrence samples, compared to normal brain tissue. C) Log₂ fold changes of cancer stem cell marker expression in the TCGA GBM cohort compared to normal brain tissue. FDR (false discovery rate) is shown. Statistical significance was determined by Mann-Whitney test (B) (***, $P \leq 0.001$; **, $P \leq 0.01$).

A hallmark of GBM malignancy is tumor recurrence (Adamson et al. 2009). Analysis of RNA sequencing data further revealed that MSI1 expression is significantly higher in GBM and paired recurrence samples, compared to normal brain tissue (Figure 7B). This suggested not only an important role in GBM, but especially a function in terms of recurrence, probably by maintaining the self-renewal potential of GBM stem cells. Besides MSI1 as a CSC marker, other well-known CSC markers, including CD44, CD133 (gene name *PROM1*), Oct-4 (gene name *POU5F1*), SOX2, BMI1 and NES were found to be upregulated in the GBM TCGA cohort compared to normal brain (Figure 7C) (Hemmati et al. 2003; Dahlrot et al. 2013; Cancer Genome Atlas Research et al. 2013). These genes represent: a cell surface marker (CD44), a transcription factor (SOX2), an intermediate filament (Nestin, NES) and an RNA-

binding protein (MSI1). The finding underlines the undifferentiated, stemness-like state of GBM as it is additionally reported for other cancers, e.g. breast or ovarian-derived malignancies (Miranda et al. 2019).

Pediatric GBM (term includes children and young adults up to the age of 18 years) are clinically and biologically distinct from adult GBM and show similar poor prognosis (Jones et al. 2012). Although MSI1 re-expression in cancer was identified in several studies, MSI1 expression in pediatric GBM was not investigated so far. Thus, MSI1 expression was analyzed on protein level via immunohistochemistry (IHC) and on RNA level via RNA sequencing of a pediatric brain tumor samples published by Jones et al. (Figure 8) (Potschke et al. 2020; Jones et al. 2015).

MSI1 IHC was performed on diffuse astrocytoma (WHO II), anaplastic astrocytoma (WHO III) and GBM (WHO IV), while fetal brain served as control tissue (Figure 8A-D). A moderate MSI1 expression was observed in foci of cerebellar origin of the fetal brain sample, as this represents proliferative tissue. Predominant MSI1 negative cells are granule cells (blue). Proliferating glia cells (i.e. *Bergmann gliosis*), as well as Purkinje cells showed MSI1 positive staining. Although diffuse and anaplastic astrocytoma revealed MSI1 expression, it was markedly enhanced in the GBM sample. To confirm the IHC findings, showing an increase of MSI1 expression with increasing WHO tumor grades, MSI1 mRNA levels were examined via analysis of RNA-sequencing data by (Jones et al. 2015) (Figure 8E). The tumor cohort comprised 64 pediatric (1-16 years of age) brain tumors: 19 WHO grade I tumors (one papillary glioneuronal, 15 Pilocytic astrocytoma, three Choroid plexus papilloma), nine WHO grade II tumors (three Diffuse astrocytoma, six Ependymoma), nine WHO grade III tumors (two Anaplastic astrocytoma, seven Ependymoma), 19 WHO grade IV tumors (five GBM, nine Medulloblastoma, five Atypical rhabdoid), and eight fetal brain controls. Additionally, eight adult brain controls were included in the analysis. Interestingly, fetal brain controls showed a higher MSI1 expression than the adult brain tumor controls. MSI1 was least expressed in WHO grade I and was not substantially enhanced to WHO grades II and III. In comparison, WHO grade IV showed a significantly higher MSI1 expression compared to WHO grade I.

Conclusively, MSI1 expression was enhanced with increasing severity of pediatric brain tumors and showed the highest expression in GBM on RNA as well as protein expression.

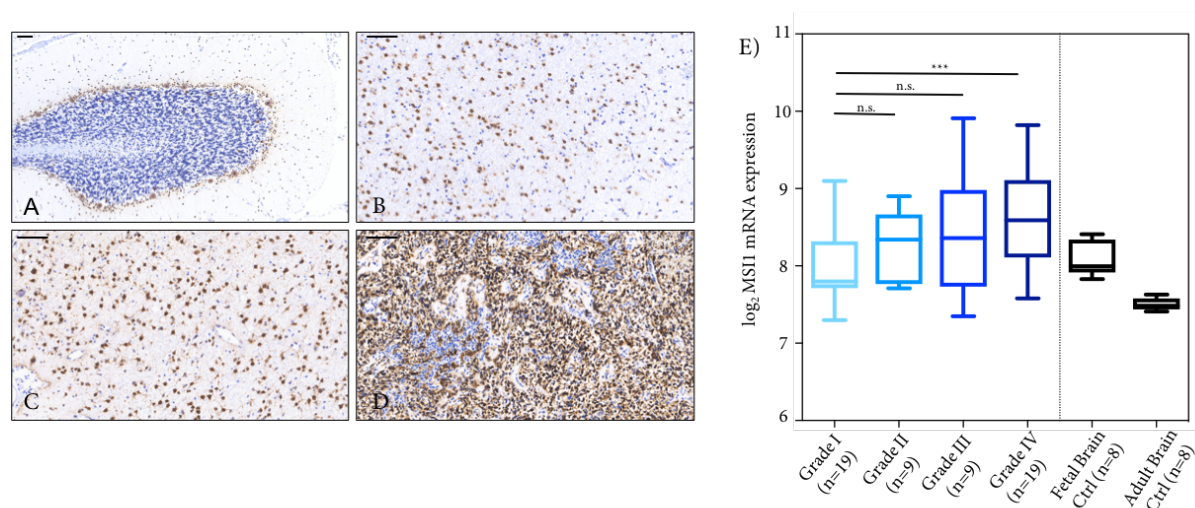


Figure 8. MSI1 expression in pediatric GBM. A-D) MSI1 expression in fetal brain control (A), diffuse astrocytoma (WHO II) (B), anaplastic astrocytoma (WHO III) (C) and GBM (WHO IV) (D) was analyzed via IHC. Scale bar, 100 μ m. E) MSI1 mRNA expression was analyzed in glioma samples of different WHO grades (I-IV), fetal and adult brain tissues (Jones et al. 2015). Statistical significance was determined by Mann-Whitney test (***) $P \leq 0.001$.

3.1.3 MSI1 expression in GBM cell lines

GBM-derived cell lines KNS42, SF188, LN18, T98G, U87MG, U251MG (USA), U251MG (Halle) and U343MG were tested for MSI1 expression, to identify a suitable model for *in vitro* studies on MSI1 function (Figure 9). Additionally, H293T (embryonic kidney) and MCF7 (breast cancer) cells were analyzed as non-GBM with known high and low MSI1 expression, respectively. While KNS42 and SF188 cell lines derived from pediatric GBM, LN18, T98G, U87MG, U251MG and U343MG originated from adult GBM. MSI1 expression of cell lines was investigated on protein level by Western blotting. MSI1 expression was detected in KNS42, U251MG and U343MG cells, which was comparable to H293T cells.

Further, Glial fibrillary acid protein (GFAP) protein expression was analyzed as it is claimed to be an astrocyte differentiation marker (Gomes et al. 1999) as well as a serum diagnostic marker for GBM (Jung et al. 2007). It was found to be expressed in KNS42 and U343MG. Further experiments were performed with MSI1-positive cell line KNS42.

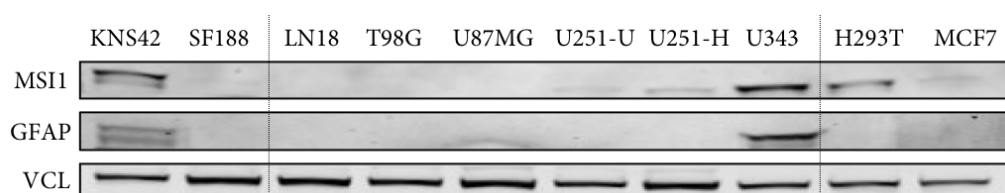


Figure 9. MSI1 expression in GBM-derived cell lines and non-GBM-derived cell lines. Representative Western blot analysis of MSI1 and GFAP protein expression in indicated cell lines. VCL served as loading control.

3.2 MSI1 affects cancer cell phenotypes

Cancer cells differ from normal cells in their genotype, consequently resulting in an altered phenotype, represented by the hallmarks of cancer (Hanahan et al. 2011). Cancer cells show sustained cell proliferation and often are insensitive to anti-growth- as well as apoptotic cell death signals, including resistance to anoikis, a form of programmed cell death (Yang et al. 2013). Due to a frequently gained anchorage-independent cell growth, cancer cells can detach from the surrounding extracellular matrix (ECM), thus facilitating invasion into the surrounding tissue. This process demands the gain of abilities to affect adhesion and migration (Friedl et al. 2011).

To decipher MSI1's oncogenic capacity, its impact on cell proliferation, apoptosis, anoikis resistance, migration and morphology changes were investigated in GBM-derived KNS42 cells, via siRNA-mediated MSI1 knockdown (KD) and CRISPR/Cas9-mediated Knockout (KO) (Figure 10).



Figure 10. MSI1 depletion (A) and knockout (B) in KNS42 cells. Representative Western blot analysis of MSI1 protein expression upon MSI1 KD (siMSI1) with respective control (siC) (A) and KO (sgMSI1) clones with respective parental and control (Cas9 only-transfected) cell populations (B). VCL served as loading control.

First, the impact of MSI1 on cell proliferation was investigated. Therefore, three MSI1 KO cell clones and two controls (one wildtype cell population and one Cas9 only-transfected clone (control) were used (Figure 11A). The number of living cells was determined via flow cytometry after two, four, six and eight days, indicating a significant reduction of growth rate for the three MSI1 KO clones, compared to wildtype and control. The reduced cell growth after MSI1 KO suggested a modulating function of MSI1 on cell proliferation. To verify this effect on physiological conditions in a three-dimensional condition, spheroid growth analyses were performed (Figure 11B). Cells were embedded in round-bottom plates to form spheroids and were analyzed after 4 days. Cell growth was determined by measuring differences in cell viability (based on ATP consumption) and altered spheroid size. Cell viability, as well as spheroid size were significantly reduced for all three MSI1 KO clones.

To evaluate a pro-proliferative role of MSI1 *in vivo*, the growth effect was investigated in an orthotopic mouse experiment (Figure 11C). KNS42 control and MSI1 KO (sgMSI1#5) cells (n = 4 per condition) injected orthotopically into the brain. After the experiment lasted three months the trial was terminated via mice execution, since neither control mice, nor sgMSI1 mice showed significant effects on survival. The histological analysis of the respective mice brains revealed, that only one control mouse developed a tumor, but none of the sgMSI1 mice showed tumor development. Although an *in vivo* experiment did not yield a significant outcome, a pro-oncogenic potential could be suggested for MSI1 from the *in vitro* data.

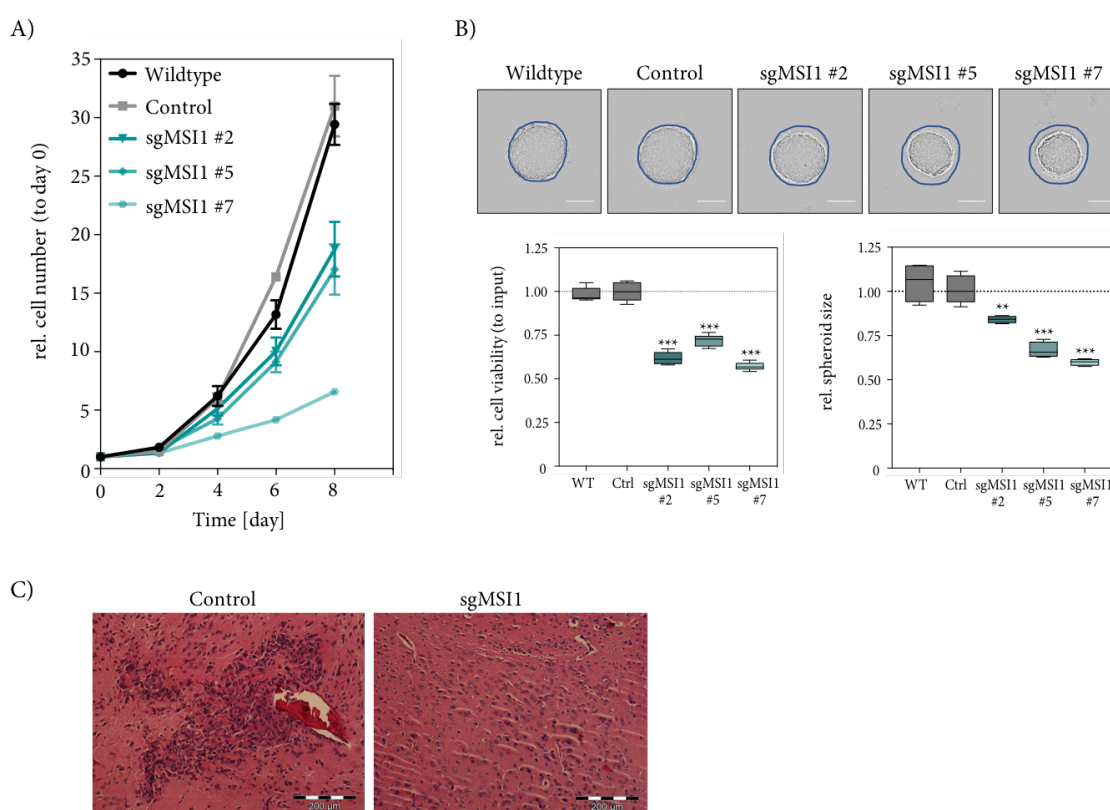


Figure 11. Impact of MSI1-knockout on KNS42 cell proliferation and spheroid viability. A) The quantification of relative cell numbers at indicated time points is shown for parental and control (Cas9-transfected only) cells, as well as for three different MSI1 KO (sgMSI1#2, #5, #7) clones. B) Relative cell viability of KNS42-derived spheroids (n=12 per condition), 72 h after seeding. Upper panel, representative images of spheroids; scale bar, 150 μm. Box plots (lower panels) show spheroid viability normalized to the median viability of control cells (set to one), determined with CellTiter-Glo®. C) Hematoxylin-eosin staining of mouse brain tissue at injection site. Mice were injected with KNS42 control cells or KNS42 MSI1 KO cells (sgMSI1#5; n=4 per condition). Scale bar, 200 μm. Statistical significance was determined from at least three independent experiments by Student's t-test (***P ≤ 0.001; **P ≤ 0.01).

To further test if MSI1 affects clonogenicity, a colony formation assay was performed (Figure 12A). This assay relies on the observation of the ability of single cells to grow into a colony

after a treatment (in this study, the treatment is the MSI1 KO) (Franken et al. 2006). KNS42 control cells were able to form approximately 600 colonies with an average size of $64 \mu\text{m}^2$. Comparatively to that finding, KNS42 MSI1 KO cells revealed a significant reduction of colony count and average colony area.

The number of cells within an organism is tightly controlled by the rate of cell division, as well as controlled cell death. This programmed cell death is mediated by intracellular proteolytic cascades via caspases. Tumor cells are able to evade apoptosis, thereby they divide and grow uncontrollably (Kaufmann et al. 2008; Hanahan et al. 2011). Thus, it was tested if MSI1 mediates apoptosis via the measurement of caspase 3/7 activity as well as detection of PARP-cleavage, a downstream event of caspase3/7 activity (Figure 12B). After MSI1 KD, cells revealed an increase of PARP-cleavage via Western blot analysis, which was associated with an increase of caspase 3/7 activity, compared to control KD.

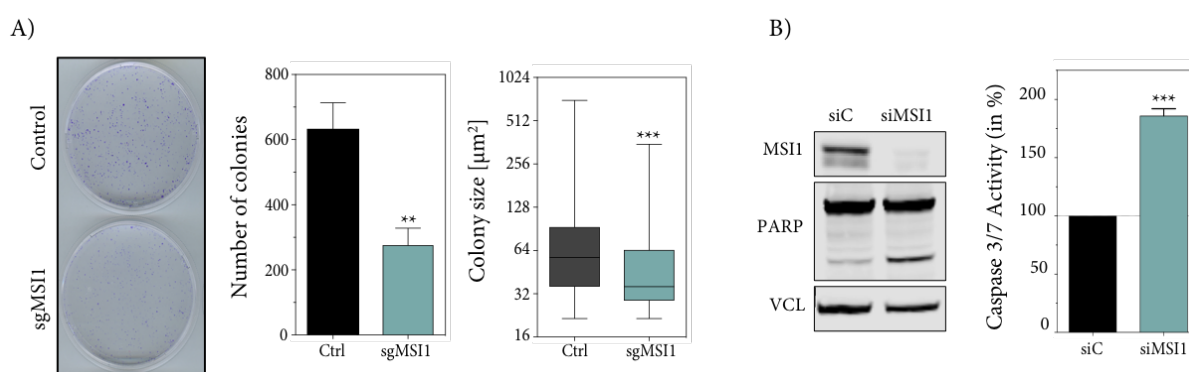


Figure 12. MSI1-knockout and knockdown affect clonogenicity and apoptosis of KNS42 cells. A) Colony formation assay with KNS42 control (Cas9-transfected only) cells and MSI1 KO (sgMSI1#5) cells. Left panel: Representative image of stained colonies in a cell culture vessel. Middle panel: Quantification of colonies for the indicated condition. Right panel: Quantification of colony size for the indicated condition. B) Representative Western blot analysis of MSI1 expression and PARP-cleavage upon MSI1 KD (siMSI1) with respective control (siC) (left panel) and the respective Caspase 3/7 activity (right panel). Statistical significance was determined from at least three independent experiments by Mann-Whitney test (A) and Student's t-test (B) (** $P \leq 0.001$; ** $P \leq 0.01$).

As MSI1 represents a marker for CSCs, it is likely that it contributes to anchorage-independent growth and anoikis resistance, a programmed cell death induced upon cell detachment from ECM or neighboring cells (Yang et al. 2013). Subsequently, this was tested in MSI1 KO cells via two different approaches.

First, clonogenicity in combination with anchorage-independent growth was investigated with the soft agar colony formation assay (Figure 13A), as described by (Borowicz et al. 2014). Control and MSI1 KO (sgMSI1#5) cells were embedded into an agar-suspension and cell

viability of formed cell colonies was tested via methylthiazolyldiphenyl-tetrazoliumbromid (MTT)-staining after 14 days. The control cells were able to grow twice as many colonies compared to MSI1 KO cells. In addition, colony size was significantly higher for control cells compared to MSI1 KO cells.

Second, it was tested if MSI1 is involved in resistance to anoikis (Figure 13B). KNS42 control cells were able to grow in spheroids on an ultra-low adhesion plate in low-serum growth media after seven days. KNS42 MSI1 KO (sgMSI1#5) cells revealed a reduced cell viability, compared to KNS42 control cells, suggesting a role for MSI1 in promoting anchorage-independent growth and anoikis resistance and concomitantly cancer stemness.

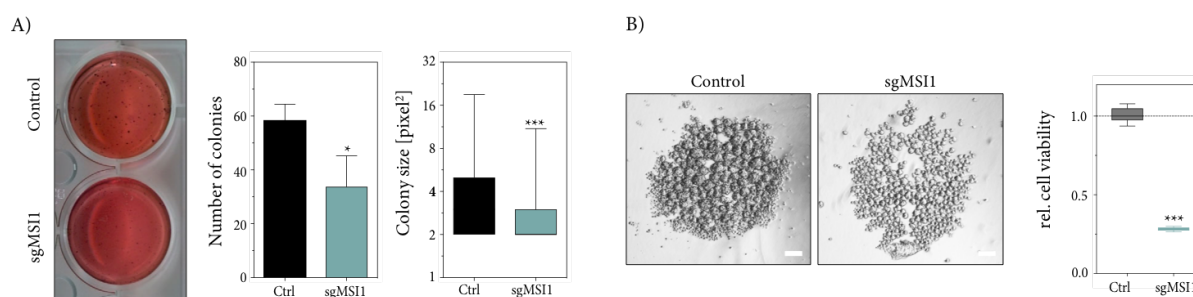


Figure 13: Impact of MSI1-knockout on anchorage-independent growth and anoikis resistance of KNS42 cells. A) Soft agar-assay with KNS42 control (Cas9-transfected only) cells and MSI1 KO (sgMSI1#5) cells. Left panel: Representative image of stained colonies in a cell culture vessel. Middle panel: Quantification of colonies for the indicated condition. Right panel: Quantification of colony size for the indicated condition. B) Anoikis-resistance of KNS42 control and MSI1 KO cells (sgMSI1#5). Left panel: Representative images of cell aggregates; scale bar, 150 μm. Right panel: Quantification of cell viability was determined with CellTiter-Glo®. Statistical significance was determined from at least three independent experiments by Mann-Whitney test (A) and Student's t-test (B) (** $P \leq 0.001$; * $P \leq 0.05$).

Patients with GBM suffer from recurrence due to the infiltrative nature of tumor growth. Thus, some cells are able to invade into the adjacent brain tissue and migrate away from the tumor bulk (Di et al. 2010). In this context, it was of interest, if MSI1 mediates cell adhesion and migration. As KNS42 show no migratory behavior, they did not represent a suitable model for migration and invasion experiments. Therefore, U251MG cells were used for this approach. In a single-cell migration analysis, U251MG control cells showed a significantly increased mean migration speed and covered a longer distance compared to U251MG MSI1 KD cells (Figure 14).

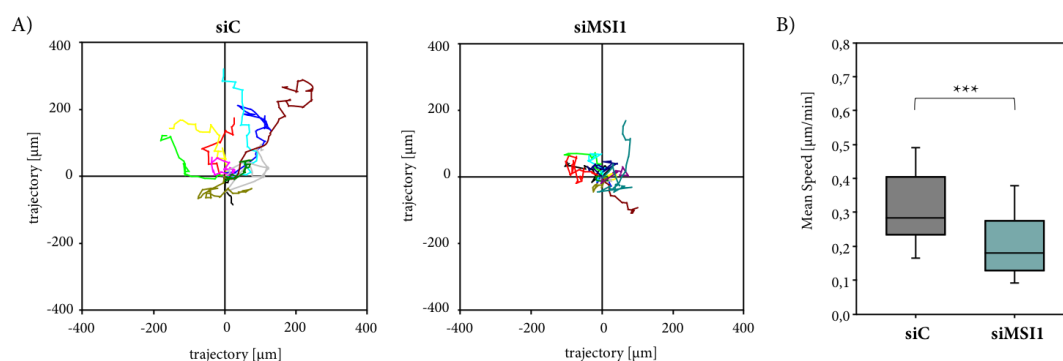


Figure 14. MSI1 affects single cell migration speed. A) Representative cell tracks for 10 cells are shown for control (siC) (left panel) and MSI1 KD (siMSI1) cells (right panel). B) The mean speed of cells was determined by the manual tracking plugin for ImageJ in three independent analyses ($n > 40$ cells per condition). Statistical significance was determined by Mann-Whitney test (***, $P \leq 0.001$).

Further experiments revealed significant morphological changes and a significant increase in 2D-cell area upon MSI1 KD in U251MG cells, compared to respective control cells (Figure 15A). Although 2D-cell area did not increase, changes in morphology could also be observed for KNS42 cells (Figure 15B). Upon MSI1 KD, cell morphology changed from a predominant diamond- to spindle-shape. In addition, MSI1 KD cells increasingly formed neurite-like extensions. The quantification revealed a threefold higher outgrowth-length, compared to control cells. Furthermore, the number of branch points was increased by twofold.

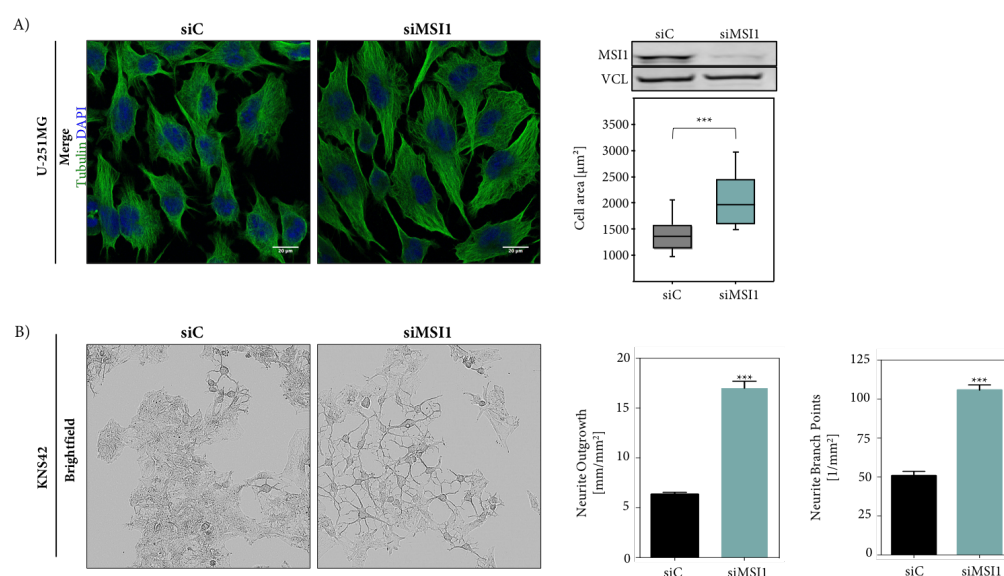


Figure 15. Effect of MSI1 on cell morphology. A) Left panel: Representative immunofluorescence images of U251MG control (siC) and MSI1 KD (siMSI1) cells. Scale bar, 20 μm. Upper right panel: Representative Western blot analysis upon MSI1 protein expression upon indicated KD. VCL served as loading control. Lower right panel: The quantification of cell area of transfected cells ($n=25$) is shown as box plots. B) Left panel: Representative brightfield image of KNS42 control and MSI1 KD cells. Right panel: Quantification of neurite outgrowth and branch points. Statistical significance was determined from at least three independent experiments by Student's t-test (A) and Mann-Whitney test (B) (***, $P \leq 0.001$).

3.3 MSI1 conveys oncogenic potential in GBM-derived cells

Due to the observed impact on cancer cell phenotypes in the here presented study, it is suggested that MSI1 functions in maintaining stemness in GBM, as previously reported for neural stem cells (Okano et al. 2005). To validate the findings from the GBM TCGA cohort, the investigation of GBM-CSC marker mRNA in respect of MSI1 expression was further analyzed in an independent cohort, provided by the Neuropathology Department Magdeburg. The here analyzed set of GBMs comprised CD44, SOX2 and NES, as those were initially identified to be co-upregulated together with MSI1 in the GBM cohort provided by TCGA (see Figure 7C). The cohort included 15 GBM and 13 LGG samples (Figure 16A). The analysis revealed a significant increase of mRNA expression of MSI1, CD44, SOX2 and NES in GBM compared to LGG. This finding supported the initial observation from the GBM TCGA cohort.

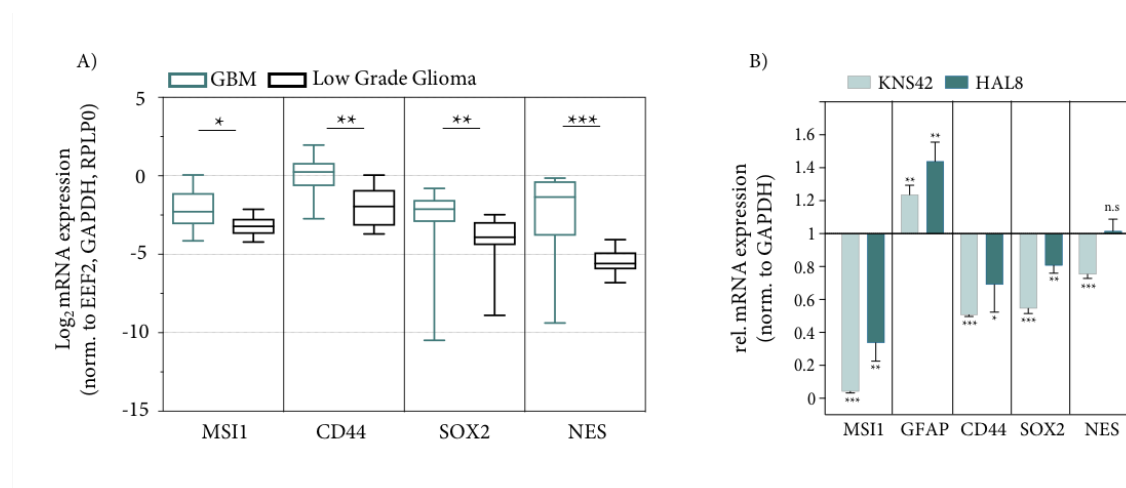


Figure 16. Stem cell marker expression is upregulated in GBM. A) Log₂ mRNA expression of cancer stem cell marker expression in GBM compared to LGG. B) mRNA expression of cancer stem cell marker and GFAP expression upon siRNA-mediated MSI1 KD in KNS42 cells and HAL8 GBM-CSC. Statistical significance was determined by Mann-Whitney test (A) or from three independent experiments by Student's t-test (B) (* $P \leq 0.05$, ** $P \leq 0.01$, *** $P \leq 0.001$).

If MSI1 is linked to the expression of the co-upregulated markers was further analyzed by MSI1 depletion in KNS42 cells (Figure 16B). Interestingly, CD44, SOX2 and NES mRNAs were significantly downregulated upon MSI1 depletion. GFAP mRNA expression, as astrocytic differentiation marker, was significantly increased, suggesting a differentiation-like phenotype. To confirm the findings from KNS42 cells, a MSI1 KD was performed in isolated CSCs (HAL8) from a primary GBM tissue. Intriguingly, the depletion revealed effects on the expression of indicated mRNAs, comparable to those from KNS42. GFAP expression was

significantly increased. In contrast, GBM-CSC markers, with the exception of NES, were downregulated. The changed expression pattern could indicate a differentiation-like process similar to KNS42 cells. Nonetheless, the observations in primary CSCs confirmed a critical role of MSI1 in GBM and further support an idea of MSI1 regulating stem cell marker expression.

MSI1 was initially identified as a translational repressor or activator of its target mRNAs (Imai et al. 2001; Battelli et al. 2006; Charlesworth et al. 2006). In addition to this function, previous studies described a post-transcriptional regulatory function for MSI1 via stabilizing its mRNA target (Cambuli et al. 2015) or revealed MSI1-associated changes in alternative splicing (Katz et al. 2014). In the here presented study, the mRNA co-upregulation of CSC-markers in GBM was observed, suggesting a potential post-transcriptional stabilizing role of MSI1 to increase cancer stemness. mRNA-sequencing of KNS42 samples upon MSI1 KD was performed to determine differentially expressed genes (DEGs; Figure 17A). In total, the analysis revealed 2779 significantly DEGs (threshold FDR < 0.01). Amongst, 1267 genes were up- and 1512 downregulated. A GO-analysis (gene ontology, biological process) indicated an enrichment of genes being involved in cell cycle progression, DNA replication, microtubule cytoskeleton and synthesis of DNA for downregulated transcripts (Figure 17B). Upregulated transcripts tend to code for proteins being involved in positive regulation of cell communication, negative regulation of cell proliferation, positive regulation of apoptotic signaling pathway and positive regulation of cell differentiation. The enrichment of DEGs of these biological processes support the identified phenotypic changes upon MSI1 KD in KNS42 cells (see 3.2.).

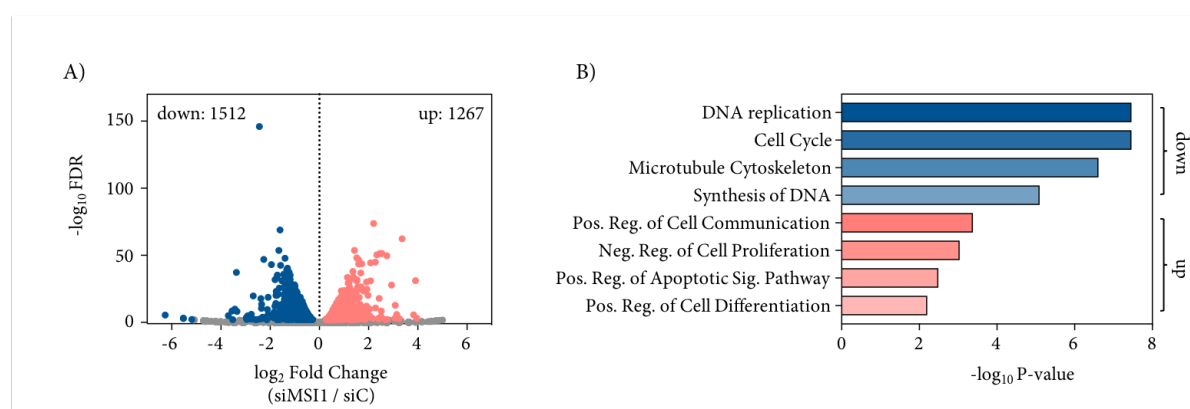


Figure 17. Analysis of RNA-Sequencing of MSI1 KD in KNS42. A) Volcano plot of \log_2 mRNA fold changes plotted against the $-\log_{10}$ FDR for MSI1 KD (siMSI1) versus control (siC) in KNS42 cells. The horizontal dashed line indicates the threshold (FDR \leq 0.01) for identification of significantly altered gene expression (orange dots represent upregulated, blue dots represent downregulated genes). B) Enrichment levels (P-values) for GO-term enrichment analyses (gene ontology, biological process) significantly enriched (P \leq 0.01) in upregulated and downregulated genes upon MSI1 KD (orange represents GO terms with the lowest P-values of upregulated, blue represents enrichment of downregulated genes).

To further identify novel downstream targets being post-transcriptionally regulated by MSI1-binding, MSI1 iCLIP data from a study in U251MG cells was included in the analysis (Figure 18A) (Uren et al. 2015). Regarding mRNA *cis*-element preferences, MSI1-binding was predominantly observed within 3'UTRs, whereas the majority of targeted transcripts were amongst downregulated DEGs. This implied that MSI1 could post-transcriptionally enhance mRNA stability in GBM cells by binding to respective 3'UTRs.

For identification of potentially stabilized transcripts by MSI1 post-transcription, genes had to fit following three criteria (Figure 18B): 1) significantly upregulated expression in the TCGA GBM cohort (GBM upregulated); 2) significant downregulation upon MSI1 depletion in KNS42 (MSI1 KD); 3) identified MSI1-CLIP site in all three replicates within the 3'UTR (iCLIP 3'UTR). This analysis identified following eight genes fulfilling all three criteria: MKI67 (marker for proliferation), MSN (localized in filopodia, important for cell-cell recognition and cell migration), TNPO1 (interacts with NLS to target nuclear proteins to the nucleus), GNA12 (G protein involved in transmembrane signaling systems), RBBP4 (Histone binding protein), LIMD1 (scaffold protein, assembly of protein complexes), TGFBR1 (Transforming growth factor beta receptor I) and CD44 (cell surface protein involved in cell-cell interaction and proliferation as stem cell marker). Amongst identified target transcripts CD44, a well-studied stem cell marker, was further analyzed in this study.

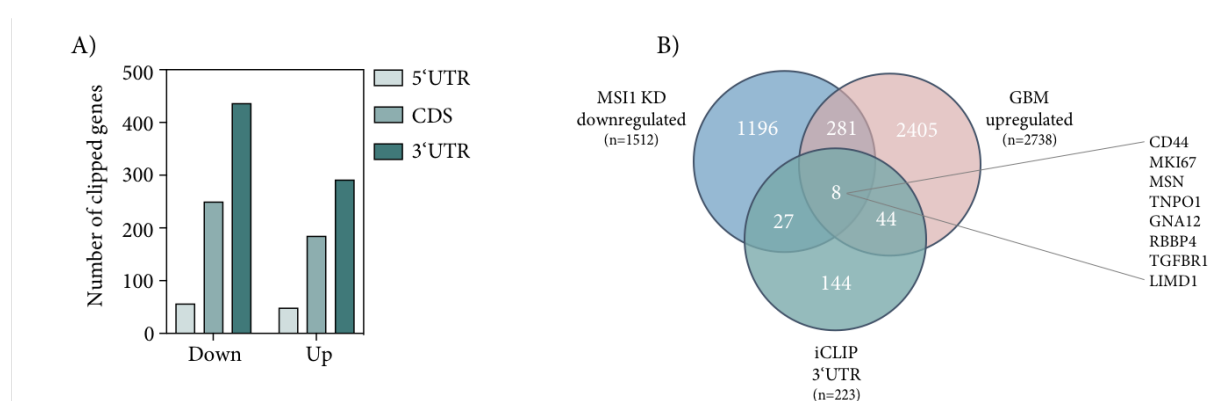


Figure 18. Identification of potentially stabilized MSI1 downstream target mRNAs in GBM. A) Number of clipped mRNA *cis*-elements (5'UTR, coding sequence (CDS), 3'UTR) of down- and upregulated transcripts in U251MG cells upon MSI1 KD in KNS42 cells. B) Venn diagram, depicting the numbers of transcripts: 1) significantly upregulated in the TCGA GBM cohort (GBM upregulated); 2) significantly downregulated in MSI1 KD in KNS42 cells (MSI1 KD downregulated); 3) identified MSI1-CLIP site within the 3'UTR (iCLIP3'UTR) in three replicates.

3.4 MSI1 regulates CD44 expression in a 3'UTR-dependent manner

As demonstrated in the previous chapters, MSI1 and CD44 mRNAs are upregulated in GBM. Interestingly, CD44 expression was found to be downregulated upon MSI1 KD in KNS42 (GBM-derived cell line) and in HAL8 (GBM-CSC) cells. An iCLIP analysis revealed that MSI1 binds the CD44 3'UTR. Thus, it was of interest if the RBP MSI1 directly regulates CD44 expression and if so, how this regulation is mediated.

Reduction of CD44 expression upon MSI1 KD, as well as in three different KO clones was confirmed on protein level by Western blot analysis (Figure 19A). Furthermore, CD44-positive cells within the MSI1 KD-population were significantly reduced, as confirmed via flow cytometry analysis (Fig. 19B).

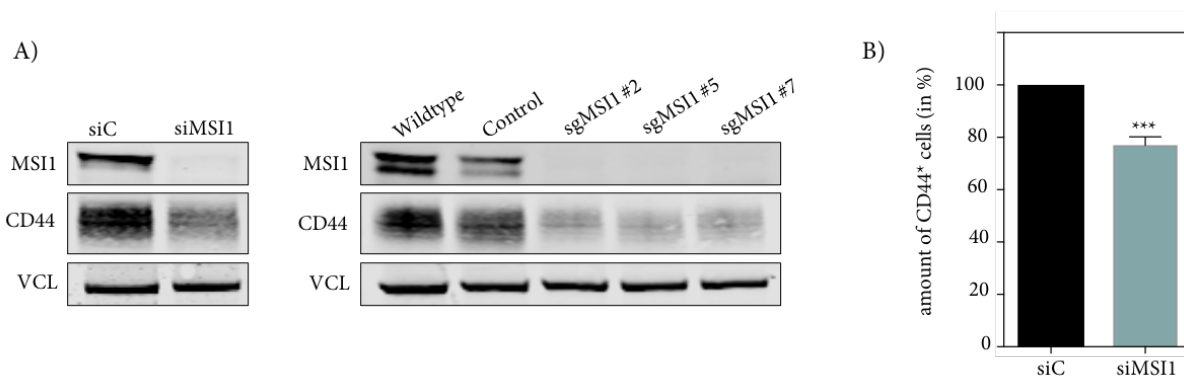


Figure 19. CD44 Expression upon MSI1 KD or KO. A) Representative Western blot analysis of MSI1 and CD44 detection of siRNA depleted (left panel) and MSI1 knockout KNS42 cells (right panel). VCL served as loading control. B) Flow cytometry analysis of CD44-positive cells (n= 10,000 cells per condition) in MSI1 KD cells. Statistical significance from at least three independent experiments was determined by Student's *t*-test (***P* ≤ 0.001).

As the iCLIP experiments were performed in U251MG cells, it was necessary to confirm the finding on binding information in KNS42 cells. An association of MSI1 with the CD44 mRNA was validated via RNA-immunoprecipitation (RIP) (Figure 20A). Compared to control (GFP) or cells expressing an RNA-binding deficient MSI1 mutant (GFP-MSI1mut, three mutated AA within RRM1: AA 63F->L, AA 65F->L, AA 68F->L, (Imai et al. 2001)), PABP protein and NUMB mRNA (positive controls) were enriched for wild type GFP-MSI1, as previously reported. In contrast to the GAPDH mRNA (negative control), selective association with GFP-MSI1 was also determined for the CD44 mRNA. This suggested the CD44 mRNA as a novel target of MSI1.

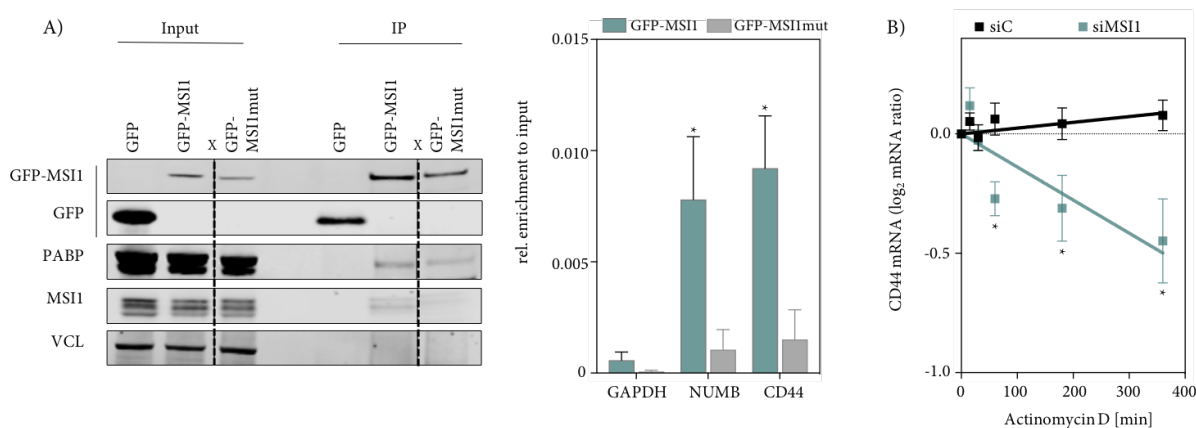


Figure 20. Regulation of CD44 expression via MSI1. A) RNA-immunoprecipitation of GFP, GFP-MSI1 and GFP-MSI1mut overexpressed in KNS42 cells. Left panel: Representative Western blot analysis of indicated proteins. PABP served as positive control and VCL as loading/negative control. Lane ‘X’ was excluded and explained in detail in chapter 6. Right panel: qRT-PCR analyses of mRNAs co-purified with GFP, GFP-MSI1 or GFP-MSI1mut by immunoprecipitation. The enrichment of indicated mRNAs was determined relative to their co-purification with GFP upon input normalization. GAPDH served as negative control. B) qRT-PCR analyses of CD44 mRNA decay in control (siC) and MSI1 KD (siMSI1) cells. RNA synthesis was inhibited by actinomycin D (ActD; 5 μ M) for indicated time. Transcript abundance was normalized to input levels. Statistical significance was determined from at least three independent experiments by Student’s t-test (* $P \leq 0.05$).

To examine if CD44 mRNA underlies stability control via MSI1, an RNA decay analysis with actinomycin D treatment was performed for up to 6 h (Figure 20B). Control cells did not show a CD44 mRNA decay within the respective time frame, as previously reported to be comparably high ($t_{1/2} > 14$ h; (Vikesaa et al. 2006)). Upon MSI1 KD CD44 mRNA showed a significantly increased decay rate already after 60 min. This finding indicated a stability control of CD44 mRNA by MSI1.

Two different experimental approaches were selected to further investigate the 3’UTR-dependency of the CD44 mRNA stability control via MSI1. First, the regulation was analyzed by monitoring the activity of a CD44 3’UTR-luciferase reporter, comprising the longest annotated 3’UTR, being expressed in KNS42. All potentially expressed alternatively polyadenylated 3’UTRs were identified to be expressed in KNS42 cells via RNA-sequencing (Figure 21A). The relative activity of the luciferase reporter was significantly enhanced by GFP-MSI1 overexpression, compared to GFP and GFP-MSI1mut (Figure 21B). Upon siRNA-mediated depletion of MSI1 (MSI1 KD) the relative reporter activity was significantly decreased, suggesting that MSI1 impairs the turnover of the CD44 mRNA in a 3’UTR-dependent manner (Figure 21C).

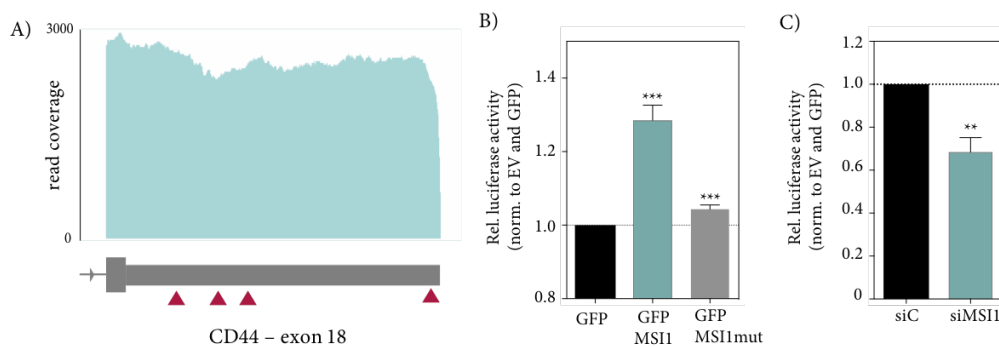


Figure 21. MSI1 regulates CD44 in a 3'UTR dependent manner. A) Read coverage of CD44 3'UTR (CD44 exon 18) in RNA-sequencing data from KNS42 cells. Alternative polyadenylation signals within the 3'UTR of CD44 are indicated by red triangles. B) Relative activity of the CD44-3'UTR luciferase reporter was determined in KNS42 cells expressing GFP, GFP-MSI1 or GFP-MSI1mut. A reporter comprising the vector-encoded 3'UTR (EV) served for normalization. C) Relative activity of the CD44-3'UTR luciferase reporter was determined in control (siC) and MSI1 KD (siMSI1) KNS42 cells. A reporter comprising the vector-encoded 3'UTR served for normalization. Statistical significance was determined from at least three independent experiments by Student's t-test (** $P \leq 0.01$, *** $P < 0.001$).

As second experimental approach, the CRISPR/Cas9-mediated deletion of the CD44 3'UTR was chosen, as previously described for the transcription factor SRF (Muller et al. 2019). This should lead to an abolished MSI1-dependency of CD44 expression. To achieve a maximum of deleted MSI1-binding sites, identified by iCLIP (see Figure 18), two sgRNAs were chosen leaving as little as 40 bp downstream of the stop codon and 100 bp upstream of the last annotated polyadenylation signal within the *CD44* gene upon Cas9-mediated cleavage (Figure 22A, B). Thus, translation of CD44 protein should still be feasible. To proof the successful partial deletion of the CD44 3'UTR, a genomic PCR was performed. Cell clones with the expected successful event of homozygous 3'UTR-deletion were identified with a genomic PCR-product of 500bp in length, according to the chosen set of primers (Figure 22B, C). Control cells were identified with a product of 1000bp, indicating the existence of both unaltered genetic CD44 alleles. Two clones with homozygous deletion of the 3'UTR were selected for the subsequent analyses. To investigate the MSI1-dependent enhancement of CD44 expression via its 3'UTR a MSI1 KD was done in control cells, as well as in both clones with deleted CD44 3'UTR (Figure 22D). In accordance with previous experiments from this study, control cells revealed a 50% decrease of CD44 mRNA and protein expression (Figure 22D, E). For both clones with deleted CD44 3'UTR an already significantly reduced protein and mRNA expression upon control transfection was observed, which likely is a consequence of clonal variability. Further, only a minor reduction of protein and mRNA was revealed upon MSI1 KD. These findings proved the MSI1-dependent stability control of CD44 mRNA via the 3'UTR.

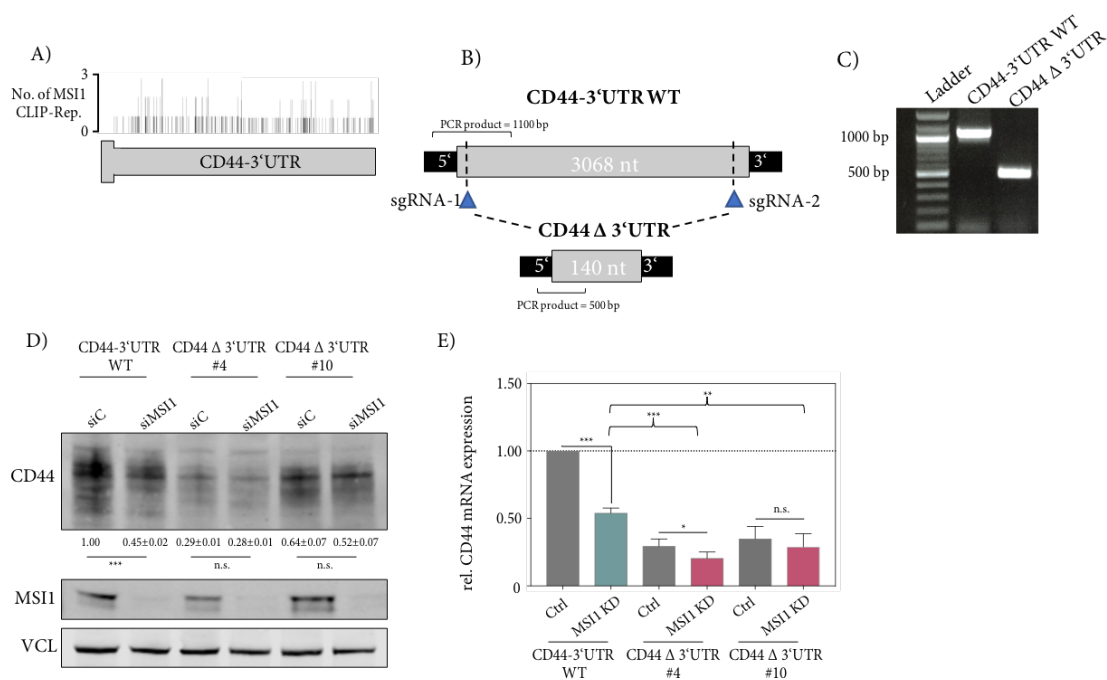


Figure 22. CD44 3'UTR-deletion in KNS42 cells. A) MSI1 binding sites within the CD44 3'UTR, identified by iCLIP with U251MG cells in three replicates. B) Schematic of the generation of CD44 3'UTR-deletion. sgRNA sites for specific cleavage are indicated. C) Representative genomic DNA analysis of control (Cas9-only transfected) and CD44 3'UTR-deleted KNS42 cells. Respective PCR product sizes as indicated in (B). D) Representative Western blot analysis of indicated proteins upon of MSI1 KD in CD44-3'UTR WT (Cas9-transfected only) and CD44 Δ 3'UTR (CD44 3'UTR-deleted; clones #4, #10) cells. E) Quantification of CD44 mRNA expression upon MSI1 KD in CD44-3'UTR WT (Cas9-transfected only) and CD44 Δ 3'UTR (CD44 3'UTR-deleted; clones #4, #10) cells. Statistical significance was determined from at least three independent experiments by Student's t-test (* $P \leq 0.05$, ** $P \leq 0.01$, *** $P \leq 0.001$).

The miRNA-dependency of CD44 expression is frequently reported in cancer cells (Chen et al. 2018). Thus, MSI1 could potentially interfere with RISC-function to prevent miRNA-mediated mRNA decay. Potential miRNA candidates, being involved in CD44 regulation, were predicted via the TargetScan database (Agarwal et al. 2015). Their respective expression was analyzed via miRNA-sequencing in KNS42 cells (Figure 23A). Only miRNA-27b-3p (two miRNA recognition elements (MREs)) and miRNA-143-3p revealed comparably high expression. Both are already reported to target the CD44 3'UTR (Takahashi et al. 2015; Pagliuca et al. 2013). The CD44 3'UTR targeting miRNA-199-3p showed low expression in KNS42 cells (Cheng et al. 2012). MiRNA activity was investigated via transfection of luciferase reporter constructs, comprising the complementary site of the respective miRNA sequence, in KNS42 cells (Figure 23B). The relative activity was significantly reduced for miRNA-27b-3p and miRNA-143-3p. The activity of the reporter, comprising the anti-sense sequence for miRNA-199-3p, was not significantly affected, as expected. Interestingly, predicted miRNA-27-3p and miRNA-143-3p MREs seemed to overlap with identified MSI1-binding sites (each

position clipped at least in two replicates) (Figure 23C). To investigate effects of MSI1 on these three CD44 3'UTR regions in a miRNA-dependent manner, a luciferase reporter assay was used (Figure 23D). For this purpose, parts of the CD44 3'UTR (ranging from 24 bp upstream to 24 bp downstream of the respective miRNA seed region) was cloned downstream of the firefly luciferase coding region. Upon transfection in control and MSI1 KO cells, the indicated reporter constructs revealed significantly reduced relative activity (Figure 23D). This suggested a potential role for MSI1 in impeding RISC association with the CD44 3'UTR. Recently, a RISC-directing function for MSI1 was shown in GBM-derived cells (Chen et al. 2020). But the here presented data suggested a contrary role, which was evidenced by the weak detectable signals for MSI1 protein enrichment upon AGO2 immunoprecipitation with KNS42 cell lysate (Figure 23E). This rather suggested a lack of MSI1 binding to transcripts being already targeted for miRNA-dependent decay, further indicating that MSI1 might interfere with a miRNA-dependent downregulation of CD44 by preventing miRNA/RISC-association with the 3'UTR.

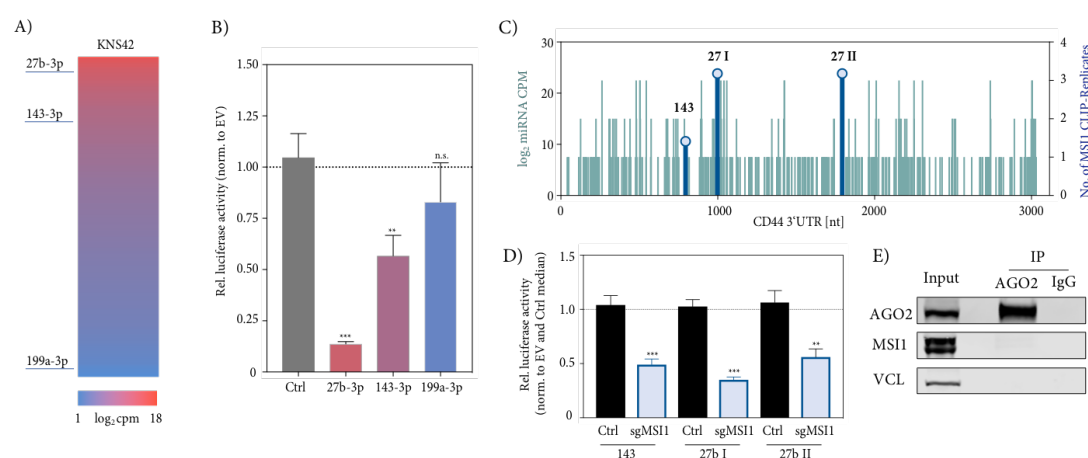


Figure 23. Effect of MSI1 in miRNA-dependent regulation of CD44 3'UTR. A) Heatmap indicating miRNA expression (log₂ counts per million, cpm) in KNS42 cells, analyzed via miRNA-sequencing. Two highly expressed miRNAs (27b-3p, 143-3p) and one low expressed miRNA (199a-3p), which were predicted to target the CD44 3'UTR by TargetScan, are indicated. B) Relative activity of the luciferase reporters, comprising the complementary sequence to the indicated miRNAs as 3'UTR, was determined in KNS42 cells. A reporter comprising the vector-encoded 3'UTR (empty vector, EV) served for normalization. C) The number of iCLIP-replicates (right axis, green) showing MSI1 binding at the indicated positions within the CD44 3'UTR, further indicating microRNA-recognition elements (MREs) and expression values (derived from KNS42 miRNA-sequencing) for indicated miRNAs. miRNA abundance (left y-axis, blue) is indicated as log₂ cpm. D) Relative activity of luciferase reporters, comprising predicted MREs for miR-143-3p and miR-27b-3p and 24 bp down- and upstream of the CD44 3'UTR, was determined in control and MSI1 KO cells. Note, that miRNA-seed regions overlap with identified MSI1-binding sites, identified by iCLIP analyses. E) Representative Western blot analysis of indicated proteins upon AGO2 immunoprecipitation (IP) in KNS42 cells. VCL served as negative control. Statistical significance from at least three independent experiments was determined by Student's *t*-test (***P* ≤ 0.01, ****P* ≤ 0.001).

3.5 Treatment with MSI1 inhibitor luteolin

As described in the here presented study, MSI1 expression increases GBM malignancy by post-transcriptionally promoting cancer hallmarks. Thus, targeting MSI1 by aiming at inhibition of its function or reduction of its expression may provide an effective therapy option. Decreasing the impact of MSI1 within the tumor could promote cell differentiation and thus, increase the sensitivity to radiochemotherapy (Auffinger et al. 2015). Unfortunately, at present no clinically evaluated direct therapeutic inhibitor of MSI1 is available. Recently, Luteolin displayed a strong inhibitory interaction with MSI1 in GBM-derived cells (Yi et al, 2017).

Thus, MSI1 inhibition experiments were performed with KNS42 cells and tested on identified phenotypes and the MSI1-dependent CD44 expression. In addition, the isolated GBM-CSCs HAL8 were used to confirm the findings in patient-derived cells. The determined EC_{50} (half maximal effective concentration) of Luteolin in KNS42 cells, 72 h after application, was 25 μ M (Figure 24A). To evaluate if the treatment affects CD44 expression, KNS42 cells were exposed to Luteolin at its determined EC_{50} concentration (Figure 24B).

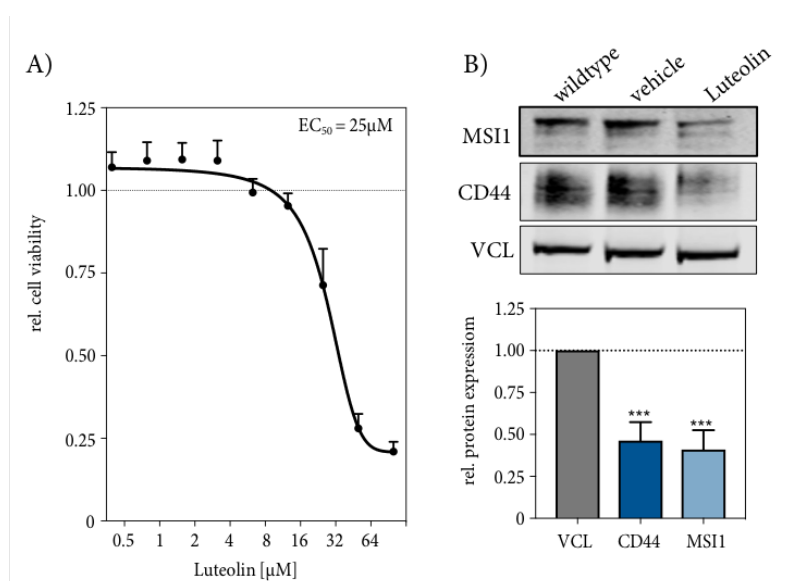


Figure 24. KNS42 treatment with MSI1 inhibitor Luteolin. A) Cell viability ratios (to DMSO) of KNS42 cells exposed to Luteolin at increasing concentrations for 72h. The response curve and respective EC_{50} are shown. B) Upper panel: Representative western blot analysis of MSI1 and CD44 after Luteolin treatment. VCL served as loading control. Lower panel: Quantification of protein expression. Statistical significance was determined from at least three independent experiments by Student's *t*-test (***) $P \leq 0.001$.

Besides an altered protein expression, phenotypic changes could be observed upon Luteolin treatment. KNS42 cells changed from the predominant diamond- to spindle-shape morphology (see Figure 15B). Further, the cells formed significantly longer neurite-like outgrowths (Figure 25A). Also, 3D-cell viability and spheroid growth were altered upon Luteolin application (Figure 25B). Cell viability was decreased to 60% compared to control cells, as expected upon a treatment at an EC_{50} concentration.

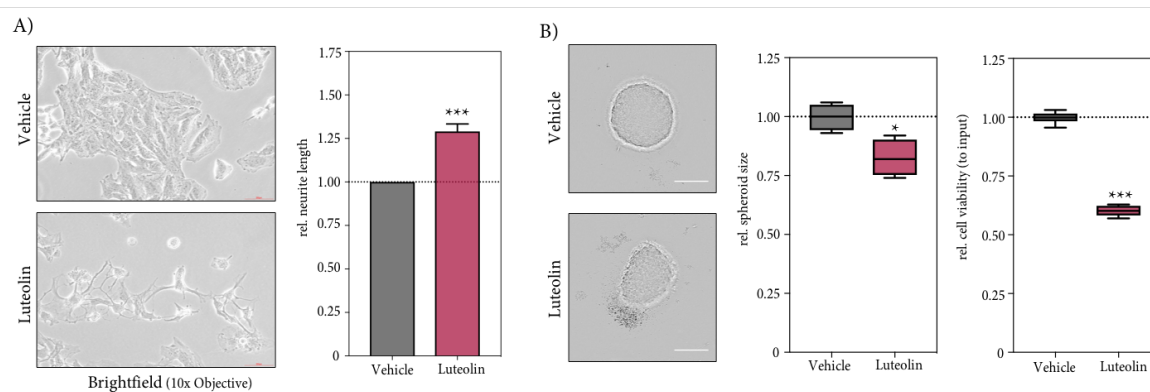


Figure 25. Cell phenotypes in KNS42 upon Luteolin treatment. A) Left panel: Representative brightfield image of KNS42 cells upon DMSO (vehicle) and Luteolin treatment. Right panel: Quantification of relative neurite outgrowth. B) Relative cell viability of KNS42 spheroids, 72 h after treatment. Left panels: Representative images of spheroids; scale bar, 150 μm . Middle and right panels: Box plots show spheroid size and cell viability normalized to the median of control cells ($n=12$). Statistical significance was determined from at least three independent experiments by Mann-Whitney test (A) and Student's t-test (B) (** $P \leq 0.01$; * $P \leq 0.05$).

To confirm the findings from KNS42 cells, the primary GBM-CSC HAL8 were treated with Luteolin. The determined EC_{50} (20 μM) was similar to KNS42 cells (Figure 26A). Although the effect on CD44 protein expression was not clear yet by Western blot analysis or qRT-PCR, an application of increasing Luteolin concentrations revealed an impact on spheroid formation and viability for this primary cell line that grows in suspension (Figure 26B). With increasing concentrations of Luteolin, the number and size of spheroids were significantly reduced. Taken together, a treatment with Luteolin at EC_{50} confirmed an impact on CD44 protein expression and on phenotypes upon MSI1-depletion and deletion.

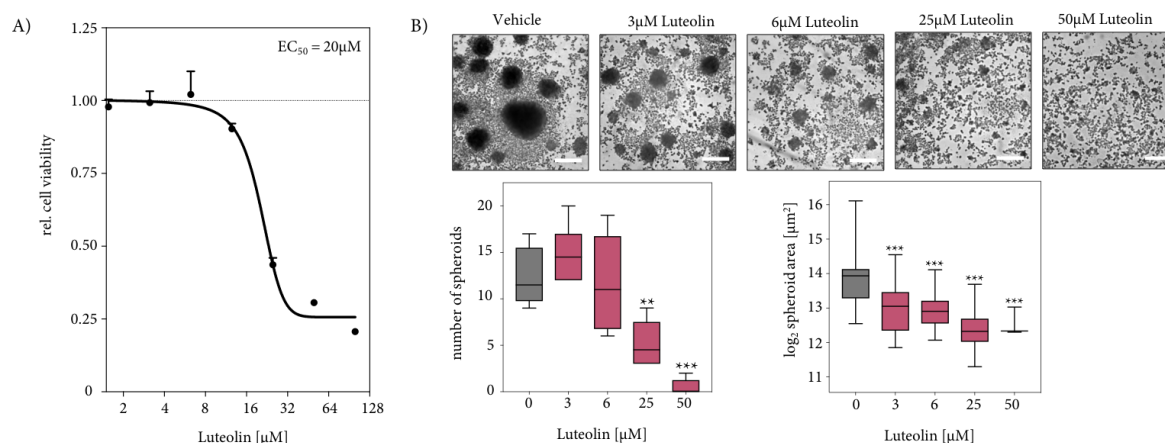


Figure 26. GBM-CSC HAL8 treatment with MSI1 inhibitor Luteolin. A) Cell viability ratios (to DMSO) of HAL8 cells exposed to Luteolin at increasing concentrations for 72h. The response curve and respective EC_{50} values are shown. B) Relative cell viability of HAL8 spheroids, 72 h after treatment. Upper panel: Representative images of spheroids. Scale bar, 150 μm . Lower panels: Box plots show spheroid numbers and area with increasing concentrations, normalized to the median of control cells. Statistical significance was determined by Mann-Whitney test (** $P \leq 0.01$, *** $P \leq 0.001$).

3.6 MSI1 impacts on chemoresistance *in vitro*

The current standard therapy of GBM includes surgical resection, followed by radiation and usually chemotherapy with Temozolomide (TMZ) (Kramm et al. 2006). New therapy strategies have evolved to increase chemotherapy response. For example, various HDAC inhibitors (HDACi), which are claimed to induce apoptosis, cell cycle arrest and DNA damage repair in cells, are tested in clinical studies (Mottamal et al. 2015). This study aimed to investigate MSI1's influence on the combined drug treatment of the HDACi Valproic acid (VPA) and the alkylating agent TMZ.

For comparative cell culture experiments, pediatric GBM cell lines KNS42 and SF188 were used. KNS42 was derived from a 16-year old male patient (Takeshita et al. 1987). SF188 was derived from an 8-year old male patient. Both cell lines are well characterized (Bjerke et al. 2013; Gaspar et al. 2010). For MSI1 expression analysis, both protein and mRNA levels were detected (Figure 27A). In comparison to KNS42 cells, SF188 showed no or only little MSI1 expression. Therefore, KNS42 cells were used for studies involving the detection of endogenous MSI1 expression upon drug treatment as well as for transient MSI1 KD studies. KNS42 cells show a predominant cytoplasmic localization of MSI1 (Figure 27B). SF188 cells were used for stable GFP-MSI1 overexpression. Comparable to endogenous MSI1, exogenous MSI1 localizes predominantly within the cytoplasm, but also within the nucleus (Figure 27C). MSI1 overexpression was verified on the protein level and it significantly increased number of viable cells, confirming previous findings from the here presented study (Figure 27D).

The effect of TMZ, VPA and the combination of both chemotherapeutics on cell viability was evaluated in KNS42 cells (Figure 28). For studies on MSI1 expression upon drug treatment in KNS42, EC_{50} for both drugs were determined. These analyses revealed that KNS42 cells show a high resistance to both drugs. Even at 300 μ M, TMZ treatment resulted in less than 40 % reduction of cell viability and cells apparently tolerated high drug doses. The determined EC_{50} was 10 μ M for TMZ (Figure 28A). VPA was used at concentrations up to 30 mM without achieving a plateau for the cell viability curve as it was achieved for TMZ treatment. This suggested that the cells do not respond to the treatment. Therefore, a precise EC_{50} could not be determined. Comparable studies and the applied concentrations of both drugs reported in GBM treatment were inspected (Hosein et al. 2015; Van Nifterik et al. 2012). According to drug concentrations used in these studies, 5 mM VPA was used in further *in vitro* experiments with KNS42 cells.

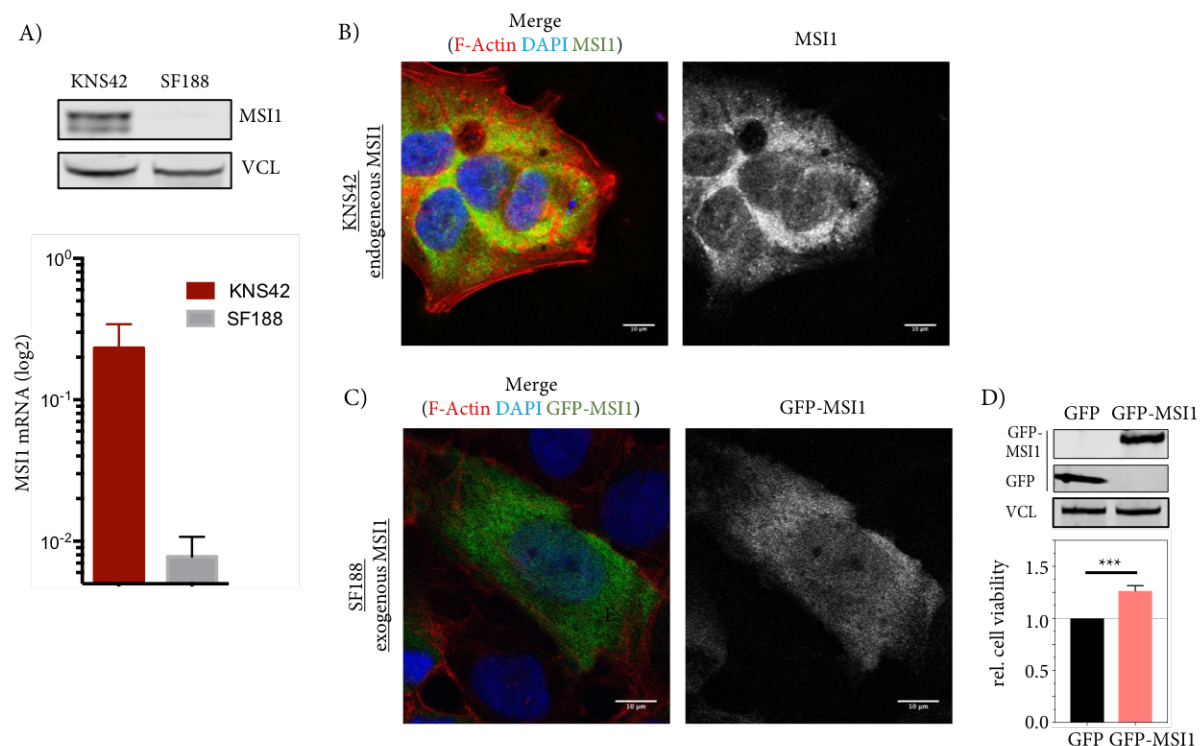


Figure 27. Expression of MSI1 in pediatric glioblastoma cell lines. A) Upper panel: Representative Western blot analysis of MSI1 expression in KNS42 and SF188 cells. VCL served as loading control. Lower panel: Quantification of MSI1 mRNA, normalized to GAPDH. B, C) Representative immunofluorescence images of endogenous MSI1 and exogenous GFP-MSI1 expression in KNS42 and SF188 cells, respectively. Scale bar, 10 μm. D) Upper panel: Representative Western blot analysis of indicated proteins of GFP-MSI1 overexpression in SF188 cells. VCL served as loading control. Lower panel: Cell viability of GFP and GFP-MSI1 expressing SF188 cells. Statistical significance was determined from at least three independent experiments by Student's *t*-test; ****P*<0.001.

VPA as single drug treatment in wildtype KNS42 cells showed a higher effect on the cell viability than TMZ alone (Figure 28B). For combined drug treatment, a stable concentration of 10 μM TMZ (which equals the calculated EC₅₀) was applied to KNS42 cells, while VPA concentration was variable. The combined drug treatment led to reduced cell viability compared to both single drug treatments and resulted in an EC₅₀ of 7.7 mM for VPA (Figure 28C). To evaluate the nature of interaction of both drugs in KNS42 cells, the *coefficient of drug interaction* (CDI) was determined (Figure 28D). Treatment with the combination of both drugs indicated a synergistic effect (CDI<0.7 significantly synergistic; CDI<1, synergistic; CDI=1, additive; CDI>1 antagonistic).

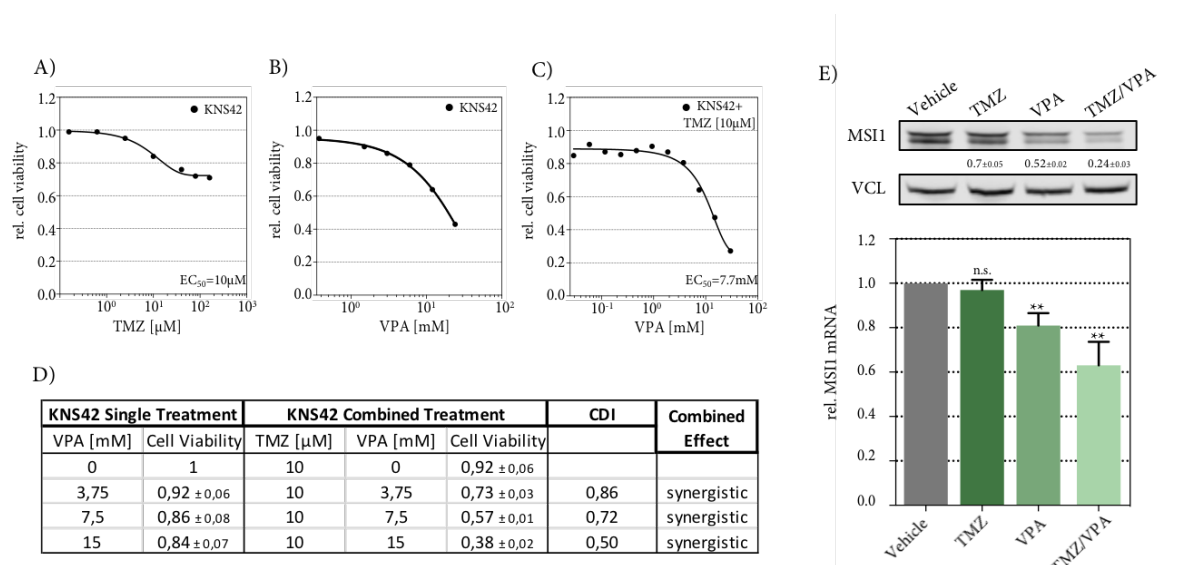


Figure 28. Effects of TMZ and VPA treatment in KNS42. A, B, C) Cell viability ratios (to DMSO) of KNS42 cells exposed to indicated compounds at increasing concentrations. The response curves and respective EC_{50} are shown.

D) Combined treatment of TMZ and VPA on KNS42 cells show synergistic effect ($\text{CDI} < 1$, synergistic; $\text{CDI} = 1$, additive; $\text{CDI} > 1$ antagonistic). E) Upper panel: Representative Western blot analysis of MSI1 protein expression upon treatment with TMZ, VPA and combination of TMZ and VPA in KNS42 cells. VCL served as loading control. Lower panel: MSI1 mRNA expression was normalized to GAPDH and vehicle. Statistical significance was determined from at least three independent experiments by Student's *t*-test (** $P \leq 0.01$, n.s. not significant).

Aiming to evaluate if MSI1 protein expression is altered due to the drug treatment, TMZ (10 μM), VPA (5 mM) and the combination of both drugs (TMZ (10 μM), VPA (5 mM)) where applied to KNS42 cells (Figure 28E). TMZ showed no significant effect on MSI1 expression on the mRNA level but effected a minor decrease on MSI1 protein. VPA treatment showed a significant reduction of MSI1 on the protein and mRNA level. This downregulation was further pronounced by the combined treatment.

The poor prognosis and substantial therapy resistance of GBMs is thought to largely rely on the resistance of GBM-CSCs. In view of MSI1's expression in neural stem cells and upregulated synthesis in GBMs, it remained to be determined, if the protein contributes to therapy resistance. This was tested by depleting MSI1 in KNS42 cells to mimic a putative therapeutic benefit by the pharmacological targeting of the protein in the future, like by Luteolin. Additionally, MSI1 overexpression in SF188 was evaluated to test if elevated MSI1 abundance confers to higher therapy resistance. In both single drug treatments, no effect on cell viability was observed upon MSI1 KD (Figure 29A). For combined drug treatment, control cells and MSI1 KD cells were supplied with 10 μM TMZ and varying VPA concentrations of 1.8 mM , 3.75 mM , and 7.5 mM . For all three concentrations, control cells

showed significantly higher cell viability compared to MSI1 KD cells (Figure 29C). For a 3.75 mM VPA dose in combination with 10 μ M TMZ, a difference of 27 % in cell viability between control cells and MSI1 KD was the highest observed impact of the combined drug treatment. In SF188 cells, stably expressing GFP-MSI1, EC_{50} of 80 μ M for TMZ and 4 mM for VPA were determined (Figure 29B). Thus, for combined drug treatment experiments, control cells, as well as GFP-MSI1 expressing cells, were exposed to 80 μ M TMZ and varying doses of VPA (1.8 mM, 3.75 mM, and 7.5 mM). Since MSI1 overexpressing cells show a proliferation effect as well, normalization was performed to GFP- and GFP-MSI1 cells, respectively, treated with vehicle. For all three conditions, GFP-MSI1 cells showed significantly higher cell viability compared to GFP cells (Figure 29D). Here, the highest effect on cell viability (22 % difference between GFP vs. GFP-MSI1) was achieved at the lowest applied VPA concentration of 1.8 mM and 80 μ M of TMZ. These findings provide strong evidence that MSI1 expressing cells show a higher resistance to a combination of TMZ and VPA drug treatment.

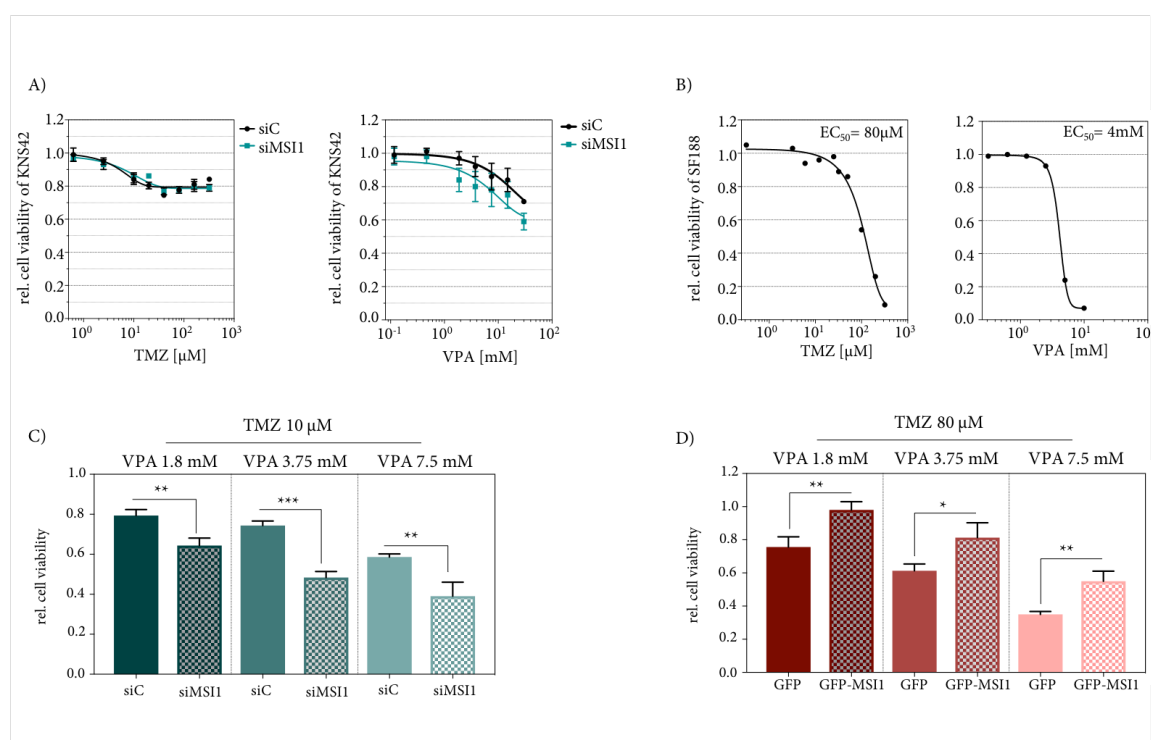


Figure 29. Effect of MSI1 on chemoresistance in TMZ and VPA treatment. A) Cell viability ratios (to DMSO) of control (siC) and MSI1 KD (siMSI1) in KNS42 cells exposed to indicated compounds at increasing concentrations. The response curves for both conditions are shown. B) Cell viability ratios (to DMSO) of SF188 cells exposed to indicated compounds at increasing concentrations. The response curve and respective EC_{50} are shown. C, D) Cell viability ratios (to DMSO) of KNS42 and SF188 cells, exposed to indicated compound upon transient MSI1 KD in KNS42 cells (C) or GFP-MSI1 overexpression in SF188 cells (D), respectively. Statistical significance was determined from at least three independent experiments by Student's *t*-test (* $P \leq 0.05$, ** $P \leq 0.01$, *** $P \leq 0.001$).

3.7 Additional Results:

Alternative Splicing results in a second functional MSI1 isoform

Western blot analysis revealed a second detectable MSI1 protein isoform of lower molecular weight in KNS42 cells (around 40kDa). This isoform is not expressed in the other MSI1-positive GBM cell lines U251-H, U251-U and U343 (Figure 30A). Knockdown of MSI1 (Figure 30B) and MSI1-immunoprecipitation with KNS42 cells (Figure 30C) confirmed the lower signal to be MSI1 isoform. The analysis of publicly available mouse and human RNA-sequencing data of brain tissue from VastDB revealed alternative splicing of MSI1 exon 11 (57 nt) (Tapial et al. 2017). Interestingly, this MSI1 isoform is not described so far. Semiquantitative RT-PCR confirmed, that KNS42 cells express the MSI1 variant with a missing exon 11 in addition to the full length MSI1. Compared to KNS42 cells, U251MG did not show a double band in the semiquantitative RT-PCR, revealing that there is no alternative splice-out event of exon 11 in these GBM-derived cell lines (Figure 30D).

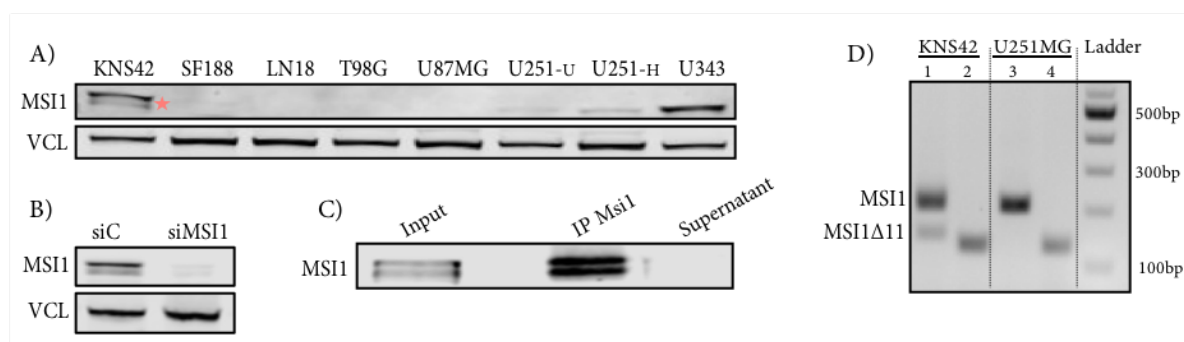


Figure 30. Detection of MSI1 isoform. A) Representative Western blot analysis of MSI1 protein in different GBM-derived cell lines. KNS42 showed a double band (marked with a pink star). VCL served as loading control. B) Representative western blot analysis of MSI1 protein upon MSI1 KD (siMSI1) in KNS42 cells. VCL served as loading control. C) MSI1-immunoprecipitation with KNS42 cell lysate. D) Detection of MSI1 PCR products via semiquantitative RT-PCR from cDNAs derived from KNS42 or U251MG cells on an agarose gel. A size ladder is indicated (lane 5). Lanes 2 and 4 are amplicons from exon 12 which served as positive control.

Exon 11, as part of the MSI1 CDS, is coding for 19 amino acids (AA 246-264), localizing c-terminal of the two RRM and between the PABP- and LIN28-binding motifs (Figure 31A). Thus, deletion of exon 11 leads to a MSI1 protein isoform with reduced molecular weight. To further investigate the functionality of the MSI1 isoform with a missing exon 11 (MSI1 Δ 11), it was cloned via fusion PCR and inserted into the lentiviral transfer vector pLVX-GFP. The respective overexpression of the constructs GFP, GFP-MSI1, GFP-MSI1 Δ 11 and GFP-MSI1mut was performed in KNS42 cells. The Western blot analysis revealed the expected shift in molecular weight for GFP-MSI1 Δ 11, compared to the other constructs (Figure 31B).

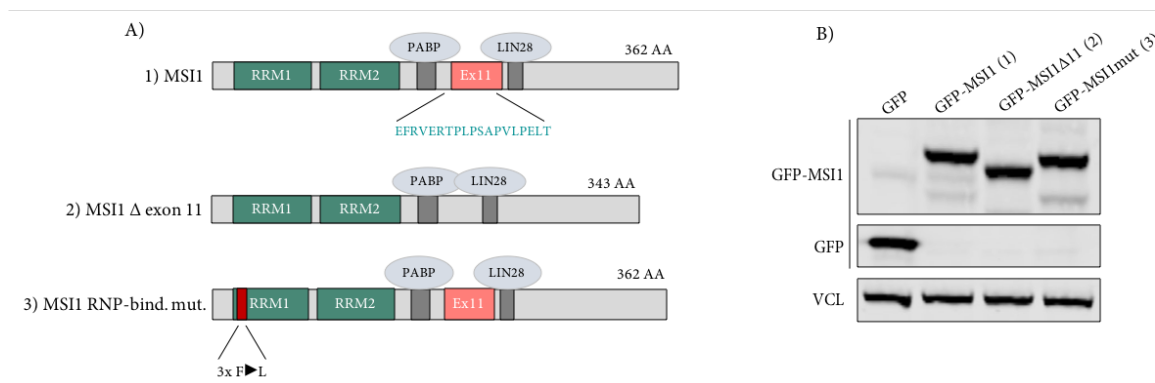


Figure 31. Generation of MSI1 variants. A) Schematic of the structural components of MSI1 proteins, used throughout this study. RRM, RNA-recognition motif; PABP, PABP-binding site; LIN28, LIN28-binding site; Exon11, amino acid (AA) sequence in blue encoded by the respective MSI1 exon 11. B) Representative Western blot analysis of indicated proteins in KNS42 cells, overexpressing GFP or GFP-MSI1 constructs. VCL served as loading control.

It is not clarified yet which function is exerted by MSI1 Δ 11. The use of ASPedia (Alternative splicing encyclopedia of human, (ASpedia 2017)) revealed experimentally validated post-translational modifications (PTMs) of amino acids encoded by exon 11 (Figure 32, red). Thus, amino acid 251(threonine) and 255 (serine) seem to get phosphorylated. The skipping of this exon removes both PTM sites, potentially resulting in an altered biological function of MSI1 Δ 11, compared to the full-length protein.

An RNA-immunoprecipitation with lysates from KNS42 cells overexpressing GFP, GFP-MSI1, GFP-MSI1 Δ 11 and GFP-MSI1mut, a significant enrichment of NUMB mRNA (a well-known translationally repressed target of MSI1 (Imai et al. 2001)) was observed for GFP-MSI1 as well as for GFP-MSI1 Δ 11 (Figure 33A). This indicated, that the resulting MSI1 protein upon exclusion of exon 11 is not hindered, but maybe even more efficient in RNA- and PABP-binding, which remains elusive in the here presented study. Comparably, GFP-MSI1mut did not reveal a significant enrichment of NUMB mRNA and PABP.

Upon overexpression of GFP and GFP-MSI1 constructs, spheroid viability was analyzed (Figure 33B). Spheroids, derived from KNS42 overexpressing GFP-MSI1 or GFP-MSI1 Δ 11, showed a significantly increased cell viability compared to GFP expressing cells. Spheroid viability upon GFP-MSI1mut overexpression did not change significantly. Thus, GFP-MSI1 Δ 11 variant is putatively biologically active, while the mutation of three amino acids within the first RRM (MSI1mut) disrupts the ability to contribute to an increased cell viability.

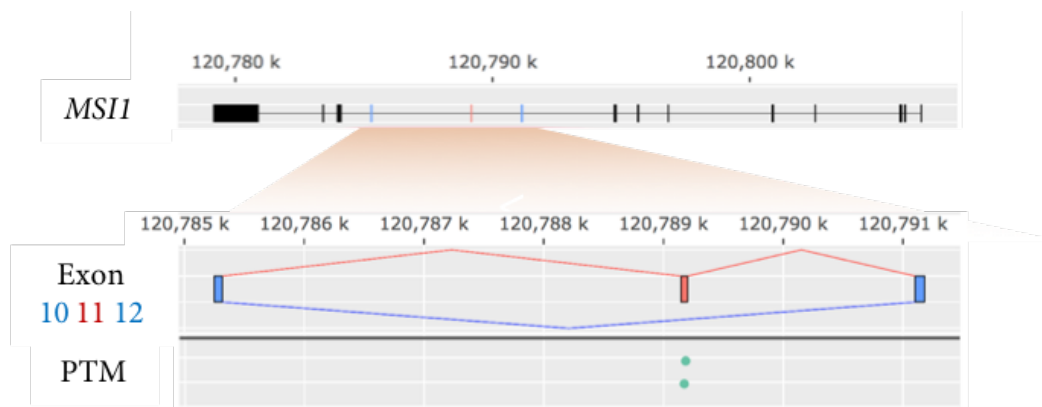


Figure 32. MSI1 Δ 11 lacks two putative post-translational modification sites. Upper and middle panel: Enlargement of the indicated genomic region shows *MSI1* exons 10 (blue), 11 (red) and 12 (blue). By using ASPedia (ASpedia 2017), Exon 11 was identified to potentially being excluded by alternative splicing (blue lines). Lower panel: Exon 11 codes for two amino acids, which were experimentally validated to be post-translationally modified (PTMs, green) in the resulting *MSI1* protein with included exon 11.

Supporting a functional role of *MSI1 Δ 11*, an RNA-sequencing analysis of mouse neural differentiation showed differential inclusion of *MSI1* exon 11 over different developmental stages (Figure 33C). Eight different stages of differentiation of cortical glutamatergic neurons were analyzed (embryonic stem cells (ESC), neuroepithelial stem cells (NESC), radial glia, neurons (days *in vitro*, DIV 1-28) (Hubbard et al. 2013)). *MSI1 Δ 11* inclusion declines from 95% in ESC to 76% in radial glia. Maturing and differentiated neurons show a 95%-100% inclusion of *MSI1* exon 11 again. Interestingly, total *MSI1* mRNA, including full length and the *MSI1 Δ 11* mRNA, revealed its highest expression in radial glia cells and decreases during maturation of neurons (red line). Thus, *MSI1* and *MSI1 Δ 11* expression seems to be enriched in precursor cells.

To examine the expression of the *MSI1 Δ 11* mRNA in human (primary) cancer-derived cells and GBM tissue (provided by the Neuropathology Department Magdeburg), semiquantitative RT-PCR was performed on cDNA (Figure 33D). Results showed, that *MSI1 Δ 11* is expressed in GBM-derived cell lines KNS42 and in U343MG. Further, three different isolated GBM-CSC lines showed expression of *MSI1 Δ 11*, although the signal was only weak for two of them. Intriguingly, all analyzed GBM samples were positive for *MSI1 Δ 11*.

In summary, *MSI1 Δ 11* seems to exert a biologically relevant function – independent of a distinct phosphorylation pathway – at a distinct developmental stage, which could potentially be represented by GBM-CSCs.

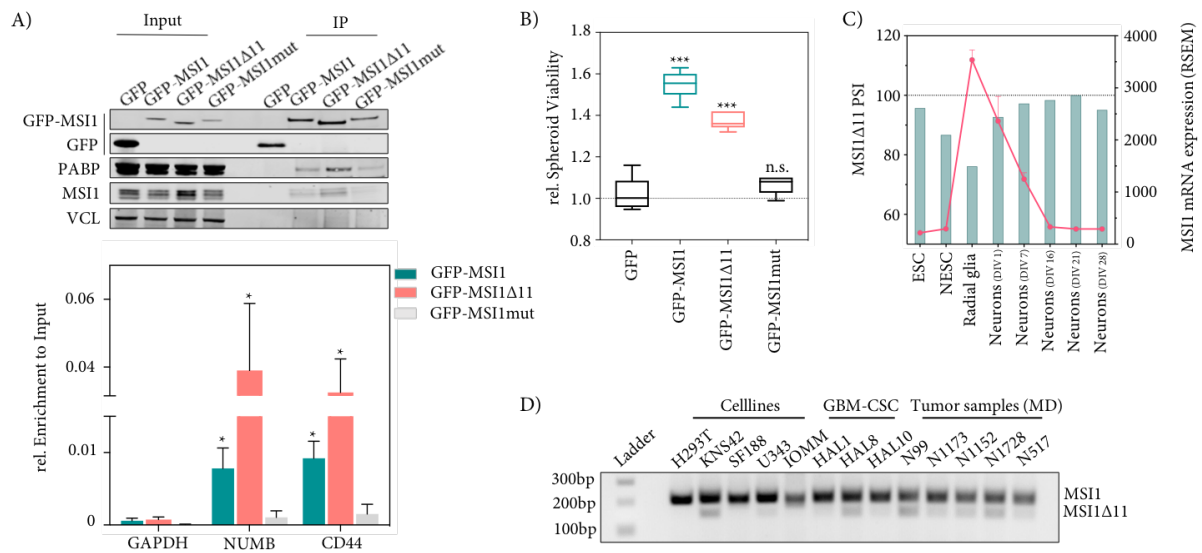


Figure 33. Biological functionality and expression pattern of MSI1Δ11. A) MSI1 RNA-immunoprecipitation in KNS42 cells overexpressing GFP-MSI1 constructs. B) Spheroid cell viability of KNS42 cells stably overexpressing GFP-MSI1 constructs (n=12). C) MSI1 mRNA expression (pink line) and percent of spliced-in (PSI) of MSI1 exon 11 (green bars) in neurogenesis of cortical glutamatergic neurons from murine ESCs. D) Detection of MSI1 Δ11 isoform via semiquantitative RT-PCR in five different cell lines (H293T (embryonic kidney cell line), KNS42, SF188 (pediatric GBM-derived cell lines), U343 (adult GBM-derived cell line), IOMM (Meningioma-derived cell line)), three primary GBM-CSC (HAL1, HAL8, HAL10) and five GBM tumor samples. Statistical significance was determined from at least three independent experiments by Student's *t*-test (* $P \leq 0.05$, *** $P \leq 0.001$)

4 Discussion

The here presented study aimed to further characterize the function of the RBP MSI1 in GBM and how it impacts the severity of this aggressive brain tumor. Regarding its expression pattern it was found to be upregulated in GBM, but also in recurrent brain tissue (Cancer Genome Atlas Research et al. 2013). In addition, a co-upregulation of well-studied CSC markers could be reported on the basis of RNA-sequencing. The subsequent analysis of MSI1's impact as oncofetal and CSC-relevant protein on promoting hallmarks of cancer, revealed striking evidence *in vitro*. In this respect, this study reports on a mechanism on MSI1 as a post-transcriptional promoter of CD44 expression by impairing the miRNA-dependent mRNA degradation. This dependency is targetable via the recently describe MSI1 inhibitor Luteolin, which alters growth of the KNS42 cells, but also of isolated primary GBM-CSCs. Further, MSI1 affected chemoresistance in pediatric GBM, providing another rational for targeting this oncofetal RBP in this severe malignancy. Irrespective of that, a so far undescribed functional MSI1 protein isoform, resulting from alternative splicing, was identified. During normal development of neuronal cells its expression is restricted to a distinct stage of cell development. Interestingly, GBM samples as well as primary GBM-CSC also revealed the expression of this unknown MSI1 isoform.

4.1 MSI1 is an oncofetal RBP

MSI1 is described to promote and maintain stem cell state (Siddall et al. 2006). Thus, its highest expression is found in the early organism's development, predominantly within the brain. Sakakibara et al reported a decrease of murine *Msi1* mRNA between embryonic day 12 to postnatal day 20 and adult state within the brain (Sakakibara et al. 1996). According to this, RNA-sequencing data of human developing brain was analyzed in comparison in the here presented study. MSI1 mRNA in the developing human hippocampus declines in the observed timeframe from nine post conceptional week to eleven years after birth. Additionally, expression pattern of another oncofetal protein, IGF2BP1, revealed similar reduction of expression over time. This further underlines MSI1 as an oncofetal protein in humans. Interestingly, expression of its homolog MSI2 shows a substantially distinct expression. Its mRNA rather stays expressed until later timepoints of development, as already reported in mice (Sakakibara et al. 2001). A possible cause of such tight regulation MSI1

expression as part of a stem cell-like expression signature could be regulatory mechanisms with increased importance during development, including altered DNA methylation and histone modifications (Cholewa-Waclaw et al. 2016). But also, transcription factors with restricted expression to certain stages are likely to be responsible for the regulation of MSI1 expression pattern (Swift et al. 2017). To explain this phenomenon of decreasing expression for MSI1 in detail, further experiments have to be performed.

Several studies reported a MSI1 re-expression in several cancer types (Kudinov et al. 2017). Especially, in the early beginnings of this century, elevated MSI1 expression was linked to malignancies of the brain (Toda et al. 2001). High-throughput analysis of brain tumor cohorts via micro-arrays and RNA-sequencing confirmed the observations (Katz et al. 2014). MSI1 showed the highest expression in GBM compared to other cancer types. An important observation from TCGA analysis is the high MSI1 expression also in recurrent GBM, compared to normal brain tissue. This finding suggests that MSI1 expressing cells can overcome chemotherapeutic treatment, since the initiating cells of a GBM recurrence most likely represent CSCs, which are considered to show higher therapy resistance (Osuka et al. 2017). Possibly, this is one strategy how MSI1 contributes to GBM malignancy. Thus, not only the major tumor bulk is positive for MSI1 expression, but also those cells which are claimed to be responsible for tumor recurrence, called GBM-CSCs (Lathia et al. 2015). In addition, GBM tumors revealed high expression of other (cancer) stem cell markers – CD44, CD133 (*PROM1*), Oct-4 (*POU5F1*), SOX2, BMI1 and NES, indicating a stemness character of dedifferentiated cells with properties including high proliferation rates, increased migration potential and resistance to programmed cell death (Zhao et al. 2017; Bao et al. 2013).

In the here presented study, enhanced MSI1 expression is shown in pediatric GBM on the mRNA and protein level and MSI1 expression is identified to be associated with increasing tumor grade. The findings suggested MSI1 as an oncofetal RBP and as a marker of pediatric GBM.

4.2 MSI1 affects cancer cell phenotypes

To identify a suitable *in vitro*-model for experimental studies, different GBM-derived cell lines (two cell lines derived from pediatric GBM, six cell lines derived from adult GBM) were analyzed in respect to MSI1 protein expression. Interestingly, only one pediatric GBM cell line

and one adult GBM cell line revealed a substantially high expression of MSI1 protein. In two additional adult GBM cell lines only minor MSI1 expression was detectable. The less positive GBM cell lines could indicate, that a majority of cells are not able to keep the undifferentiated cell state promoted by MSI1 and only a minor proportion are adapting to MSI1 expression for growth in adherent cell culture. Interestingly, MSI1 negative cell lines were shown to start to express MSI1 upon culturing under neuronal stem cell conditions (serum-free medium DMEM/F12, supplemented with EGF, bFGF and N-2) (Iacopino et al. 2014). Similar observations could be made in breast and lung cancer cell lines (Wang, Penalva, et al. 2010; Wang et al. 2013). Thus, cells are able to modulate MSI1 expression under cell culture conditions already.

Experiments to monitor altered phenotypes dependent on MSI1 were predominantly performed with KNS42 upon siRNA-mediated MSI1 depletion or stable MSI1 KO. In this study, the MSI1 KO reduced cell proliferation *in vitro* in 2D growth and spheroid (3D) growth assays. Further, a colony formation assay revealed a reduced capacity of MSI1 KO cells to form colonies. To test, whether these effects can be translated into *in vivo* analysis, experiments in swiss nude mice were performed with orthotopically injected wildtype or KO cells. Although, none of the four mice with injected MSI1 KO cells showed any tumor growth by histological analysis, only one of four control mice developed a tumor. None of any animals died due to the injected cells. Thus, it is not possible to draw conclusions out of the experiment. Initially, KNS42 were described to be suitable for subcutaneous injection in nude mice, but orthotopic models were not reported so far. In addition, protocols suggest $\sim 4 \times 10^6$ KNS42 cells to be used per injection (Yamashita et al. 1981). In contrast, for the here presented study only 5×10^5 cells were injected. It is likely that the cell number was not sufficient and should be adjusted for future orthotopic experiments or a subcutaneous xenograft should be considered. Further, clonal variability, a frequently observed issue derived from the generation of CRISPR/Cas9-mediated single-cell clone (Giuliano et al. 2019) may have led to an inability of collective growth in an *in vivo* environment.

Irrespective of that, MSI1 KD cells showed increased caspase3/7 activity and PARP cleavage *in vitro*. Both enzymes play essential roles during apoptosis (Shalini et al. 2015). The observation implied a potential role for MSI1 in overcoming programmed cell death. This was further evidenced after challenging the cells with anchorage-independent growth and additional pressure by generating non-permissive growth conditions (no FBS, ultra-low attachment

plates) in an anoikis resistance assay. The MSI1 KO severely impaired non-adhesive growth. It suggested a role for MSI1 in facilitating anoikis resistance by disturbing apoptosis pathways. Upon detachment from an appropriate extra-cellular matrix cells run into a programmed cell death, called “anoikis”. This process is essential during development, but is deregulated in cancers. The respective cells then are anoikis resistant which is a necessity for a mesenchymal-like cell for successful migration and invasion (Yang et al. 2013)

GBM is characterized by extensive growth of the tumor bulk, but also by the invasive potential of cells, which migrate into the surrounding brain tissue and finally lead to a recurrent tumor (Di et al. 2010). Invasion into adjacent brain tissue depends on the interaction between the cell and the extracellular matrix, as well as on intrinsic changes to the cell itself to allow for active cell migration (Zhong et al. 2010). Therefore, the cell body must change its morphology/polarization and adhere itself to the surrounding extracellular matrix. Thus, tumor malignancy is driven by proteins which play a role in cell adhesion and invasion (Friedl et al. 2011). A GO analysis of MSI1 iCLIP data showed that numerous MSI1 targets are identified to play a role in cell morphology, migration, cell adhesion and invasion and thereby revealing a function of MSI1 in these pathways (Uren et al. 2015). In the here presented study, MSI1 KD decreased cell migration speed. This finding confirmed that MSI1 interferes with migration and adhesion pathways. Lin et al verified the initial findings from Uren et al by overexpressing MSI1. This promoted invasion and motility and linked these phenotypes to an enhanced translation of ICAM1 by MSI1 (Lin et al. 2019).

Interestingly, MSI1 KD in KNS42 cells altered their cell morphology. KNS42 control cells usually grow with a diamond shaped, flat and large cell body. Upon MSI1 KD, the cell body forms neuronal- and spindle-like outgrowths with several branch points. This finding suggests a role for MSI1 in blocking a differentiation-like process in KNS42 cells, which is already reported for normal neurogenesis (Sakakibara et al. 1997; Kuwako et al. 2010). Noteworthy, the morphology effects could only be observed upon MSI1 KD, but not upon its KO. A likely, but speculative explanation could be, that KO cell clones represent cells which, to some extent, overcame the consequences of the MSI1 KO – at least to maintain cell proliferation. Thus, the MSI1 KO cell clones might need an additional stressor to trigger these morphology effects, which remains elusive.

4.3 Identification of CD44 as a new post-transcriptionally regulated target of MSI1

The impact of MSI1 on cancer phenotypes complies with certain hallmarks of cancer (Hanahan et al. 2011). By using the GBM TCGA RNA-sequencing dataset, the CSC marker MSI1 was identified as highly expressed, together with other yet well-studied CSC markers. Importantly, this enhancement of CSCs could be confirmed with an independent, small tumor cohort (GBM vs LGG). In detail, the mRNA expression of MSI1, CD44, SOX2 and NES was analyzed. All four markers revealed elevated expression in GBM compared to LGG, representing the undifferentiated state of GBM. This marker set was analyzed upon MSI1 KD in KNS42 cells, as well as in GBM-CSCs (HAL8), which were isolated in the course of the here presented study and cultured in neuronal stem cell media. Intriguingly, both cell lines revealed similar effects on CSC marker expression, suggesting a conservation of a distinct GBM CSC marker expression pattern. Interestingly, it was reported that MSI1 maintains the expression of MYC, NANOG, SOX2, BMI1 and OCT4 in breast cancer cells (Wang, Penalva, et al. 2010). This even stretches the potential conservation of CSC marker expression over different entities, and even further suggests, that the observations from the here presented study could, at least in part, depend on MSI1 expression.

The co-upregulation of CSC markers, potentially MSI1-dependent, would imply a post-transcriptional mechanism by mRNA stabilization. So far, MSI1 has predominantly been described to affect translation, rather than affecting mRNA stabilization (Pereira et al. 2017; Cambuli et al. 2015). But as the depletion of MSI1 resulted in the downregulation of CSC marker mRNA expression, transcriptome profiling via mRNA-sequencing upon MSI1 KD in KNS42 cells was performed. Interestingly, among mRNAs being (1) downregulated upon MSI1 KD, (2) upregulated in the TCGA-provided GBM cohort and (3) associated with MSI1 protein (identified via iCLIP, (Uren et al. 2015)) was CD44. SOX2 or NES did not fulfill all three criteria, thus suggesting an indirect regulation. Importantly, the iCLIP experiment was performed with GBM-derived U251MG cell line. Thus, the association of MSI1 protein with the CD44 mRNA in KNS42 cells was confirmed via RIP analysis. The iCLIP data revealed binding to 3'UTRs by MSI1 as preferred *cis*-element, including in the CD44 mRNA. This finding indicated a potential post-transcriptional regulation of mRNA expression via the

3'UTR in GBM-derived cells. A similar function was already proposed and extensively validated for the IGF2BPs. They 'shield' target transcripts from miRNA-dependent decay (Schneider et al. 2019; Muller et al. 2018). Thus, MSI1 could potentially participate in a similar mechanism, as the CD44 3'UTR has frequently been described to be a prone miRNA-target (Liu et al. 2011; Jeyapalan et al. 2011; Yang et al. 2016). Of note, iCLIP experiments in a mouse model with Msi1 overexpression in intestinal epithelium showed binding at the CD44 3'UTR, suggesting a conserved mechanism across humans and mice (Cambuli et al. 2015).

The 3'UTR-dependent enhancement of CD44 mRNA expression by MSI1 was experimentally validated with a luciferase reporter assay, a rather artificial approach, upon overexpression and siRNA-mediated depletion of MSI1 (see Figure 21). Intriguingly, the homozygous CRISPR/Cas9-mediated deletion of the CD44 3'UTR confirmed the previous findings, as a MSI1 KD was not sufficient anymore to further decrease the already reduced CD44 expression, most likely due to the loss of MSI1-binding elements (see Figure 22). Both experimental approaches together evidenced the 3'UTR-dependent enhancement of CD44 expression by MSI1 in a GBM-derived cell line. Hence, it is likely that MSI1 'shields' from miRNA-dependent regulation, which could explain the effect of mRNA reduction upon MSI1 KD in cells with intact CD44 3'UTR. This does not occur anymore upon the deletion of the CD44 3'UTR. The decreased CD44 protein and mRNA expression upon CD44 3'UTR deletion, irrespective of MSI1-KD, could be explained by clonal variability and the impact of multiple additional RBPs, which now lack influence. Besides, MSI1 protein directly interacts with PABP1. Subsequently, CD44 mRNA could be degraded due to a (potentially RISC-independent) poly(A) tail-shortening (deadenylation) upon MSI1 loss. Shortened 3'-terminal adenosine extensions serve as a landing pad for complexes which stimulate cap hydrolysis, followed by a 5' to 3'-decay, or exosome-dependent 3'-5' decay (Labno et al. 2016).

Irrespective of that, the here presented study provides compelling evidence that MSI1 impairs miRNA-dependent downregulation of CD44 expression. As previously introduced, the CD44 mRNA has been extensively investigated in terms of RISC-dependent regulation and it was reported that the CD44 3'UTR can function as a miRNA-sponge (Rutnam et al. 2012). Here, two already reported CD44 3'UTR-targeting miRNAs have been identified, which regulate CD44 expression. Obviously, MSI1 impairs their function, likely due to the incorporation of the CD44 mRNA into a MSI1-containing RNP, which actively excludes the RISC, as described for IGF2BP1 (Busch et al. 2016). This was shown by performing a luciferase reporter assay. Interestingly, the here presented findings stand in contrast to a recent report on an association

of MSI1 with AGO2 in GBM cells (Chen et al. 2020). The authors claimed, that MSI1 stimulates miRNA-dependent mRNA decay by recruiting AGO2 to 3'UTRs of certain mRNAs under hypoxia. But the association was also evidenced by AGO2 immunoprecipitation under normoxia. Hence, in the here presented study an AGO2 immunoprecipitation did not, or barely, reveal a co-precipitation of MSI1. The finding indicates that MSI1 does not associate with mRNAs targeted by the RISC. Further, MSI1 most likely does not recruit AGO2 in KNS42 cells, supporting the hypothesis of miRNA shielding. A following experiment would be an AGO IP in MSI1 KO cells with identification if CD44 mRNA shows increased enrichment.

4.4 A treatment with the MSI1 inhibitor Luteolin resembles MSI1 KD and KO phenotypes

The here presented study indicates, that a direct inhibition of MSI1 function could be beneficial in GBM treatment. Recently, Yi et al identified Luteolin via a large-scale compound screen as an inhibitor of MSI1 (Yi et al. 2018). Interestingly, Luteolin is a common flavonoid. It is enriched in many plants used for Chinese traditional medicine and was reported to have anti-cancer properties (Lin et al. 2008). Luteolin disrupts the binding capacity to MSI1 target mRNA, which influences its regulatory activity. Therefore, it was of interest, if a treatment of KNS42 cells revealed similar effects comparable to MSI1 KD and KO. The results shown in this work indicate, that Luteolin decreased cell viability of KNS42 as well as of primary GBM CSCs (HAL8). In KNS42 cells, the compound induced a morphological change similar to MSI1 KD and led to a reduced spheroid growth. In accordance, Luteolin treatment reduced MSI1, as well as CD44 protein expression. Although Luteolin was reported to specifically block the interaction between MSI1 and its target mRNAs, it unlikely only affects MSI1 downstream-signaling. Hence, Luteolin was already reported to alter antioxidant activity, modulate the MAPK and p-IGF-1R/PI3K/AKT/mTOR signaling pathways, and induce apoptosis by mitochondrial dysfunction and in GBM or colorectal cancers (Wang, Wang, Jia, Pan, et al. 2017; Wang, Wang, Jia, Ding, et al. 2017; Liu et al. 2017). In HAL8, Luteolin treatment seemed to interfere with the ability of spheroid formation of this suspension cell line. Further, the compound has been investigated as a potential therapeutic agent for different cancer types in several studies (Cook et al. 2017; Zang et al. 2017). To attack a tumor at multiple layers, combined drug therapy becomes attractive, since current therapy with

TMZ and radiotherapy after tumor resection does not yield satisfying survival outcome for patients. Fortunately, recent studies already showed that Luteolin can be used in combined compound application (Chakrabarti et al. 2015; Sonoki et al. 2017), although the determined EC_{50} in KNS42 and HAL8 cells is rather high (~25 μ M). Still, in future it should be investigated if Luteolin further enhances the synergistic effect of VPA on TMZ in pediatric glioma (Potschke et al. 2020).

4.5 MSI1 affects chemoresistance *in vitro*

Two studies reported the involvement of MSI1 in promoting therapy resistance in adult GBM. In GBM-derived cells treated with cisplatin, it was proposed that MSI1 inhibits drug-induced apoptosis via an AKT/IL6 regulatory pathway (Chen et al. 2016). De Araujo et al. described the impact of MSI1 on DNA damage repair and radioresistance by controlling the expression of DNA-PKcs (de Araujo et al. 2016). Both studies used adult GBM cell lines. In the here presented study, MSI1 was predominantly investigated in pediatric GBM cells. The two cell lines used, KNS42 and SF188, showed a high drug resistance, which was already documented by other studies (Bjerke et al. 2013; Gaspar et al. 2010). KNS42 cells are TMZ resistant, although their MGMT promotor is hypermethylated, suggesting MGMT-independent mechanisms of TMZ resistance. SF188 cells are also TMZ resistant, which is potentially mediated by MGMT expression (Gaspar et al. 2010). In both cell lines, MSI1 expression was clearly associated with enhanced cell survival. Nifterik et al. investigated the interaction of VPA on TMZ and radiation, by showing that a combination of VPA and TMZ increases radiation response compared to TMZ and radiation only (independent of MGMT protein). They assumed, that the synergistic effect of VPA and TMZ resulted from a loosening of chromatin structure through VPA, and subsequent increase of DNA methylation as well as damage through TMZ (Van Nifterik et al. 2012). In the here presented study, MSI1 was revealed as a *bona fide* marker of the combined treatment of TMZ and/or VPA. Although MSI1 expression remained unaffected by TMZ, the combined treatment led to a significantly pronounced downregulation of the protein. This supports the conclusion, that combined treatments are generally more effective than monotherapies. A study by Hosein et al. revealed that VPA is effective as a monotherapy in primary GBM lines (at clinically achievable serum concentrations [1-10mM]) (Hosein et al. 2015). There are different clinical studies, which investigated a combination of VPA and TMZ with radiation, or VPA treatment with radiation

alone (Weller et al. 2011; Felix et al. 2011). The here presented data supports these findings, as in KNS42 cells VPA as monotherapy already significantly affected MSI1 expression and cell viability. In addition to revealing MSI1 as a therapeutic marker, its potential in modulating therapy resistance was evaluated. Consistent with its proposed expression and role in GBM-CSCs (Hemmati et al. 2003), it was observed that MSI1 promotes therapy resistance to combined TMZ/VPA treatment. Thus, targeting of MSI1, for instance by Luteolin, is expected to impair therapy resistance and improve the efficacy of combined TMZ/VPA treatment. Although it has to be clarified whether Luteolin promotes the efficacy of combined TMZ/VPA treatment in pediatric GBM via MSI1 inhibition, Luteolin indicates a promising starting point to improve drug efficacy. Further, the findings suggest that MSI1 could be a marker and potential drug target to improve therapy of pediatric GBM.

4.6 Alternative splicing results in a second functional MSI1 protein isoform

Initial Western blot analysis revealed the detection of a second MSI1 isoform of slightly lower molecular weight in KNS42. The use of siRNAs and immunoprecipitation confirmed the finding – a novel and undescribed MSI1 protein isoform. Interestingly, the very first reports on MSI1 expression and function detection via Western blot already showed a double band for MSI1 detection ((Sakakibara et al. 2002; Kawahara et al. 2008), but it was not further addressed. A database research revealed a potential alternative splicing event of MSI1 exon 11 during normal neurogenesis (ASpedia 2017). Indeed, a semi-quantitative RT-PCR revealed two MSI1 isoforms in KNS42, whereas the second lacked exon 11. Thus, this isoform was termed MSI1 Δ 11. Exon 11 is 57bp in size and codes for the AA 246 to 264. Interestingly, in the wildtype MSI1 protein these AA locate between the PABP- and the LIN28 binding sites.

The stable overexpression of GFP-MSI1 Δ 11 revealed a significant induction of spheroid growth and NUMB mRNA immunoprecipitation, similar to GFP-MSI1. This suggested that it exerts a comparable function as the full-length protein. From the here presented data it is not clear what MSI1 Δ 11 distinguishes from the full-length protein. But within the exon 11-encoded amino acid sequence, two phosphorylation sites are predicted (ASpedia 2017). This could be a first hint for a different function of the MSI1 variant and why cells, representing a certain developmental stage, might favor its expression. Further experiments on deciphering the role of the MSI1 variant should be localization studies with stress experiments and the mutation of sites for post-translational modifications. Further, mass spectrometry analysis

could reveal differences in the MSI1 interactomes and stable re-expression of MSI1 Δ 11 in a MSI1 KO background could show if the shortened protein functionally relies on the full-length protein.

The MSI1 Δ 11 isoform is predominantly expressed in radial glia cells – the first neural stem cells – and is absent in differentiated neurons. Interestingly, total MSI1 mRNA expression peaks in radial glia cells and declines during the maturation of neurons (Tapial et al. 2017). Interestingly, in early embryonal stages and CSCs proliferation and self-renewal is, to some extent, depending on mitogen-activated protein kinase (MAPK) signaling. The canonical function of MAPKs is the phosphorylation of threonine and serine (Pimienta et al. 2007). Hypothetically, MSI1 Δ 11 could be independent of this signaling and thus an enhancer of pro-proliferative properties, because it does not, at least in part, rely on MAPK-activating growth factors to perform its functions. Surprisingly, in the here presented study, MSI1 Δ 11 expression was detected in all three tested GBM-CSC lines and GBM tumor samples. Intriguingly, two independent, very recently published articles report on the existence of radial glia-like cells within heterogeneous GBM populations, which seem to contribute to the invasive/metastatic behavior of GBM (Wang et al. 2020; Bhaduri et al. 2020). In consequence, the expression of MSI1 Δ 11 could possibly be seen as a specific marker for GBM-CSCs at a distinct stage of differentiation.

5 Summary

The RNA-binding protein (RBP) Musashi (MSI1) is reported to control the mRNA translation of various target transcripts to promote cell cycle progression. It is highly abundant during embryogenesis in stem cells, where it was found to support stem cell self-renewal and to inhibit differentiation. Interestingly, MSI1 is upregulated in various cancers, with the highest expression in Glioblastoma (GBM), where it is presumed to promote an aggressive stemness-like tumor cell phenotype. GBM is the most prevalent and lethal primary brain tumor. It is characterized by radiochemoresistant cancer stem cells (CSC), which invade the adjacent brain tissue, thus leading to tumor recurrence. Unfortunately, conventional therapy options barely increase the poor survival probability.

The here presented study aimed to further characterize the function of the oncofetal RBP MSI1 in GBM and how it impacts the severity of this aggressive brain tumor. Besides its high expression in the primary GBM, it was also observed in recurrent tumors. Subsequent analysis of MSI1 on promoting hallmarks of cancers (for instance sustained proliferation and resistance to cell death) revealed striking evidence on support of cancer cell phenotypes, *in vitro*. Intriguingly, a co-upregulation of well-studied CSC markers could be reported on the basis of RNA-sequencing in GBM, including CD44, SOX2 and NES. This potential dependency was validated *in vitro* in KNS42 and primary GBM-CSCs upon MSI1 depletion. In this respect, a novel mechanism for MSI1 is reported: a post-transcriptional 3'UTR-dependent enhancement of CD44 expression by impairing miRNA/RISC-mediated decay. This dependency is targetable via the recently describe MSI1 inhibitor Luteolin, which alters growth of the KNS42 cells, but also of primary GBM-CSCs. Furthermore, MSI1 affected chemoresistance in GBM to temozolomide and valproic acid treatment, providing an additional rational for targeting this oncofetal RBP in this severe malignancy.

In addition to the so far presented data, an undescribed functional MSI1 protein isoform, resulting from alternative splicing, was identified. During normal development of neuronal cells its expression is restricted to a distinct stage of cell development. Interestingly, GBM samples as well as primary GBM-CSC also revealed the expression of this so far unknown MSI1 isoform.

The here presented data identify MSI1 as regulator of stemness in GBM and spots mRNA stability control as a new function for the well described translational modulator. The study provides rationales for potential treatment options of this highly malignant brain tumor.

6 References

- Adamson, C., O. O. Kanu, et al. 2009. 'Glioblastoma multiforme: a review of where we have been and where we are going', *Expert Opin Investig Drugs*, 18: 1061-83.
- Agarwal, V., G. W. Bell, et al. 2015. 'Predicting effective microRNA target sites in mammalian mRNAs', *Elife*, 4.
- Al-Hajj, M., M. S. Wicha, et al. 2003. 'Prospective identification of tumorigenic breast cancer cells', *Proc Natl Acad Sci U S A*, 100: 3983-8.
- Ameres, S. L., and P. D. Zamore. 2013. 'Diversifying microRNA sequence and function', *Nat Rev Mol Cell Biol*, 14: 475-88.
- Ardekani, A. M., and M. M. Naeini. 2010. 'The Role of MicroRNAs in Human Diseases', *Avicenna J Med Biotechnol*, 2: 161-79.
- Arumugam, K., M. C. Macnicol, et al. 2012. 'Autoregulation of Musashi1 mRNA translation during *Xenopus* oocyte maturation', *Mol Reprod Dev*, 79: 553-63.
- Ascano, M., S. Gerstberger, et al. 2013. 'Multi-disciplinary methods to define RNA-protein interactions and regulatory networks', *Curr Opin Genet Dev*, 23: 20-8.
- ASpedia. 2017. 'ASpedia: a comprehensive encyclopedia of human alternative splicing'. http://combio.snu.ac.kr/aspedia/search_result.php.
- Auffinger, B., D. Spencer, et al. 2015. 'The role of glioma stem cells in chemotherapy resistance and glioblastoma multiforme recurrence', *Expert Rev Neurother*, 15: 741-52.
- Azari, H., S. Millette, et al. 2011. 'Isolation and expansion of human glioblastoma multiforme tumor cells using the neurosphere assay', *J Vis Exp*: e3633.
- Babic, I., A. Jakymiw, et al. 2004. 'The RNA binding protein Sam68 is acetylated in tumor cell lines, and its acetylation correlates with enhanced RNA binding activity', *Oncogene*, 23: 3781-9.
- Baltz, A. G., M. Munschauer, et al. 2012. 'The mRNA-bound proteome and its global occupancy profile on protein-coding transcripts', *Mol Cell*, 46: 674-90.
- Bao, B., A. Ahmad, et al. 2013. 'Overview of cancer stem cells (CSCs) and mechanisms of their regulation: implications for cancer therapy', *Curr Protoc Pharmacol*, Chapter 14: Unit 14 25.

- Bao, S., Q. Wu, et al. 2006. 'Glioma stem cells promote radioresistance by preferential activation of the DNA damage response', *Nature*, 444: 756-60.
- Barbouti, A., M. Hoglund, et al. 2003. 'A novel gene, MSI2, encoding a putative RNA-binding protein is recurrently rearranged at disease progression of chronic myeloid leukemia and forms a fusion gene with HOXA9 as a result of the cryptic t(7;17)(p15;q23)', *Cancer Res*, 63: 1202-6.
- Barker, C. A., A. J. Bishop, et al. 2013. 'Valproic acid use during radiation therapy for glioblastoma associated with improved survival', *Int J Radiat Oncol Biol Phys*, 86: 504-9.
- Bartel, D. P. 2004. 'MicroRNAs: genomics, biogenesis, mechanism, and function', *Cell*, 116: 281-97.
- Bartel, D. P. 2009. 'MicroRNAs: target recognition and regulatory functions', *Cell*, 136: 215-33.
- Batista, C. M., E. D. Mariano, et al. 2014. 'Adult neurogenesis and glial oncogenesis: when the process fails', *Biomed Res Int*, 2014: 438639.
- Battelli, C., G. N. Nikopoulos, et al. 2006. 'The RNA-binding protein Musashi-1 regulates neural development through the translational repression of p21WAF-1', *Mol Cell Neurosci*, 31: 85-96.
- Bell, J. L., R. Turlapati, et al. 2015. 'IGF2BP1 harbors prognostic significance by gene gain and diverse expression in neuroblastoma', *J Clin Oncol*, 33: 1285-93.
- Bell, J. L., K. Wachter, et al. 2013. 'Insulin-like growth factor 2 mRNA-binding proteins (IGF2BPs): post-transcriptional drivers of cancer progression?', *Cell Mol Life Sci*, 70: 2657-75.
- Bendall, L. J., K. F. Bradstock, et al. 2000. 'Expression of CD44 variant exons in acute myeloid leukemia is more common and more complex than that observed in normal blood, bone marrow or CD34+ cells', *Leukemia*, 14: 1239-46.
- Bhaduri, A., E. Di Lullo, et al. 2020. 'Outer Radial Glia-like Cancer Stem Cells Contribute to Heterogeneity of Glioblastoma', *Cell Stem Cell*, 26: 48-63 e6.
- Bjerke, L., A. Mackay, et al. 2013. 'Histone H3.3. mutations drive pediatric glioblastoma through upregulation of MYCN', *Cancer Discov*, 3: 512-9.
- Bonnet, D., and J. E. Dick. 1997. 'Human acute myeloid leukemia is organized as a hierarchy that originates from a primitive hematopoietic cell', *Nat Med*, 3: 730-7.
- Borowicz, S., M. Van Scoyk, et al. 2014. 'The soft agar colony formation assay', *J Vis Exp*: e51998.

- Bourguignon, L. Y., K. Peyrollier, et al. 2008. 'Hyaluronan-CD44 interaction activates stem cell marker Nanog, Stat-3-mediated MDR1 gene expression, and ankyrin-regulated multidrug efflux in breast and ovarian tumor cells', *J Biol Chem*, 283: 17635-51.
- Bourguignon, L. Y., G. Wong, et al. 2012. 'Hyaluronan-CD44v3 interaction with Oct4-Sox2-Nanog promotes miR-302 expression leading to self-renewal, clonal formation, and cisplatin resistance in cancer stem cells from head and neck squamous cell carcinoma', *J Biol Chem*, 287: 32800-24.
- Boyerinas, B., S. M. Park, et al. 2008. 'Identification of let-7-regulated oncofetal genes', *Cancer Res*, 68: 2587-91.
- Burd, C. G., and G. Dreyfuss. 1994. 'Conserved structures and diversity of functions of RNA-binding proteins', *Science*, 265: 615-21.
- Busch, B., N. Bley, et al. 2016. 'The oncogenic triangle of HMGA2, LIN28B and IGF2BP1 antagonizes tumor-suppressive actions of the let-7 family', *Nucleic Acids Res*, 44: 3845-64.
- Cambuli, F. M., B. R. Correa, et al. 2015. 'A Mouse Model of Targeted Musashi1 Expression in Whole Intestinal Epithelium Suggests Regulatory Roles in Cell Cycle and Stemness', *Stem Cells*, 33: 3621-34.
- Cancer Genome Atlas Research, Network. 2008. 'Comprehensive genomic characterization defines human glioblastoma genes and core pathways', *Nature*, 455: 1061-8.
- Cancer Genome Atlas Research, Network, J. N. Weinstein, et al. 2013. 'The Cancer Genome Atlas Pan-Cancer analysis project', *Nat Genet*, 45: 1113-20.
- Castello, A., B. Fischer, et al. 2012. 'Insights into RNA biology from an atlas of mammalian mRNA-binding proteins', *Cell*, 149: 1393-406.
- Castello, A., B. Fischer, et al. 2016. 'Comprehensive Identification of RNA-Binding Domains in Human Cells', *Mol Cell*, 63: 696-710.
- Chakrabarti, M., and S. K. Ray. 2015. 'Synergistic anti-tumor actions of luteolin and silibinin prevented cell migration and invasion and induced apoptosis in glioblastoma SNB19 cells and glioblastoma stem cells', *Brain Res*, 1629: 85-93.
- Chanmee, T., P. Ontong, et al. 2015. 'Key Roles of Hyaluronan and Its CD44 Receptor in the Stemness and Survival of Cancer Stem Cells', *Front Oncol*, 5: 180.
- Charlesworth, A., A. Wilczynska, et al. 2006. 'Musashi regulates the temporal order of mRNA translation during *Xenopus* oocyte maturation', *EMBO J*, 25: 2792-801.

- Chen, C., S. Zhao, et al. 2018. 'The biology and role of CD44 in cancer progression: therapeutic implications', *J Hematol Oncol*, 11: 64.
- Chen, H. Y., L. T. Lin, et al. 2016. 'Musashi-1 regulates AKT-derived IL-6 autocrinal/paracrine malignancy and chemoresistance in glioblastoma', *Oncotarget*, 7: 42485-501.
- Chen, H. Y., M. L. Wang, et al. 2020. 'Musashi-1 promotes stress-induced tumor progression through recruitment of AGO2', *Theranostics*, 10: 201-17.
- Chen, J., Y. Li, et al. 2012. 'A restricted cell population propagates glioblastoma growth after chemotherapy', *Nature*, 488: 522-6.
- Chen, P. X., Q. Y. Li, et al. 2015. 'Musashi-1 Expression is a Prognostic Factor in Ovarian Adenocarcinoma and Correlates with ALDH-1 Expression', *Pathol Oncol Res*, 21: 1133-40.
- Cheng, C., N. Bhardwaj, et al. 2009. 'The relationship between the evolution of microRNA targets and the length of their UTRs', *BMC Genomics*, 10: 431.
- Cheng, L., Q. Wu, et al. 2011. 'Elevated invasive potential of glioblastoma stem cells', *Biochem Biophys Res Commun*, 406: 643-8.
- Cheng, W., T. Liu, et al. 2012. 'MicroRNA-199a targets CD44 to suppress the tumorigenicity and multidrug resistance of ovarian cancer-initiating cells', *FEBS J*, 279: 2047-59.
- Cholewa-Waclaw, J., A. Bird, et al. 2016. 'The Role of Epigenetic Mechanisms in the Regulation of Gene Expression in the Nervous System', *J Neurosci*, 36: 11427-34.
- Chomczynski, P., and N. Sacchi. 1987. 'Single-step method of RNA isolation by acid guanidinium thiocyanate-phenol-chloroform extraction', *Anal Biochem*, 162: 156-9.
- Clingman, C. C., L. M. Deveau, et al. 2014. 'Allosteric inhibition of a stem cell RNA-binding protein by an intermediary metabolite', *Elife*, 3.
- Cook, M. T., Y. Liang, et al. 2017. 'Luteolin inhibits lung metastasis, cell migration, and viability of triple-negative breast cancer cells', *Breast Cancer (Dove Med Press)*, 9: 9-19.
- Cragle, C., and A. M. MacNicol. 2014. 'Musashi protein-directed translational activation of target mRNAs is mediated by the poly(A) polymerase, germ line development defective-2', *J Biol Chem*, 289: 14239-51.
- Cuadrado, A., L. F. Garcia-Fernandez, et al. 2002. 'Regulation of tau RNA maturation by thyroid hormone is mediated by the neural RNA-binding protein musashi-1', *Mol Cell Neurosci*, 20: 198-210.

- Dahlrot, R. H., S. K. Hermansen, et al. 2013. 'What is the clinical value of cancer stem cell markers in gliomas?', *Int J Clin Exp Pathol*, 6: 334-48.
- Dahlstrand, J., V. P. Collins, et al. 1992. 'Expression of the class VI intermediate filament nestin in human central nervous system tumors', *Cancer Res*, 52: 5334-41.
- Das, S., M. Srikanth, et al. 2008. 'Cancer stem cells and glioma', *Nat Clin Pract Neurol*, 4: 427-35.
- de Araujo, P. R., A. Gorthi, et al. 2016. 'Musashi1 Impacts Radio-Resistance in Glioblastoma by Controlling DNA-Protein Kinase Catalytic Subunit', *Am J Pathol*, 186: 2271-8.
- Di, C., A. K. Mattox, et al. 2010. 'Emerging therapeutic targets and agents for glioblastoma migrating cells', *Anticancer Agents Med Chem*, 10: 543-55.
- Eramo, A., F. Lotti, et al. 2008. 'Identification and expansion of the tumorigenic lung cancer stem cell population', *Cell Death Differ*, 15: 504-14.
- Esteller, M., J. Garcia-Foncillas, et al. 2000. 'Inactivation of the DNA-repair gene MGMT and the clinical response of gliomas to alkylating agents', *N Engl J Med*, 343: 1350-4.
- Fabian, M. R., G. Mathonnet, et al. 2009. 'Mammalian miRNA RISC recruits CAF1 and PABP to affect PABP-dependent deadenylation', *Mol Cell*, 35: 868-80.
- Fabian, M. R., and N. Sonenberg. 2012. 'The mechanics of miRNA-mediated gene silencing: a look under the hood of miRISC', *Nat Struct Mol Biol*, 19: 586-93.
- Fang, D., T. K. Nguyen, et al. 2005. 'A tumorigenic subpopulation with stem cell properties in melanomas', *Cancer Res*, 65: 9328-37.
- Felix, F. H., N. M. Trompieri, et al. 2011. 'Potential role for valproate in the treatment of high-risk brain tumors of childhood-results from a retrospective observational cohort study', *Pediatr Hematol Oncol*, 28: 556-70.
- Ferrarese, R., G. R. th Harsh, et al. 2014. 'Lineage-specific splicing of a brain-enriched alternative exon promotes glioblastoma progression', *J Clin Invest*, 124: 2861-76.
- Filatova, A., T. Acker, et al. 2013. 'The cancer stem cell niche(s): the crosstalk between glioma stem cells and their microenvironment', *Biochim Biophys Acta*, 1830: 2496-508.
- Fouad, Y. A., and C. Aanei. 2017. 'Revisiting the hallmarks of cancer', *Am J Cancer Res*, 7: 1016-36.
- Fox, R. G., F. D. Park, et al. 2015. 'Musashi signaling in stem cells and cancer', *Annu Rev Cell Dev Biol*, 31: 249-67.

- Franken, N. A., H. M. Rodermond, et al. 2006. 'Clonogenic assay of cells in vitro', *Nat Protoc*, 1: 2315-9.
- Friedl, P., and S. Alexander. 2011. 'Cancer invasion and the microenvironment: plasticity and reciprocity', *Cell*, 147: 992-1009.
- Fulci, V., S. Chiaretti, et al. 2007. 'Quantitative technologies establish a novel microRNA profile of chronic lymphocytic leukemia', *Blood*, 109: 4944-51.
- Furnari, F. B., T. Fenton, et al. 2007. 'Malignant astrocytic glioma: genetics, biology, and paths to treatment', *Genes Dev*, 21: 2683-710.
- Garneau, N. L., J. Wilusz, et al. 2007. 'The highways and byways of mRNA decay', *Nat Rev Mol Cell Biol*, 8: 113-26.
- Gaspar, N., L. Marshall, et al. 2010. 'MGMT-independent temozolomide resistance in pediatric glioblastoma cells associated with a PI3-kinase-mediated HOX/stem cell gene signature', *Cancer Res*, 70: 9243-52.
- Gerstberger, S., M. Hafner, et al. 2014. 'A census of human RNA-binding proteins', *Nat Rev Genet*, 15: 829-45.
- Giuliano, C. J., A. Lin, et al. 2019. 'Generating Single Cell-Derived Knockout Clones in Mammalian Cells with CRISPR/Cas9', *Curr Protoc Mol Biol*, 128: e100.
- Glisovic, T., J. L. Bachorik, et al. 2008. 'RNA-binding proteins and post-transcriptional gene regulation', *FEBS Lett*, 582: 1977-86.
- Gomes, F. C., D. Paulin, et al. 1999. 'Glial fibrillary acidic protein (GFAP): modulation by growth factors and its implication in astrocyte differentiation', *Braz J Med Biol Res*, 32: 619-31.
- Good, P., A. Yoda, et al. 1998. 'The human Musashi homolog 1 (MSI1) gene encoding the homologue of Musashi/Nrp-1, a neural RNA-binding protein putatively expressed in CNS stem cells and neural progenitor cells', *Genomics*, 52: 382-4.
- Grimson, A., K. K. Farh, et al. 2007. 'MicroRNA targeting specificity in mammals: determinants beyond seed pairing', *Mol Cell*, 27: 91-105.
- Hadziselimovic, N., V. Vukojevic, et al. 2014. 'Forgetting is regulated via Musashi-mediated translational control of the Arp2/3 complex', *Cell*, 156: 1153-66.
- Hanahan, D., and R. A. Weinberg. 2011. 'Hallmarks of cancer: the next generation', *Cell*, 144: 646-74.

- Hayashita, Y., H. Osada, et al. 2005. 'A polycistronic microRNA cluster, miR-17-92, is overexpressed in human lung cancers and enhances cell proliferation', *Cancer Res*, 65: 9628-32.
- Hegi, M. E., A. C. Diserens, et al. 2005. 'MGMT gene silencing and benefit from temozolomide in glioblastoma', *N Engl J Med*, 352: 997-1003.
- Hemmati, H. D., I. Nakano, et al. 2003. 'Cancerous stem cells can arise from pediatric brain tumors', *Proc Natl Acad Sci U S A*, 100: 15178-83.
- Hentze, M. W., A. Castello, et al. 2018. 'A brave new world of RNA-binding proteins', *Nat Rev Mol Cell Biol*, 19: 327-41.
- Hong, I. S., and K. S. Kang. 2013. 'The effects of Hedgehog on the RNA-binding protein Msi1 in the proliferation and apoptosis of mesenchymal stem cells', *PLoS One*, 8: e56496.
- Hosein, A. N., Y. C. Lim, et al. 2015. 'The effect of valproic acid in combination with irradiation and temozolomide on primary human glioblastoma cells', *J Neurooncol*, 122: 263-71.
- Hubbard, K. S., I. M. Gut, et al. 2013. 'Longitudinal RNA sequencing of the deep transcriptome during neurogenesis of cortical glutamatergic neurons from murine ESCs', *F1000Res*, 2: 35.
- Huntzinger, E., and E. Izaurralde. 2011. 'Gene silencing by microRNAs: contributions of translational repression and mRNA decay', *Nat Rev Genet*, 12: 99-110.
- Huse, J. T., and E. C. Holland. 2009. 'Genetically engineered mouse models of brain cancer and the promise of preclinical testing', *Brain Pathol*, 19: 132-43.
- Iacopino, F., C. Angelucci, et al. 2014. 'Isolation of cancer stem cells from three human glioblastoma cell lines: characterization of two selected clones', *PLoS One*, 9: e105166.
- Imai, T., A. Tokunaga, et al. 2001. 'The neural RNA-binding protein Musashi1 translationally regulates mammalian numb gene expression by interacting with its mRNA', *Mol Cell Biol*, 21: 3888-900.
- Iorio, M. V., and C. M. Croce. 2012. 'Causes and consequences of microRNA dysregulation', *Cancer J*, 18: 215-22.
- Islam, S., U. Kjallquist, et al. 2011. 'Characterization of the single-cell transcriptional landscape by highly multiplex RNA-seq', *Genome Res*, 21: 1160-7.
- Jankowsky, E., and M. E. Harris. 2015. 'Specificity and nonspecificity in RNA-protein interactions', *Nat Rev Mol Cell Biol*, 16: 533-44.

- Jansson, M. D., and A. H. Lund. 2012. 'MicroRNA and cancer', *Mol Oncol*, 6: 590-610.
- Jeyapalan, Z., Z. Deng, et al. 2011. 'Expression of CD44 3'-untranslated region regulates endogenous microRNA functions in tumorigenesis and angiogenesis', *Nucleic Acids Res*, 39: 3026-41.
- Jonas, S., and E. Izaurralde. 2015. 'Towards a molecular understanding of microRNA-mediated gene silencing', *Nat Rev Genet*, 16: 421-33.
- Jones, C., L. Perryman, et al. 2012. 'Paediatric and adult malignant glioma: close relatives or distant cousins?', *Nat Rev Clin Oncol*, 9: 400-13.
- Jones, T. A., J. N. Jeyapalan, et al. 2015. 'Molecular analysis of pediatric brain tumors identifies microRNAs in pilocytic astrocytomas that target the MAPK and NF-kappaB pathways', *Acta Neuropathol Commun*, 3: 86.
- Jung, C. S., C. Foerch, et al. 2007. 'Serum GFAP is a diagnostic marker for glioblastoma multiforme', *Brain*, 130: 3336-41.
- Kagara, N., K. T. Huynh, et al. 2012. 'Epigenetic regulation of cancer stem cell genes in triple-negative breast cancer', *Am J Pathol*, 181: 257-67.
- Kaneko, Y., S. Sakakibara, et al. 2000. 'Musashi1: an evolutionally conserved marker for CNS progenitor cells including neural stem cells', *Dev Neurosci*, 22: 139-53.
- Kanemura, Y., K. Mori, et al. 2001. 'Musashi1, an evolutionarily conserved neural RNA-binding protein, is a versatile marker of human glioma cells in determining their cellular origin, malignancy, and proliferative activity', *Differentiation*, 68: 141-52.
- Katz, Y., F. Li, et al. 2014. 'Musashi proteins are post-transcriptional regulators of the epithelial-luminal cell state', *Elife*, 3: e03915.
- Kaufmann, S. H., S. H. Lee, et al. 2008. 'Apoptosis-associated caspase activation assays', *Methods*, 44: 262-72.
- Kawahara, H., T. Imai, et al. 2008. 'Neural RNA-binding protein Musashi1 inhibits translation initiation by competing with eIF4G for PABP', *J Cell Biol*, 181: 639-53.
- Kawahara, H., Y. Okada, et al. 2011. 'Musashi1 cooperates in abnormal cell lineage protein 28 (Lin28)-mediated let-7 family microRNA biogenesis in early neural differentiation', *J Biol Chem*, 286: 16121-30.
- Kawase, S., K. Kuwako, et al. 2014. 'Regulatory factor X transcription factors control Musashi1 transcription in mouse neural stem/progenitor cells', *Stem Cells Dev*, 23: 2250-61.

- Kechavarzi, B., and S. C. Janga. 2014. 'Dissecting the expression landscape of RNA-binding proteins in human cancers', *Genome Biol*, 15: R14.
- Kharas, M. G., C. J. Lengner, et al. 2010. 'Musashi-2 regulates normal hematopoiesis and promotes aggressive myeloid leukemia', *Nat Med*, 16: 903-8.
- Kim, D., B. Langmead, et al. 2015. 'HISAT: a fast spliced aligner with low memory requirements', *Nat Methods*, 12: 357-60.
- Kozomara, A., and S. Griffiths-Jones. 2014. 'miRBase: annotating high confidence microRNAs using deep sequencing data', *Nucleic Acids Res*, 42: D68-73.
- Kramm, C. M., S. Wagner, et al. 2006. 'Improved survival after gross total resection of malignant gliomas in pediatric patients from the HIT-GBM studies', *Anticancer Res*, 26: 3773-9.
- Kudinov, A. E., J. Karanicolas, et al. 2017. 'Musashi RNA-Binding Proteins as Cancer Drivers and Novel Therapeutic Targets', *Clin Cancer Res*, 23: 2143-53.
- Kuwako, K., K. Kakumoto, et al. 2010. 'Neural RNA-binding protein Musashi1 controls midline crossing of precerebellar neurons through posttranscriptional regulation of Robo3/Rig-1 expression', *Neuron*, 67: 407-21.
- Kwak, P. B., S. Iwasaki, et al. 2010. 'The microRNA pathway and cancer', *Cancer Sci*, 101: 2309-15.
- Labno, A., R. Tomecki, et al. 2016. 'Cytoplasmic RNA decay pathways - Enzymes and mechanisms', *Biochim Biophys Acta*, 1863: 3125-47.
- Langmead, B., and S. L. Salzberg. 2012. 'Fast gapped-read alignment with Bowtie 2', *Nat Methods*, 9: 357-9.
- Larsen, J. E., V. Nathan, et al. 2016. 'ZEB1 drives epithelial-to-mesenchymal transition in lung cancer', *J Clin Invest*, 126: 3219-35.
- Lathia, J. D., J. M. Heddleston, et al. 2011. 'Deadly teamwork: neural cancer stem cells and the tumor microenvironment', *Cell Stem Cell*, 8: 482-5.
- Lathia, J. D., S. C. Mack, et al. 2015. 'Cancer stem cells in glioblastoma', *Genes Dev*, 29: 1203-17.
- Lee, E. K. 2012. 'Post-translational modifications of RNA-binding proteins and their roles in RNA granules', *Curr Protein Pept Sci*, 13: 331-6.
- Lelli, K. M., M. Slattery, et al. 2012. 'Disentangling the many layers of eukaryotic transcriptional regulation', *Annu Rev Genet*, 46: 43-68.

- Li, D., X. Peng, et al. 2011. 'Msi-1 is a predictor of survival and a novel therapeutic target in colon cancer', *Ann Surg Oncol*, 18: 2074-83.
- Liao, Y., G. K. Smyth, et al. 2014. 'featureCounts: an efficient general purpose program for assigning sequence reads to genomic features', *Bioinformatics*, 30: 923-30.
- Lin, J. C., J. T. Tsai, et al. 2019. 'Musashi-1 Enhances Glioblastoma Migration by Promoting ICAM1 Translation', *Neoplasia*, 21: 459-68.
- Lin, Y., R. Shi, et al. 2008. 'Luteolin, a flavonoid with potential for cancer prevention and therapy', *Curr Cancer Drug Targets*, 8: 634-46.
- Liu, C., K. Kelnar, et al. 2011. 'The microRNA miR-34a inhibits prostate cancer stem cells and metastasis by directly repressing CD44', *Nat Med*, 17: 211-5.
- Liu, Y., T. Lang, et al. 2017. 'Luteolin inhibits colorectal cancer cell epithelial-to-mesenchymal transition by suppressing CREB1 expression revealed by comparative proteomics study', *J Proteomics*, 161: 1-10.
- Lundell, B. I., J. B. McCarthy, et al. 1997. 'Activation of beta1 integrins on CML progenitors reveals cooperation between beta1 integrins and CD44 in the regulation of adhesion and proliferation', *Leukemia*, 11: 822-9.
- Malzkorn, B., M. Wolter, et al. 2010. 'Identification and functional characterization of microRNAs involved in the malignant progression of gliomas', *Brain Pathol*, 20: 539-50.
- Marinov, G. K., B. A. Williams, et al. 2014. 'From single-cell to cell-pool transcriptomes: stochasticity in gene expression and RNA splicing', *Genome Res*, 24: 496-510.
- Mayr, C., and D. P. Bartel. 2009. 'Widespread shortening of 3'UTRs by alternative cleavage and polyadenylation activates oncogenes in cancer cells', *Cell*, 138: 673-84.
- McHugh, C. A., P. Russell, et al. 2014. 'Methods for comprehensive experimental identification of RNA-protein interactions', *Genome Biol*, 15: 203.
- Mestdagh, P., A. K. Bostrom, et al. 2010. 'The miR-17-92 microRNA cluster regulates multiple components of the TGF-beta pathway in neuroblastoma', *Mol Cell*, 40: 762-73.
- Miller, J. A., S. L. Ding, et al. 2014. 'Transcriptional landscape of the prenatal human brain', *Nature*, 508: 199-206.
- Miranda, A., P. T. Hamilton, et al. 2019. 'Cancer stemness, intratumoral heterogeneity, and immune response across cancers', *Proc Natl Acad Sci U S A*, 116: 9020-29.
- Mottamal, M., S. Zheng, et al. 2015. 'Histone deacetylase inhibitors in clinical studies as templates for new anticancer agents', *Molecules*, 20: 3898-941.

- Muller, S., N. Bley, et al. 2018. 'IGF2BP1 enhances an aggressive tumor cell phenotype by impairing miRNA-directed downregulation of oncogenic factors', *Nucleic Acids Res*, 46: 6285-303.
- Muller, S., M. Glass, et al. 2019. 'IGF2BP1 promotes SRF-dependent transcription in cancer in a m6A- and miRNA-dependent manner', *Nucleic Acids Res*, 47: 375-90.
- Nair, V. S., L. S. Maeda, et al. 2012. 'Clinical outcome prediction by microRNAs in human cancer: a systematic review', *J Natl Cancer Inst*, 104: 528-40.
- Nakamura, M., H. Okano, et al. 1994. 'Musashi, a neural RNA-binding protein required for Drosophila adult external sensory organ development', *Neuron*, 13: 67-81.
- Nakano, A., Y. Kanemura, et al. 2007. 'Expression of the Neural RNA-binding protein Musashi1 in pediatric brain tumors', *Pediatr Neurosurg*, 43: 279-84.
- Noushmehr, H., D. J. Weisenberger, et al. 2010. 'Identification of a CpG island methylator phenotype that defines a distinct subgroup of glioma', *Cancer Cell*, 17: 510-22.
- Ohyama, T., A. Furukawa, et al. 2008. 'Structural analysis of Musashi-RNA complex on the basis of long-range structural information', *Nucleic Acids Symp Ser (Oxf)*: 193-4.
- Ohyama, T., T. Nagata, et al. 2012. 'Structure of Musashi1 in a complex with target RNA: the role of aromatic stacking interactions', *Nucleic Acids Res*, 40: 3218-31.
- Okano, H., H. Kawahara, et al. 2005. 'Function of RNA-binding protein Musashi-1 in stem cells', *Exp Cell Res*, 306: 349-56.
- Oliferenko, S., I. Kaverina, et al. 2000. 'Hyaluronic acid (HA) binding to CD44 activates Rac1 and induces lamellipodia outgrowth', *J Cell Biol*, 148: 1159-64.
- Oskarsson, T., S. Acharyya, et al. 2011. 'Breast cancer cells produce tenascin C as a metastatic niche component to colonize the lungs', *Nat Med*, 17: 867-74.
- Osuka, S., and E. G. Van Meir. 2017. 'Overcoming therapeutic resistance in glioblastoma: the way forward', *J Clin Invest*, 127: 415-26.
- Pagliuca, A., C. Valvo, et al. 2013. 'Analysis of the combined action of miR-143 and miR-145 on oncogenic pathways in colorectal cancer cells reveals a coordinate program of gene repression', *Oncogene*, 32: 4806-13.
- Pereira, B., M. Billaud, et al. 2017. 'RNA-Binding Proteins in Cancer: Old Players and New Actors', *Trends Cancer*, 3: 506-28.
- Perkins, A., and G. Liu. 2016. 'Primary Brain Tumors in Adults: Diagnosis and Treatment', *Am Fam Physician*, 93: 211-7.

- Pimienta, G., and J. Pascual. 2007. 'Canonical and alternative MAPK signaling', *Cell Cycle*, 6: 2628-32.
- Pointer, K. B., P. A. Clark, et al. 2014. 'Glioblastoma cancer stem cells: Biomarker and therapeutic advances', *Neurochem Int*, 71: 1-7.
- Potschke, R., G. Gielen, et al. 2020. 'Musashi1 enhances chemotherapy resistance of pediatric glioblastoma cells in vitro', *Pediatr Res*, 87: 669-76.
- Preca, B. T., K. Bajdak, et al. 2015. 'A self-enforcing CD44s/ZEB1 feedback loop maintains EMT and stemness properties in cancer cells', *Int J Cancer*, 137: 2566-77.
- Reya, T., S. J. Morrison, et al. 2001. 'Stem cells, cancer, and cancer stem cells', *Nature*, 414: 105-11.
- Rezza, A., S. Skah, et al. 2010. 'The overexpression of the putative gut stem cell marker Musashi-1 induces tumorigenesis through Wnt and Notch activation', *J Cell Sci*, 123: 3256-65.
- Ricci-Vitiani, L., D. G. Lombardi, et al. 2007. 'Identification and expansion of human colon-cancer-initiating cells', *Nature*, 445: 111-5.
- Richter, K., P. J. Good, et al. 1990. 'A developmentally regulated, nervous system-specific gene in *Xenopus* encodes a putative RNA-binding protein', *New Biol*, 2: 556-65.
- Robinson, M. D., D. J. McCarthy, et al. 2010. 'edgeR: a Bioconductor package for differential expression analysis of digital gene expression data', *Bioinformatics*, 26: 139-40.
- Rutnam, Z. J., and B. B. Yang. 2012. 'The non-coding 3' UTR of CD44 induces metastasis by regulating extracellular matrix functions', *J Cell Sci*, 125: 2075-85.
- Sakakibara, S., T. Imai, et al. 1996. 'Mouse-Musashi-1, a neural RNA-binding protein highly enriched in the mammalian CNS stem cell', *Dev Biol*, 176: 230-42.
- Sakakibara, S., Y. Nakamura, et al. 2001. 'Rna-binding protein Musashi2: developmentally regulated expression in neural precursor cells and subpopulations of neurons in mammalian CNS', *J Neurosci*, 21: 8091-107.
- Sakakibara, S., Y. Nakamura, et al. 2002. 'RNA-binding protein Musashi family: roles for CNS stem cells and a subpopulation of ependymal cells revealed by targeted disruption and antisense ablation', *Proc Natl Acad Sci U S A*, 99: 15194-9.
- Sakakibara, S., and H. Okano. 1997. 'Expression of neural RNA-binding proteins in the postnatal CNS: implications of their roles in neuronal and glial cell development', *J Neurosci*, 17: 8300-12.

- Sandberg, R., J. R. Neilson, et al. 2008. 'Proliferating cells express mRNAs with shortened 3' untranslated regions and fewer microRNA target sites', *Science*, 320: 1643-7.
- Sassen, S., E. A. Miska, et al. 2008. 'MicroRNA: implications for cancer', *Virchows Arch*, 452: 1-10.
- Schlegel, U.; Weller, M.; Westphal, M. 2009. 'Neuroonkologische Therapie ', W. Kohlhammer Verlag. <https://www.medfuehrer.de/Gehirntumor-Hintergrund>.
- Schneider, T., L. H. Hung, et al. 2019. 'Combinatorial recognition of clustered RNA elements by the multidomain RNA-binding protein IMP3', *Nat Commun*, 10: 2266.
- Sebestyen, E., B. Singh, et al. 2016. 'Large-scale analysis of genome and transcriptome alterations in multiple tumors unveils novel cancer-relevant splicing networks', *Genome Res*, 26: 732-44.
- Shalini, S., L. Dorstyn, et al. 2015. 'Old, new and emerging functions of caspases', *Cell Death Differ*, 22: 526-39.
- Siddall, N. A., E. A. McLaughlin, et al. 2006. 'The RNA-binding protein Musashi is required intrinsically to maintain stem cell identity', *Proc Natl Acad Sci U S A*, 103: 8402-7.
- Singh, G., G. Pratt, et al. 2015. 'The Clothes Make the mRNA: Past and Present Trends in mRNP Fashion', *Annu Rev Biochem*, 84: 325-54.
- Singh, S. K., I. D. Clarke, et al. 2003. 'Identification of a cancer stem cell in human brain tumors', *Cancer Res*, 63: 5821-8.
- Sonoki, H., A. Tanimae, et al. 2017. 'Kaempferol and Luteolin Decrease Claudin-2 Expression Mediated by Inhibition of STAT3 in Lung Adenocarcinoma A549 Cells', *Nutrients*, 9.
- Stupp, R., M. E. Hegi, et al. 2009. 'Effects of radiotherapy with concomitant and adjuvant temozolomide versus radiotherapy alone on survival in glioblastoma in a randomised phase III study: 5-year analysis of the EORTC-NCIC trial', *Lancet Oncol*, 10: 459-66.
- Sturm, D., H. Witt, et al. 2012. 'Hotspot mutations in H3F3A and IDH1 define distinct epigenetic and biological subgroups of glioblastoma', *Cancer Cell*, 22: 425-37.
- Sureban, S. M., R. May, et al. 2008. 'Knockdown of RNA binding protein musashi-1 leads to tumor regression in vivo', *Gastroenterology*, 134: 1448-58.
- Sutherland, J. M., N. A. Siddall, et al. 2015. 'RNA binding proteins in spermatogenesis: an in depth focus on the Musashi family', *Asian J Androl*, 17: 529-36.

- Swift, J., and G. M. Coruzzi. 2017. 'A matter of time - How transient transcription factor interactions create dynamic gene regulatory networks', *Biochim Biophys Acta Gene Regul Mech*, 1860: 75-83.
- Takahashi, R. U., H. Miyazaki, et al. 2015. 'Loss of microRNA-27b contributes to breast cancer stem cell generation by activating ENPP1', *Nat Commun*, 6: 7318.
- Takeshita, I., T. Takaki, et al. 1987. 'Characteristics of an established human glioma cell line, KNS-42', *Neurol Med Chir (Tokyo)*, 27: 581-7.
- Tapial, J., K. C. H. Ha, et al. 2017. 'An atlas of alternative splicing profiles and functional associations reveals new regulatory programs and genes that simultaneously express multiple major isoforms', *Genome Res*, 27: 1759-68.
- Taylor, O. G., J. S. Brzozowski, et al. 2019. 'Glioblastoma Multiforme: An Overview of Emerging Therapeutic Targets', *Front Oncol*, 9: 963.
- Tenenbaum, S. A., C. C. Carson, et al. 2000. 'Identifying mRNA subsets in messenger ribonucleoprotein complexes by using cDNA arrays', *Proc Natl Acad Sci U S A*, 97: 14085-90.
- Toda, M., Y. Iizuka, et al. 2001. 'Expression of the neural RNA-binding protein Musashi1 in human gliomas', *Glia*, 34: 1-7.
- Uren, P. J., D. T. Vo, et al. 2015. 'RNA-Binding Protein Musashi1 Is a Central Regulator of Adhesion Pathways in Glioblastoma', *Mol Cell Biol*, 35: 2965-78.
- Uziel, T., F. V. Karginov, et al. 2009. 'The miR-17~92 cluster collaborates with the Sonic Hedgehog pathway in medulloblastoma', *Proc Natl Acad Sci U S A*, 106: 2812-7.
- Van Nifterik, K. A., J. Van den Berg, et al. 2012. 'Valproic acid sensitizes human glioma cells for temozolomide and gamma-radiation', *J Neurooncol*, 107: 61-7.
- Van Nostrand, E. L., G. A. Pratt, et al. 2016. 'Robust transcriptome-wide discovery of RNA-binding protein binding sites with enhanced CLIP (eCLIP)', *Nat Methods*, 13: 508-14.
- Venere, M., H. A. Fine, et al. 2011. 'Cancer stem cells in gliomas: identifying and understanding the apex cell in cancer's hierarchy', *Glia*, 59: 1148-54.
- Verhaak, R. G., K. A. Hoadley, et al. 2010. 'Integrated genomic analysis identifies clinically relevant subtypes of glioblastoma characterized by abnormalities in PDGFRA, IDH1, EGFR, and NF1', *Cancer Cell*, 17: 98-110.
- Vikesaa, J., T. V. Hansen, et al. 2006. 'RNA-binding IMPs promote cell adhesion and invadopodia formation', *EMBO J*, 25: 1456-68.

- Vo, D. T., K. Abdelmohsen, et al. 2012. 'The oncogenic RNA-binding protein Musashi1 is regulated by HuR via mRNA translation and stability in glioblastoma cells', *Mol Cancer Res*, 10: 143-55.
- Vo, D. T., M. Qiao, et al. 2011. 'The oncogenic RNA-binding protein Musashi1 is regulated by tumor suppressor miRNAs', *RNA Biol*, 8: 817-28.
- Vogelbaum, M. A. 2012. 'Does extent of resection of a glioblastoma matter?', *Clin Neurosurg*, 59: 79-81.
- Wang, J., T. P. Wakeman, et al. 2010. 'Notch promotes radioresistance of glioma stem cells', *Stem Cells*, 28: 17-28.
- Wang, Q., H. Wang, et al. 2017. 'Luteolin reduces migration of human glioblastoma cell lines via inhibition of the p-IGF-1R/PI3K/AKT/mTOR signaling pathway', *Oncol Lett*, 14: 3545-51.
- Wang, Q., H. Wang, et al. 2017. 'Luteolin induces apoptosis by ROS/ER stress and mitochondrial dysfunction in gliomablastoma', *Cancer Chemother Pharmacol*, 79: 1031-41.
- Wang, R., R. Sharma, et al. 2020. 'Adult Human Glioblastomas Harbor Radial Glia-like Cells', *Stem Cell Reports*, 14: 338-50.
- Wang, X. Y., L. O. Penalva, et al. 2010. 'Musashi1 regulates breast tumor cell proliferation and is a prognostic indicator of poor survival', *Mol Cancer*, 9: 221.
- Wang, X. Y., H. Yu, et al. 2013. 'Musashi1 as a potential therapeutic target and diagnostic marker for lung cancer', *Oncotarget*, 4: 739-50.
- Wang, Z. L., B. Li, et al. 2018. 'Comprehensive Genomic Characterization of RNA-Binding Proteins across Human Cancers', *Cell Rep*, 22: 286-98.
- Wei, K. C., C. Y. Huang, et al. 2010. 'Evaluation of the prognostic value of CD44 in glioblastoma multiforme', *Anticancer Res*, 30: 253-9.
- Weller, M., T. Gorlia, et al. 2011. 'Prolonged survival with valproic acid use in the EORTC/NCIC temozolomide trial for glioblastoma', *Neurology*, 77: 1156-64.
- Yamashita, M., H. Egami, et al. 1981. 'Alternate culture and animal passage of human glioma', *Acta Neuropathol*, 53: 35-40.
- Yan, L. X., X. F. Huang, et al. 2008. 'MicroRNA miR-21 overexpression in human breast cancer is associated with advanced clinical stage, lymph node metastasis and patient poor prognosis', *RNA*, 14: 2348-60.

- Yang, J., Z. Zheng, et al. 2013. 'Integration of autophagy and anoikis resistance in solid tumors', *Anat Rec (Hoboken)*, 296: 1501-8.
- Yang, Z., D. Chen, et al. 2016. 'MicroRNA143 targets CD44 to inhibit breast cancer progression and stem cell-like properties', *Mol Med Rep*, 13: 5193-9.
- Yates, A., W. Akanni, et al. 2016. 'Ensembl 2016', *Nucleic Acids Res*, 44: D710-6.
- Yi, C., G. Li, et al. 2018. 'Luteolin inhibits Musashi1 binding to RNA and disrupts cancer phenotypes in glioblastoma cells', *RNA Biol*, 15: 1420-32.
- Yoshida, T., Y. Matsuda, et al. 2012. 'CD44 in human glioma correlates with histopathological grade and cell migration', *Pathol Int*, 62: 463-70.
- Zang, M. D., L. Hu, et al. 2017. 'Luteolin suppresses gastric cancer progression by reversing epithelial-mesenchymal transition via suppression of the Notch signaling pathway', *J Transl Med*, 15: 52.
- Zearfoss, N. R., L. M. Deveau, et al. 2014. 'A conserved three-nucleotide core motif defines Musashi RNA binding specificity', *J Biol Chem*, 289: 35530-41.
- Zhang, B., X. Pan, et al. 2007. 'microRNAs as oncogenes and tumor suppressors', *Dev Biol*, 302: 1-12.
- Zhang, M., J. Zhang, et al. 2013. 'Glycogen synthase kinase 3 promotes p53 mRNA translation via phosphorylation of RNPC1', *Genes Dev*, 27: 2246-58.
- Zhao, W., Y. Li, et al. 2017. 'Stemness-Related Markers in Cancer', *Cancer Transl Med*, 3: 87-95.
- Zhong, J., A. Paul, et al. 2010. 'Mesenchymal migration as a therapeutic target in glioblastoma', *J Oncol*, 2010: 430142.
- Zoller, M. 2011. 'CD44: can a cancer-initiating cell profit from an abundantly expressed molecule?', *Nat Rev Cancer*, 11: 254-67.

7 Appendix

7.1 Abbreviations

AA	Amino acid
AML	Acute myeloid leukemia
APC	Astrocyte progenitor cell
ATP	Adenosintriphosphate
bFGF	Basic fibroblast growth factor
bp	Basepairs
BSA	Bovine serum albumin
CDI	Coefficient of drug interaction
cDNA	Complementary DNA
CDS	Coding sequence
CLIP	Cross-Linking and Immunoprecipitation
CNS	Central nervous system
cm	Centimeter
CRISPR	Clustered Reuglatory Interspaced Short Palindromic Repeats
CSC	Cancer Stem cells
Ctrl	Control
DAPI	4',6-Diamidin-2-phenylindol
DCP2	Decapping protein 2
DEG	Differentially expressed gene
DIV	Days <i>in vitro</i>
DMEM	Dulbecco's Modified Eagle's Medium
DMSO	Dimethylsulfoxid
DNA	Desoxynucleic acid
eCLIP	enhanced CLIP
ECM	Extracellular matrix
EGF	Epidermal growth factor
eIF4G	Eukaryotic initiation factor 4 G
EMT	Epithelial-mesenchymal transition
ENCDOE	Encyclopedia of DNA elements
ESC	Embryonic stem cells
FBS	Fetal bovine serume
FDR	False discovery rate
fw	Forward
g	Gramm
GBM-CSC	GBM-Cancer stem cells
GBM	Glioblastoma

GFAP	Glial fibrillary acidic protein
GFP	Green fluorescing protein
GLD2	Germ Line Development
GO	Gene ontology
h	Hours
HDAC	Histone deacetylase
HDACi	HDAC-inhibitor
HGG	High grade glioma
hnRNP	heterogenous nuclear ribonucleoprotein
iCLIP	individual-nucleotide resolution CLIP
IGF2BP1	IGF2 mRNA-binding protein
IHC	Immunohistochemistry
IP	Immunoprecipitation
kb	Kilobasepairs
kDa	Kilodalton
KD	Knockdown
KH	K-homology
KO	Knock-out
LGG	Low Grade Glioma
M	Molar
mg	Milligramm
min	Minutes
miRISC	miRNA-induced silencing complex
miRNA	microRNA
MGMT	Methyl guanine methyltransferase
ml	Milliliter
mM	Millimolar
mm	Millimeter
MRE	miRNA recognition element
mRNA	messenger RNA
mRNP	messenger RNP
MSI1	Musashi1
MTT	Methylthiazolyldiphenyl-tetrazoliumbromid
NESC	Neuroepithelial stem cells
ng	Nanogramm
NLS	Nuclear localization signal
nM	Nanomolar
nm	Nanometer
NPC	Neural progenitor cell
n.s.	Not significant
NSC	Neural stem cells
nt	Nucleotide
OE	Overexpression

OPC	Oligodendrocyte progenitor cell
PABPC	Cytoplasmic poly(A)-binding protein
PARP-1	poly (ADP-ribose) polymerase-1
PBS	Phosphate-buffered saline
PCR	Polymerase chain reaction
pcw	Post-conception week
PKc	Protein-kinase catalytic subunit
PTM	Posttranslation modification
qRT-PCR	Quantitative Real Time PCR
RBP	RNA-binding protein
rev	Reverse
RFP	Red fluorescent protein
RFX	Regulatory factor X
RIC	RNA interactome capture
RIP	RNA-Immunoprecipitation
RISC	RNA-induced silencing complex
RNA	Ribonucleic acid
RNP	Ribonucleoprotein
RPKM	Reads per kilobase per million mapped reads
rpm	revolutions per minute
RRM	RNA-recognition motif
RTK	Receptor tyrosine kinase
RT-PCR	Reverse transcription PCR
RT	Reverse transcriptase
RT	Room Temperature
sec	Seconds
SCNA	Somatic copy number alterations
Seq	Sequencing
sgRNA	Single guide RNA
SHH	Sonic Hedgehog
TCGA	The Cancer Genome Atlas
TMZ	Temozolomide
UTR	Untranslated region
V	Volt
VPA	Valproic acid
WB	Western blot
WT	Wildtype
Yrs	Years
%	Percent
°C	Centigrade
µg	Mikrogramm
µl	Mikroliter
µm	Micrometer

7.2 List of Figures

- Figure 1. Mechanisms of posttranscriptional gene regulation by RBPs.
- Figure 2: Schematic illustration of miRNA-mediated silencing in animals
- Figure 3: Schematic of MSI1 protein domain composition.
- Figure 4: Mechanism of MSI1-dependent translational repression of its target mRNA.
- Figure 5: MRT of a patient's brain suffering from GBM.
- Figure 6. Expression of MSI1, MSI2 and IGF2BP1 across human fetal hippocampus development.
- Figure 7. MSI1 expression in TCGA cancer cohorts.
- Figure 8. MSI1 expression in pediatric GBM.
- Figure 9. MSI1 expression in GBM-derived cell lines and non-GBM-derived cell lines.
- Figure 10. MSI1 depletion and knockout in KNS42 cells.
- Figure 11. Impact of MSI1-knockout on KNS42 cell proliferation and spheroid viability.
- Figure 12. MSI1-knockout and knockdown affect clonogenicity and apoptosis of KNS42 cells.
- Figure 13: Impact of MSI1-knockout on anchorage-independent growth and anoikis resistance of KNS42 cells.
- Figure 14. MSI1 affects single cell migration speed.
- Figure 15. Effect of MSI1 on cell morphology.
- Figure 16. Stem cell marker expression is upregulated in GBM.
- Figure 17. Analysis of RNA-Sequencing of MSI1 KD in KNS42.
- Figure 18. Identification of potentially stabilized MSI1 downstream target mRNAs in GBM.
- Figure 19. CD44 Expression upon MSI1 KD or KO.
- Figure 20. Regulation of CD44 expression via MSI1.
- Figure 21. MSI1 regulates CD44 in a 3'UTR dependent manner.
- Figure 22. CD44 3'UTR-deletion in KNS42 cells.
- Figure 23. Effect of MSI1 in miRNA-dependent regulation of CD44 3'UTR.
- Figure 24. KNS42 treatment with MSI1 inhibitor Luteolin.
- Figure 25. Cell phenotypes in KNS42 upon Luteolin treatment.
- Figure 26. GBM-CSC HAL8 treatment with MSI1 inhibitor Luteolin.
- Figure 27. Expression of MSI1 in pediatric glioblastoma cell lines.
- Figure 28. Effects of TMZ and VPA treatment in KNS42.
- Figure 29: Effect of MSI1 on chemoresistance in TMZ and VPA treatment.

Figure 30. Detection of MSI1 isoform.

Figure 31. Generation of MSI1 variants.

Figure 32. MSI1 Δ 11 lacks two putative post-translational modification sites.

Figure 33. Biological functionality and expression pattern of MSI1 Δ 11.

7.3 Eidesstattliche Erklärung

Hiermit versichere ich, dass ich die vorliegende Dissertation selbstständig und ohne fremde Hilfe verfasst habe. Ich habe keine anderen als die von mir angegebenen Quellen und Hilfsmittel benutzt. Die eingereichte schriftliche Fassung der Arbeit entspricht der auf dem elektronischen Speichermedium.

Mit der vorliegenden Arbeit bewerbe ich mich erstmals um die Erlangung des Doktorgrades *doctor rerum naturalium*.

Datum

Unterschrift

7.4 Danksagung

An erster Stelle möchte ich mich bei Prof. Stefan Hüttelmaier und bei Dr. Caspar Kühnöl dafür bedanken, dass ich ein so interessantes Thema als Projekt bearbeiten durfte und dadurch mein Wissen in den Neurowissenschaften vertiefen konnte. Danke Caspar, dass ich so nah am klinischen Geschehen Einblicke bekommen durfte. Danke für die stetige Unterstützung und Beratung. Danke Stefan, für dein Engagement, deine Diskussionsbereitschaft, deine konstruktive Kritik und dafür, dass ich Teil der Arbeitsgruppe werden konnte. Danke, dass du eine hervorragende Forschungsumgebung geschaffen hast, in der wir als Doktoranden wissenschaftlich und persönlich wachsen können. Danke für das Vertrauen zur Etablierung von Kooperationen und dafür, dass ich die dazugehörigen Projekte bearbeiten durfte. Danke, dass mir die Assoziation am GRK 1591 ermöglicht wurde, wodurch ich an Kongressen teilnehmen und ich wertvolle wissenschaftliche Erfahrungen machen konnte.

Thank you, Luiz, for bringing my RBP of interest into the group whereof my project could grow out. It was such a pleasure to collaborate with you.

Vielen Dank, liebe Arbeitsgruppe, für den gemeinsamen Laboralltag und die vielen Unternehmungen fernab der Wissenschaft. Ich bedanke mich bei Hendrik und Britta, die mich von Anfang an in der Arbeitsgruppe willkommen heißen haben und mit denen ich viele schöne Erinnerungen teile.

Danke an die Mensagruppe, für die tägliche kleine Auszeit unter Freunden. Ich bin schon jetzt dankbar darüber, dass unsere Freundschaften weiter bestehen werden, auch wenn wir nicht mehr im selben Labor pipettieren.

Ich möchte mich bei meinen Eltern und meinen Geschwistern bedanken, dass sie mich so oft verständnisvoll aufmuntern und mich auch in den unmöglichsten Situationen zum Lachen bringen. Kleines Mupsch, zum Glück sind wir Schwestern.

Danke an meine Freunde-dafür, dass ihr so lieb an meiner Seite steht und wir eine schöne gemeinsame Zeit haben.

Danke Jacob, für deine mentale und wissenschaftliche Unterstützung. Und natürlich dafür, dass wir zusammen mutig genug für Rosalind waren <3 Auf in unser neues wissenschaftliches Abenteuer.

7.5 Curriculum Vitae

Persönliche Details

Name: Rebecca Pötschke

Geburtsdatum: 3. November 1988

Nationalität: Deutsch

Ausbildung & Werdegang

09/1999 – 07/2007

Gotthold-Ephraim-Lessing Schule Kamenz

Abschluss: Abitur

10/2007 - 09/2010

Studiengang „Bioinformatik“

Martin-Luther-Universität Halle-Wittenberg

Abschluss: Bachelor of Science

10/2010 – 07/2013

Studiengang „Integrative Neurowissenschaften“

Otto-von-Guericke Universität Magdeburg

Abschluss: Master of Science

10/2013 -05/2019

Wissenschaftliche Mitarbeiterin und Doktorandin in der Pädiatrie I, Universitätsklinik

Halle und Institut für Molekulare Medizin der Martin-Luther-Universität Halle, GRK 1591
assoziiert

seit 05/2019

Mutterschutz und Elternzeit

Rebecca Pötschke

Halle (Saale), Mai, 2020

7.6 Publikationsliste

1.) N. von Spreckelsen*, N. Waldt*, **R. Pötschke***, C. Kessler, H. Dohmen, H.-K. Jiao, A. Nemeth, S. Schob, C. Scherlach, M. Deckert, I. Sandalcioglu, B. Krischek, F. Angenstein, P. Stavrinou, M. Timmer, M. Remke, E. Kirches, R. Goldbrunner, E. A. Chiocca, S. Hüttelmaier, T. Acker, C. Mawrin (2020). * geteilte Erstautorschaft

KLF4K409Q-mutated meningiomas show enhanced hypoxia signaling and respond to mTORC1 inhibitor treatment., *Acta Neuropathol Commun.* 2020; 8:41

2.) **R. Pötschke**, G. Gielen, T. Pietsch, C. Kramm, J-H. Klusmann, S. Hüttelmaier, C. Kühnöl (2020).

Musashi1 enhances chemotherapy resistance of pediatric glioblastoma cells *in vitro.*, *Pediatric Research* 87(4):669-676

3.) P. Uren, D. Vo, P. de Araujo, **R. Pötschke**, S. Burns, E. Bahrami-Samani, M. Qiao, R. de Sousa Abreu, H. Nakaya, B. Correa, C. Kühnöl, J. Ule, J. Martindale, K. Abdelmohsen, M. Gorospe, A. Smith, L. Penalva (2015).

RNA-Binding Protein Musashi1 Is a Central Regulator of Adhesion Pathways in Glioblastoma., *Mol Cell Biol* 35:2965-2978